

# NUMUON: NUCLEAR-NORM-CONSTRAINED MUON FOR COMPRESSIBLE LLM TRAINING

Hadi Mohaghegh Dolatabadi, Thalaiyasingam Ajanthan, Sameera Ramasinghe, Chamin P Hewa Koneputugodage, Shamane Siriwardhana, Violetta Shevchenko, Karol Pajak, James Snewin, Gil Avraham, and Alexander Long

Pluralis Research

The rapid progress of large language models (LLMs) is increasingly constrained by memory and deployment costs, motivating compression methods for practical deployment. Many state-of-the-art compression pipelines leverage the low-rank structure of trained weight matrices, a phenomenon often associated with the properties of popular optimizers such as Adam. In this context, Muon is a recently proposed optimizer that improves LLM pretraining via full-rank update steps, but its induced weight-space structure has not been characterized yet. In this work, we report a surprising empirical finding: despite imposing full-rank updates, Muon-trained models exhibit pronounced low-rank structure in their weight matrices and are readily compressible under standard pipelines. Motivated by this insight, we propose *NuMuon*, which augments Muon with a nuclear-norm constraint on the update direction, further constraining the learned weights toward low-rank structure. Across billion-parameter-scale models, we show that NuMuon increases weight compressibility and improves post-compression model quality under state-of-the-art LLM compression pipelines while retaining Muon’s favorable convergence behavior.

*Keywords: Optimization, Deep Learning, Large Language Models, Model Compression*

## 1. INTRODUCTION

Large language models (LLMs) (DeepSeek-AI et al., 2025; OpenAI, 2023; Radford et al., 2018; Yang et al., 2024) have driven rapid progress in natural language processing and enabled a wide range of applications, including coding (Bairi et al., 2024), mathematics (Romera-Paredes et al., 2024), and agentic systems (Wang et al., 2024). Much of this progress has been fueled by scaling model and data size (Hoffmann et al., 2022; Kaplan et al., 2020), which often leads to qualitative shifts in capability as model size grows (Schaeffer et al., 2023; Wei et al., 2022). However, deploying LLMs with billions of parameters incurs substantial memory, storage, and accelerator costs (Zhou et al., 2024). This has motivated a large body of work on LLM compression (Zhu et al., 2024) to reduce deployment-time footprint. Such compression methods often exploit structure in the weight matrices (e.g., low-rank structure (Wang et al., 2025b) or sparsity (Frantar and Alistarh, 2023)). Consequently, training choices directly impact how well a model can be compressed for deployment.

Recently, Muon (Bernstein and Newhouse, 2025; Jordan et al., 2024) has been proposed as an alternative optimizer for pretraining LLMs. Unlike elementwise adaptive optimizers such as Adam (Kingma and Ba, 2015) and AdamW (Loshchilov and Hutter, 2019), Muon orthogonalizes the matrix-valued momentum update (e.g., via Newton–Schulz), effectively adapting updates to spectral geometry. Empirically, Muon has shown strong performance in large-scale language model training (Bai et al., 2025; Liu et al., 2025). In contrast to common optimizers such as AdamW that are known to exhibit an implicit low-rank bias (Huh et al., 2023; Zhao, 2022), Muon’s training dynamics and the induced structure of the learned weight space remain underexplored. Understanding such implicit biases are crucial for the downstream deployability of Muon-trained models through existing LLM compression pipelines.

In this paper, we shed light on these dynamics and report a surprising phenomenon: despite using full-rank, orthogonalized update directions and imposing no explicit rank control, *Muon-trained models already exhibit*

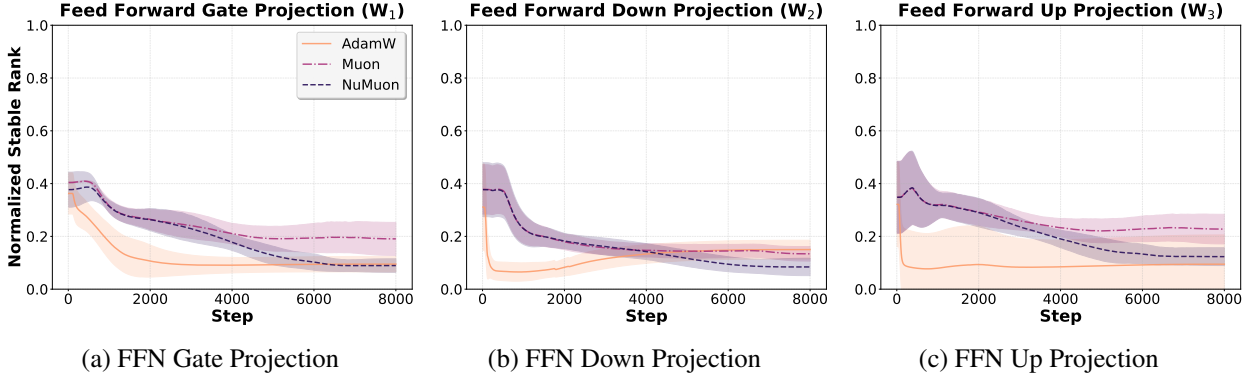


Figure 1: Normalized stable rank evolution for Qwen3-0.6B across training steps for feedforward projection matrices. Each subplot shows the mean stable rank (normalized by the maximum rank), with shaded regions indicating standard deviation across all layers. All other weight matrices exhibit a similar low-rank behavior throughout training (see Figure 13 in the Appendix).

*pronounced low-rank structure in their weight matrices* (Figure 1). As a result, we empirically observe that Muon-trained models are readily compressible under common low-rank compression pipelines. However, Muon’s emergent low-rank structure is not sufficiently robust against aggressive compression, deteriorating performance rapidly as the compression rate increases. Motivated by this limitation, we seek a principled mechanism to strengthen this low-rank structure during training to improve high-rate compressibility while preserving Muon’s favorable optimization behavior.

To this end, we view Muon’s orthogonalization step through a projection-free lens where it implements a linear minimization oracle (LMO) (Pethick et al., 2025; Riabinin et al., 2025) and returns the steepest descent direction by minimizing a linearized objective over a spectral-norm-bounded set. Building on this interpretation, we propose *NuMuon*: a variant of Muon that augments its spectral-norm LMO with an additional nuclear-norm budget on the update direction, which we use as a convex proxy to control update rank. Using an LMO formulation, we show that the NuMuon step reduces to a linear program over singular values with a closed-form solution using the top- $k$  singular vectors. NuMuon yields a rank-controlled alternative to Muon’s full orthogonalization and directly shapes the singular-value profile of the update. By constraining the update direction, we demonstrate that NuMuon consistently achieves lower stable rank in the learned weights than Muon.

We test NuMuon on models in the 0.6–1.8B parameter range, and show that it converges similarly to Muon while producing weight matrices with more concentrated spectra (lower stable rank), which in turn improves downstream compressibility. Under state-of-the-art (SoTA) LLM compression pipelines, NuMuon-trained models achieve up to 55.9% better compression–quality tradeoffs (i.e., lower perplexity at a fixed compression setting), making NuMuon attractive for large-scale or cost-sensitive deployment scenarios with strict memory requirements.

In summary, we make the following contributions:

- We show that Muon-trained models exhibit a surprisingly pronounced low-rank structure in their weight matrices despite the explicit full-rank updates in the absence of rank constraints.
- Inspired by this observation, we propose NuMuon which augments Muon with a per-layer nuclear-norm budget on the LMO update direction. We show that the resulting LMO reduces to a linear program over singular values and admits a closed-form top- $k$  singular-vector solution, yielding rank-controlled updates.
- We provide convergence guarantees for NuMuon under non-convex assumptions and describe practical techniques for efficient top- $k$  computation and rank scheduling strategies for large-scale training using

our approach.

- We empirically show that NuMuon achieves comparable performance to Muon while yielding substantially improved compressibility under SoTA LLM compression pipelines, improving deployability.

Our results clarify aspects of Muon’s implicit bias and provide a practical optimizer variant for settings where controlling low-rank structure is important.

## 2. BACKGROUND

In this section, we introduce notation and briefly review background related to our work.

**Muon Optimizer.** Muon (Jordan et al., 2024) is an optimizer that produces *geometry-aware* updates for matrix-valued parameters by orthogonalizing momentum updates. In contrast to elementwise adaptive methods such as AdamW (Loshchilov and Hutter, 2019), which rescale coordinates independently, Muon post-processes the momentum update so that its singular directions are treated uniformly.

Concretely, consider a single matrix parameter  $\mathbf{W} \in \mathbb{R}^{d_{\text{out}} \times d_{\text{in}}}$  (e.g., a linear layer weight) from a neural network.<sup>1</sup> Through training, we aim to minimize an objective with respect to the weights  $\min_{\mathbf{W}} f(\mathbf{W})$ . Let  $\mathbf{G}_t = \nabla_{\mathbf{W}} f(\mathbf{W}_t)$  be the gradient, and let  $\mathbf{M}_t$  be a momentum buffer:

$$\mathbf{M}_t = \beta \mathbf{M}_{t-1} + (1 - \beta) \mathbf{G}_t, \quad (1)$$

where  $\beta \in [0, 1)$ . Assuming a truncated SVD  $\mathbf{M}_t = \mathbf{U}_t \mathbf{S}_t \mathbf{V}_t^\top$ , Muon replaces  $\mathbf{M}_t$  by its *orthogonal (polar) factor*:

$$\text{Ortho}(\mathbf{M}_t) := \mathbf{U}_t \mathbf{V}_t^\top, \quad (2)$$

which has singular values equal to 1. The parameter update is then written as:

$$\mathbf{W}_{t+1} = \mathbf{W}_t - \gamma \text{Ortho}(\mathbf{M}_t), \quad (3)$$

where  $\gamma$  is the learning rate. Intuitively, dropping  $\mathbf{S}_t$  removes anisotropic scaling and yields an update that treats singular directions uniformly (Bernstein and Newhouse, 2025; Jordan et al., 2024). In practice, the  $\text{Ortho}(\cdot)$  operation is typically approximated efficiently, e.g., via a few rounds of Newton–Schulz approximation (see Algorithm 2).

**Linear Minimization Oracles.** Recent work by Pethick et al. (2025); Riabinin et al. (2025) has highlighted that Muon can be interpreted within a broader family of methods based on *linear minimization oracles* (LMOs) over norm balls. In particular, consider the norm-constrained problem:

$$\min_{\mathbf{W}} f(\mathbf{W}) \quad \text{s.t.} \quad \mathbf{W} \in \mathcal{W} := \{\mathbf{W} : \|\mathbf{W}\| \leq \rho\}, \quad (4)$$

for some radius  $\rho > 0$  and a chosen norm  $\|\cdot\|$ . As shown in Scion (Pethick et al., 2025), LMO-based training rules can be written in an *unconstrained* (additive) form:

$$\mathbf{W}_{t+1} = \mathbf{W}_t + \gamma_t \text{lmo}_{\mathcal{W}}(\mathbf{M}_t), \quad (5)$$

or in a *constrained* Frank–Wolfe (FW) (Frank et al., 1956) / conditional-gradient (CG) (Jaggi, 2013) form:

$$\mathbf{W}_{t+1} = (1 - \gamma_t) \mathbf{W}_t + \gamma_t \text{lmo}_{\mathcal{W}}(\mathbf{M}_t), \quad (6)$$

<sup>1</sup>For clarity, we present the update for one matrix block; in practice, Muon is applied block-wise/layer-wise.

where  $\gamma_t \in (0, 1]$  is a stepsize. Here, an LMO for  $\mathcal{W}$  is the mapping:

$$\text{lmo}_{\mathcal{W}}(\mathbf{M}) \in \arg \min_{\Delta \mathbf{W} \in \mathcal{W}} \langle \mathbf{M}, \Delta \mathbf{W} \rangle. \quad (7)$$

When  $\mathcal{W}$  is a *spectral-norm ball*, i.e.,  $\mathcal{W} = \{\Delta \mathbf{W} : \|\Delta \mathbf{W}\|_2 \leq \rho\}$ , the LMO has a closed form. Specifically, if  $\mathbf{M} = \mathbf{U} \mathbf{S} \mathbf{V}^\top$  is a thin SVD, then:

$$\text{lmo}_{\mathcal{W}}(\mathbf{M}) \in \arg \min_{\|\Delta \mathbf{W}\|_2 \leq \rho} \langle \mathbf{M}, \Delta \mathbf{W} \rangle = -\rho \mathbf{U} \mathbf{V}^\top. \quad (8)$$

Thus, up to stepsize conventions (absorbing  $\rho$  into the learning rate), the additive LMO update in Equation (5) recovers Muon’s orthogonalized step in Equation (2).

### LLM Compression via Low-Rank Structure.

LLM compression seeks to lower storage and deployment-time memory costs and speed without sacrificing accuracy (Zhou et al., 2024). To this end, prior work typically exploits low-rank structure (Wang et al., 2025b), reduced-precision representations via quantization (Dettmers et al., 2022; Huang et al., 2024; Yuan et al., 2024), and sparsification or pruning (Frantar and Alistarh, 2023; Kim et al., 2024).

A prominent line of work leverages approximate low-rank structure in weight matrices by factorizing a full-rank weight matrix into low-rank factors (Hsu et al., 2022; Wang et al., 2025a;b; Yuan et al., 2023). In particular, for a weight matrix  $\mathbf{W} \in \mathbb{R}^{d_{\text{out}} \times d_{\text{in}}}$ , a rank- $k$  factorization in such methods takes the form  $\mathbf{W} \approx \mathbf{W}_u \mathbf{W}_v^\top$ , where  $\mathbf{W}_u \in \mathbb{R}^{d_{\text{out}} \times k}$  and  $\mathbf{W}_v \in \mathbb{R}^{d_{\text{in}} \times k}$  are low-rank factors. The factors can be obtained in several ways, most commonly via truncated SVD or SVD variants that account for activation statistics (Yuan et al., 2023) and layer sensitivity (Wang et al., 2025b). These methods are often paired with lightweight post-processing and/or extensive fine-tuning to recover accuracy (Wang et al., 2025a;b). Such approaches are typically evaluated by measuring perplexity and downstream task performance at a fixed compression budget, aiming to minimize the gap to the original full-rank model (Wang et al., 2025b).

This perspective also clarifies why the optimizer matters for compressibility: training influences the singular-value profile and effective rank of learned weights (Le and Jegelka, 2022; Timor et al., 2023), which directly affects how well low-rank factorization-based compression performs. In the next section, we use this lens to study Muon’s learned weight structure and to motivate rank-controlled updates that better align training with downstream low-rank compression.

## 3. OUR METHOD

In this section, we present NuMuon. We begin by probing how Muon shapes the rank structure of transformer weight matrices during pretraining. Although Muon applies full-rank, orthogonalized update directions, we surprisingly find that the resulting weight matrices nonetheless exhibit pronounced low-rank structure throughout training. This observation suggests that low-rank structure can emerge naturally under Muon’s training dynamics. As such, Muon-trained models are readily compressible with SVD-based LLM compression methods. However, as we see in our experiments, the performance of these models deteriorate rapidly as the compression rate increases. To address this limitation, we propose to *explicitly control the rank of Muon’s update directions* by augmenting its spectral-norm LMO with an additional nuclear-norm budget on the *LMO step*. We present theoretical guarantees for NuMuon’s convergence and examine the validity of our assumptions. Finally, we describe practical considerations for using NuMuon.

### 3.1 MOTIVATION

As discussed in Section 2, many LLM compression pipelines exploit structure in weight matrices, and low-rank factorization is a particularly common mechanism for reducing memory footprint while preserving

model quality (Wang et al., 2025b; Yuan et al., 2023). A natural question, then, is how the rank structure of transformer weights evolves during training with Muon, and whether Muon produces weights that are amenable to low-rank compression.

To study this, we track the *stable rank* of transformer weight matrices during pretraining. Stable rank is a robust proxy for effective dimensionality that is less sensitive to small singular values than the exact rank, and is defined as  $\text{sr}(\mathbf{W}) = \|\mathbf{W}\|_F^2 / \|\mathbf{W}\|_2^2$ . To compare across layers and matrix shapes, we normalize by the maximum attainable rank (i.e.,  $\min(d_{\text{out}}, d_{\text{in}})$ ), yielding a *normalized stable rank* between  $1 / \min(d_{\text{in}}, d_{\text{out}})$  and 1.

We measure this quantity throughout training for all the weight matrices of a Qwen-3-0.6B decoder-only model with 28 layers (Yang et al., 2025) trained for 16.8B tokens, equivalent to  $1.4\times$  the Chinchilla compute-optimal token budget (Kaplan et al., 2020). Figure 1 summarizes the mean normalized stable rank across layers over training for the feedforward projection weights, with shaded regions denoting layer-to-layer variability.

As seen, *Muon-trained weights remain strongly low-rank throughout training* despite Muon using full-rank orthogonalized update directions. In other words, the learned weight matrices occupy a relatively low-dimensional subspace as training progresses, and this is reflected by the consistently low normalized stable rank. Compared to AdamW, Muon tends to maintain a somewhat higher (but still clearly sub-maximal) stable rank in these feed-forward projections. This indicates that Muon does not eliminate low-rank structure; instead, low-rank structure appears to be an emergent property of training that persists under both optimizers (Feng et al., 2022; Huh et al., 2023). Also note that the early training dynamics differ: under Muon, stable rank stays elevated during the first few hundred iterations before gradually settling, whereas under AdamW it drops sharply at the start of training and then stabilizes.

We observe similar qualitative behavior across other weight matrices (e.g., attention and output projections); additional results are provided in Figure 13. To validate that this phenomenon extends beyond our experiments, Figure 17 shows the normalized stable rank for Moonlight-16B-A3B (Liu et al., 2025) and Kimi-K2 (Bai et al., 2025), two large-scale models that pioneered the use of Muon for pretraining. Across both models, the stable rank of various weight matrices remains a small fraction of the maximum attainable rank, corroborating our finding that Muon-trained models exhibit pronounced low-rank structure. Taken together, these measurements indicate that Muon-trained weights admit accurate low-rank approximations, and thus should be amenable to standard low-rank compression pipelines. We confirm this empirically using SoTA LLM compression methods in Figure 2 and Table 2. However, this compressibility is brittle: while moderate compression rates preserve performance, pushing to higher compression ratios leads to a rapid degradation relative to the base model. This motivates shaping the training dynamics so that the learned weights remain reliably compressible at high rates, while retaining Muon’s favorable optimization behavior.

### 3.2 NUMUON: NUCLEAR-NORM-CONSTRAINED MUON

Motivated by our observations in the previous section, we propose to *control the rank of Muon’s update directions* so that training dynamics better align with downstream low-rank compression. Concretely, we adopt a conditional gradient view in which Muon’s orthogonalization step can be interpreted as implementing an LMO over a spectral-norm–bounded set of update directions. We then modify this update selection by adding a nuclear-norm budget. The nuclear norm is defined as the sum of singular values  $\|\mathbf{A}\|_* = \sum_i \sigma_i(\mathbf{A})$  and is a standard convex proxy to encourage low-rank structure (Recht et al., 2010).

In particular, let  $\mathbf{M}_t$  denote Muon’s matrix-valued momentum. NuMuon replaces Muon’s spectral-norm LMO with  $\mathcal{W}_*$  over the set of admissible update directions:

$$\mathcal{W}_* := \{ \Delta \mathbf{W} \mid \|\Delta \mathbf{W}\|_2 \leq \rho, \|\Delta \mathbf{W}\|_* \leq \tau \}. \quad (9)$$

Note that  $\mathcal{W}_*$  is the intersection of a spectral-norm ball and a nuclear-norm ball, hence closed and convex. We

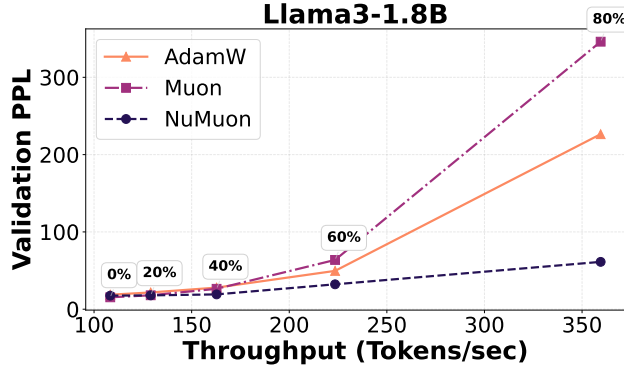


Figure 2: Validation perplexity on WikiText2 against generation inference throughput for Llama3-1.8B models compressed via SVD-LLM (Wang et al., 2025b). As seen, for a given perplexity, NuMuon-trained models provide the fastest inference for moderate to extreme compression rates (40-80%). Our results for other models can be found in Figure 20.

define

$$\Delta \mathbf{W}_t \in \text{lmo}_{\mathcal{W}_*}(\mathbf{M}_t) := \arg \min_{\Delta \mathbf{W} \in \mathcal{W}_*} \langle \mathbf{M}_t, \Delta \mathbf{W} \rangle, \quad (10)$$

and use  $\Delta \mathbf{W}_t$  in either an additive or a convex-combination (CG/FW-style) update following Pethick et al. (2025). Note that by this definition, NuMuon constrains the *update direction* and places no constraint on the weight matrices. However, under CG/FW-style updates, the iterates are convex combinations of low-rank directions from  $\mathcal{W}_*$  and are thus progressively attracted toward the feasible set (see Lemma A.6), which provides intuition for why low-rank structure reliably emerges in practice (see Figure 13).

To apply NuMuon in practice, we need to reliably and efficiently solve the LMO outlined in Equation (10). A key appeal of Muon is that its spectral norm LMO has a closed-form solution. In the following propositions, we show this property is also present in NuMuon; we first demonstrate that NuMuon’s LMO reduces to a linear program (LP) and then find a closed-form solution for this LP.

**Proposition 3.1.** Let  $\mathbf{M} \in \mathbb{R}^{d_{\text{out}} \times d_{\text{in}}}$  with thin SVD  $\mathbf{M} = \mathbf{U} \text{diag}(\boldsymbol{\sigma}) \mathbf{V}^\top$ , where  $\sigma_1 \geq \sigma_2 \geq \dots \geq 0$  and  $q = \min(d_{\text{out}}, d_{\text{in}})$ . Consider the LMO

$$\min_{\Delta \mathbf{W}} \langle \mathbf{M}, \Delta \mathbf{W} \rangle \text{ s.t. } \|\Delta \mathbf{W}\|_2 \leq \rho, \|\Delta \mathbf{W}\|_* \leq \tau.$$

There exists an optimal solution of the form  $\Delta \mathbf{W}^* = -\mathbf{U} \text{diag}(\mathbf{s}^*) \mathbf{V}^\top$  for some  $\mathbf{s}^* \in \mathbb{R}_{\geq 0}^q$  where

$$\max_{\mathbf{s} \in \mathbb{R}^q} \sum_{i=1}^q \sigma_i s_i \text{ s.t. } \mathbf{s} \in \mathcal{P}(\rho, \tau) \quad (11)$$

is a linear program over the polytope  $\mathcal{P}(\rho, \tau) := \left\{ \mathbf{s} : 0 \leq s_i \leq \rho \ \forall i, \sum_{i=1}^q s_i \leq \tau \right\}$ .

*Proof sketch.* By unitary invariance, we may rotate  $\Delta \mathbf{W}$  into the singular basis of  $\mathbf{M}$  without changing  $\|\Delta \mathbf{W}\|_2$  or  $\|\Delta \mathbf{W}\|_*$ . Von Neumann’s trace inequality (von Neumann, 1937) implies the optimum aligns singular vectors with  $\mathbf{M}$ , so the objective depends only on the singular values of  $\Delta \mathbf{W}$ , reducing to the LP in Equation (11). A full proof is provided in Appendix A.  $\square$

**Proposition 3.2.** *Under the assumptions of Proposition 3.1, the optimal solution of the LP in Equation (11) is  $s^*$  where, for  $i = 1, \dots, q$  and  $k = \lfloor \tau/\rho \rfloor$ , we have*

$$s_i^* = \begin{cases} \rho, & 1 \leq i \leq \min(k, q), \\ r, & i = k + 1 \text{ and } k + 1 \leq q, \\ 0, & k + 2 \leq i \leq q, \end{cases} \quad (12)$$

and  $r = \tau - k\rho$  is the residual singular value. Consequently,  $\text{rank}(\Delta \mathbf{W}^*) \leq \min(q, \lceil \tau/\rho \rceil)$ .

*Proof sketch.* The feasible set in Equation (11) is a capped simplex polytope. Since  $\sigma_1 \geq \sigma_2 \geq \dots$ , a standard greedy argument shows the LP is maximized by allocating as much budget as possible to the largest coefficients first, i.e.,  $s_1 = \rho, s_2 = \rho, \dots$  until the budget  $\tau$  is exhausted yielding Equation (12). Proof can be found in Appendix A.  $\square$

Now let us consider the common case where the nuclear-norm budget is an integer multiple of the spectral cap, i.e.,  $\tau = k\rho$  so that  $r = 0$  in Proposition 3.2.<sup>2</sup> Combining Propositions 3.1 and 3.2, the NuMuon update is:

$$\Delta \mathbf{W}^* = -\rho \sum_{i=1}^k \mathbf{u}_i \mathbf{v}_i^\top := -\rho \mathbf{U}_k \mathbf{V}_k^\top, \quad (13)$$

where  $\{\mathbf{u}_i, \mathbf{v}_i\}_{i=1}^k$  are the singular vector pairs of  $\mathbf{M}$  associated with the top- $k$  singular values  $\sigma_1 \geq \dots \geq \sigma_k$ . Thus, NuMuon takes a top- $k$  singular-direction update in which all nonzero update singular values are equal to  $\rho$ . Setting  $k = q$  (or equivalently, choosing  $\tau \geq q\rho$ ) recovers Muon’s full-rank spectral-norm LMO update  $\Delta \mathbf{W}^* = -\rho \mathbf{U} \mathbf{V}^\top$  (up to the same stepsize and rescaling conventions as in Equations (8) and (35)). In this sense, NuMuon interpolates between a rank-1 nuclear-norm update and Muon’s full-rank orthogonalized update by adjusting  $k$ .

### 3.3 CONVERGENCE ANALYSIS

In this section, we analyze the convergence behavior of NuMuon and show that the bounds provided by Shen et al. (2025) for Muon can be extended to NuMuon. To this end, we provide a generalization of Theorem 4.3 from Shen et al. (2025) to NuMuon. This generalization establishes a stationarity bound for non-convex functions under the nuclear norm. Apart from the standard smoothness and bounded gradient variance assumptions, our generalization requires that the gradient’s tail energy outside its top- $k$  components remain bounded. More formally, we make the following assumptions:

**Assumption 3.3** (Smoothness). The function  $f : \mathbb{R}^{d_{\text{out}} \times d_{\text{in}}} \rightarrow \mathbb{R}$  is  $L$ -smooth with respect to the Frobenius norm:

$$\|\nabla f(\mathbf{W}) - \nabla f(\mathbf{W}')\|_{\text{F}} \leq L \|\mathbf{W} - \mathbf{W}'\|_{\text{F}}.$$

**Assumption 3.4** (Unbiased gradients with bounded variance). The stochastic gradient estimator  $\mathbf{G}_t = \frac{1}{b} \sum_{i=1}^b \nabla f(\mathbf{W}_t; \xi_{t,i})$  satisfies

$$\mathbb{E}[\mathbf{G}_t] = \nabla f(\mathbf{W}_t), \quad \mathbb{E}\|\mathbf{G}_t - \nabla f(\mathbf{W}_t)\|_{\text{F}}^2 \leq \frac{\nu^2}{b},$$

where  $b$  is the batch-size.

<sup>2</sup>When  $\tau$  is not an exact multiple of  $\rho$ , the solution additionally allocates a fractional amount  $r \in (0, \rho)$  to the  $(k+1)$ -st singular direction; see Proposition 3.2. In practice, however, we ignore this term and set the rank  $k$  directly.

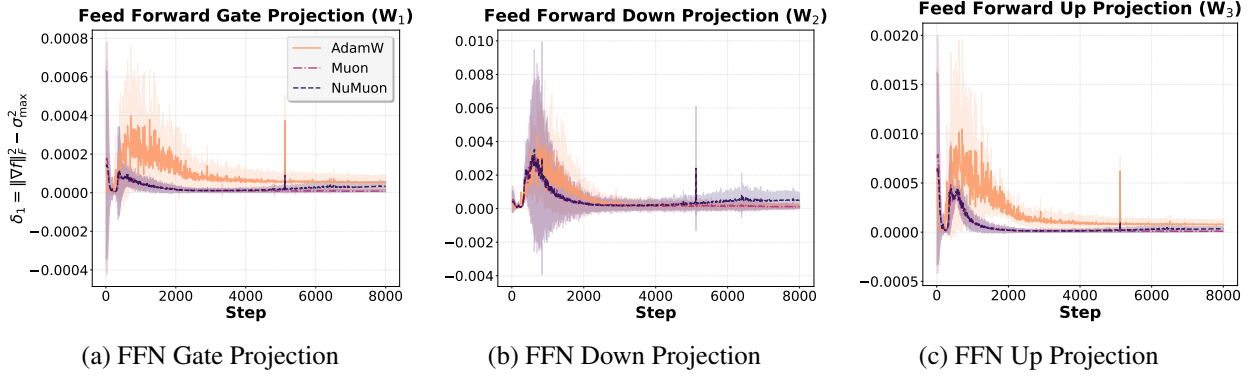


Figure 3:  $\delta_1^{(F)}$  as a proxy for the tail bound in Assumption 3.5 for the feedforward projection matrices. As we see, this quantity is bounded and close to zero for NuMuon, supporting this assumption. For other parameters, please see Figure 10.

**Assumption 3.5** (Bounded Tail Energy). Along the iterates  $\{\mathbf{W}_t\}_{t=0}^{T-1}$ , the gradient tail energy is bounded. In other words, there exists  $\delta_k \geq 0$  such that  $\mathbb{E}[\|\nabla f(\mathbf{W}_t) - (\nabla f(\mathbf{W}_t))_k\|_*] \leq \delta_k$  for all  $t$ , where  $(\nabla f(\mathbf{W}_t))_k$  denotes the best rank- $k$  approximation.

To support the validity of this assumption in practice, we measure  $\delta_k^{(F)}(\mathbf{W}) := \|\nabla f(\mathbf{W}_t) - (\nabla f(\mathbf{W}_t))_k\|_F^2$  for our Qwen3-0.6B model. In particular, we show in the Appendix that  $\delta_k^{(F)}$  is monotonically decreasing in  $k$ , and hence, it suffices to observe the behavior of  $\delta_1^{(F)}$  (Lemma A.5). As seen in Figure 3, Muon and NuMuon’s residual energy is typically small and close to zero, mirroring the validity of Assumption 3.5 in practice. Such low-rank gradient structure is consistent with prior empirical findings that neural network gradients concentrate in a small subspace during training (Vogels et al., 2019; Zhao et al., 2024). Under this assumption, we present our convergence guarantee.

**Theorem 3.6** (Nonconvex Nuclear-Norm Stationarity). Let  $f : \mathbb{R}^{d_{\text{out}} \times d_{\text{in}}} \rightarrow \mathbb{R}$  be  $L$ -smooth with respect to the Frobenius norm. Assume the stochastic gradient estimator  $\mathbf{G}_t$  is unbiased with variance bounded by  $\nu^2/b$ , where  $b$  is the batch-size. Additionally, assume that the gradient spectra has bound energy outside its top- $k$  components (Assumption 3.5). Let  $\{\mathbf{W}_t, \mathbf{M}_t\}$  be generated by NuMuon with momentum parameter  $\beta$  and constant stepsize  $\gamma$ . Then

$$\frac{1}{T} \sum_{t=0}^{T-1} \mathbb{E} \|\nabla f(\mathbf{W}_t)\|_* \leq \frac{\mathbb{E}[f(\mathbf{W}_0) - f(\mathbf{W}_T)]}{T\gamma} + \frac{Lk\gamma}{2} + \frac{2\nu\sqrt{k(1-\beta)}}{\sqrt{(1+\beta)b}} + \frac{2\beta\nu\sqrt{k}}{(1-\beta)T\sqrt{b}} + \frac{2k\gamma\beta L}{1-\beta} + \delta_k. \quad (14)$$

*Proof Sketch.* We prove this in two steps. First, following the momentum analysis framework of Shen et al. (2025) with the key modification that the update direction  $\mathbf{U}_{t,k} \mathbf{V}_{t,k}^\top$ <sup>3</sup> has Frobenius norm  $\sqrt{k}$  (rather than  $\sqrt{\min(d_{\text{out}}, d_{\text{in}})}$ ), we propagate a factor of  $k$  through the smoothness and momentum-lag terms. This establishes convergence under the Ky Fan  $k$ -norm (Definition A.1). Then, we employ Assumption 3.5 to complete the proof. The full proof is provided in Appendix A.2.  $\square$

As we can see, setting  $k = \min(d_{\text{out}}, d_{\text{in}})$  recovers Shen et al. (2025)’s bound for Muon. Furthermore, we see a trade-off in the upper bound on nuclear-norm stationarity. Choosing a smaller  $k$  reduces almost all the terms in Equation (14) but increases the tail residual  $\delta_k$ , and vice versa. An interesting theoretical direction for

<sup>3</sup>We assume that  $\rho$  has been absorbed in the stepsize  $\gamma$ .

future work is to characterize conditions under which an optimal  $k < \min(d_{\text{out}}, d_{\text{in}})$  exists that yields tighter convergence guarantees than full-rank Muon. Please see our discussion on the validity of the tail control condition in Appendix A.2.1.

### 3.4 PRACTICAL CONSIDERATIONS

To make NuMuon practical at scale, we address two implementation questions: (i) how to compute the top- $k$  singular vectors efficiently, and (ii) how to choose a per-layer rank.

**Top- $k$  SVD via Randomized Block Krylov Method.** NuMuon requires the leading  $k$  singular vector pairs of the matrix driving the LMO for each parameter block. Computing a full SVD is prohibitively expensive at scale, so we approximate the top- $k$  subspace using a randomized block Krylov method proposed by Musco and Musco (2015) (see Algorithm 3). Intuitively, the method alternates multiplying by  $\mathbf{A}$  and  $\mathbf{A}^\top$  to build a low-dimensional Krylov subspace that concentrates on  $\mathbf{A}$ 's dominant singular directions; we then compute a small SVD in this subspace to recover approximate top- $k$  singular vectors. In practice, a small number of Krylov iterations and a modest block size (we chose 2 and 8, respectively) are sufficient.

**Rank Scheduler.** As we observed in Figure 1, the stable rank of transformer weight matrices evolve over training, and enforcing very low-rank updates too early can be suboptimal. This is due to the fact that the early phase of training with Muon is typically characterized by high stable rank across layers. Motivated by this, we expose NuMuon rank as a fractional schedule rather than a fixed integer. At training step  $t$ , the scheduler outputs  $r(t) \in (0, 1]$  and we set  $k_t = \lceil r(t) \min(d_{\text{in}}, d_{\text{out}}) \rceil$  for all the layers. This makes rank control shape-agnostic across parameter blocks and enables a gradual transition from higher-rank to lower-rank updates. We consider the fixed, piece-wise, and cosine rank schedulers in our experiments (see Appendix B for a formal definition). As we show in Section 5, scheduled rank control can improve the final model performance compared to using a fixed  $k$  throughout training.

## 4. RELATED WORK

Our work sits at the intersection of three lines of research: the emergence of low-rank structure in neural networks, compression methods that exploit this structure, and optimizers that shape weight geometry during training. Below, we provide related work to our approach.

**Low-Rank Structure in Neural Networks.** Learned neural network weights often exhibit significant redundancy and lie near low-dimensional subspaces. Denil et al. (2013) provided early evidence that a large fraction of parameters can be predicted from a small subset, and subsequent work exploited low-rank decompositions to compress convolutional networks (Denton et al., 2014; Jaderberg et al., 2014). Beyond explicit compression, gradient-based training itself tends to produce low-rank weights: theoretical results for linear models show an implicit nuclear-norm bias under gradient descent (Gunasekar et al., 2017), and this rank-minimizing tendency has been observed and formalized in deeper settings (Le and Jegelka, 2022; Ramasinghe et al., 2025; Timor et al., 2023). These findings suggest that low-rank structure is an emergent property of optimization, motivating our investigation of how different optimizers shape this structure.

**LLM Compression via Low-Rank Factorization.** LLM compression encompasses quantization (Dettmers et al., 2022; Huang et al., 2024; Yuan et al., 2024), pruning (Frankle and Carbin, 2019; Kim et al., 2024), and distillation (Hinton et al., 2015; Xu et al., 2024), among other techniques (Zhou et al., 2024). Low-rank factorization has emerged as a particularly effective approach, approximating each weight matrix  $\mathbf{W}$  with a product of smaller factors (Hsu et al., 2022; Xue et al., 2013; Yu et al., 2017). Recent methods improve upon naive SVD truncation by incorporating activation statistics (ASVD; Yuan et al., 2023), layer sensitivity

Table 1: Training/validation perplexity (PPL) and efficiency metrics across optimizers for training Llama3-1.8B models. Validation PPL is computed on WikiText2 dataset.

OPTIM.	TRAIN PPL ↓	VAL. PPL ↓	TIME/STEP (S) ↓	GPU MEM. (GB) ↓
ADAMW	10.83	18.75	25.12	37.62
MUON	10.01	15.39	25.39	32.51
NUMUON	10.59	17.56	30.03	33.88

and lightweight adaptation (SVD-LLM; Wang et al., 2025b), or data-driven optimization objectives (Dobi-SVD; Wang et al., 2025a). The progression from basic truncation to these refined approaches underscores that compression quality depends critically on the singular-value distribution learned during training which is a key motivation for our work.

**Optimizers and Weight Geometry.** Optimizer choice influences the geometry of learned weights and thus downstream compressibility. While elementwise adaptive methods such as Adam and AdamW rescale coordinates independently (Kingma and Ba, 2015; Loshchilov and Hutter, 2019), recent work interprets modern optimizers through constrained-optimization and projection-free lenses (Pethick et al., 2025; Riabinin et al., 2025). Muon (Bernstein and Newhouse, 2025; Jordan et al., 2024) orthogonalizes momentum updates via the polar factor, which can be viewed as an LMO over a spectral-norm ball. Unlike standard training dynamics that exhibit implicit low-rank bias (Huh et al., 2023; Zhao, 2022), Muon applies full-rank, spectrally-uniform updates. Nevertheless, we show that Muon-trained models still develop pronounced low-rank structure (Section 3.1). Building on this observation, NuMuon augments the spectral-norm LMO with a nuclear-norm constraint, a standard convex surrogate for rank (Recht et al., 2010), to explicitly control update rank and improve alignment with downstream low-rank compression. Close to our work, Zimmer et al. (2022) uses an LMO view to encourage compression robustness by constraining the weights directly, and is tested primarily on CNN models; Lu et al. (2022) similarly studies Stochastic Frank–Wolfe for pruning-friendly training in the unstructured setting for CNNs. In contrast, NuMuon constrains the *update direction* via a nuclear-norm budget, preserving Muon’s spectral dynamics while explicitly controlling update rank for low-rank LLM compression.

## 5. EXPERIMENTAL RESULTS

**Settings.** We evaluate on three model architectures: Qwen3-0.6B (Yang et al., 2025), Olmo2-1.4B (OLMo et al., 2025), and Llama3-1.8B (Dubey et al., 2024), training each past Chinchilla optimality (Kaplan et al., 2020) using AdamW, Muon, and NuMuon. Following Semenov et al. (2025); Wen et al. (2025), we use a cosine learning rate scheduler for AdamW and a WSD (Hu et al., 2024) scheduler for Muon and NuMuon. We train on FineWeb-EDU (Penedo et al., 2024), which has been shown to yield rapid downstream performance gains (Mayilvahanan et al., 2025). For NuMuon, we use a cosine rank scheduler that anneals the relative rank from  $k = 1$  to  $k = 0.25$  across all weight matrices. Training details are provided in Appendix C.

For downstream compression, we evaluate three SoTA LLM compression methods: ASVD (Yuan et al., 2023), SVD-LLM (Wang et al., 2025b), and Dobi-SVD (Wang et al., 2025a). For SVD-LLM, we test both the whitening variant and whitening plus LoRA. All methods use their official default settings, with compression rates ranging from 20% to 80%. Note that even though these methods rely on a low-rank structure, they still do their post-processing which could involve extensive fine-tuning on a target dataset. Following standard practice, we report validation perplexity on WikiText2 and accuracy on standard benchmarks: ARC-Easy and ARC-Challenge (Bhakhavatsalam et al., 2021), HellaSwag (Zellers et al., 2019), LAMBADA (Paperno et al., 2016), OpenbookQA (Mihaylov et al., 2018), PIQA (Bisk et al., 2020), and Winogrande (Sakaguchi et al., 2020). For more information on each method, please visit their official implementation.

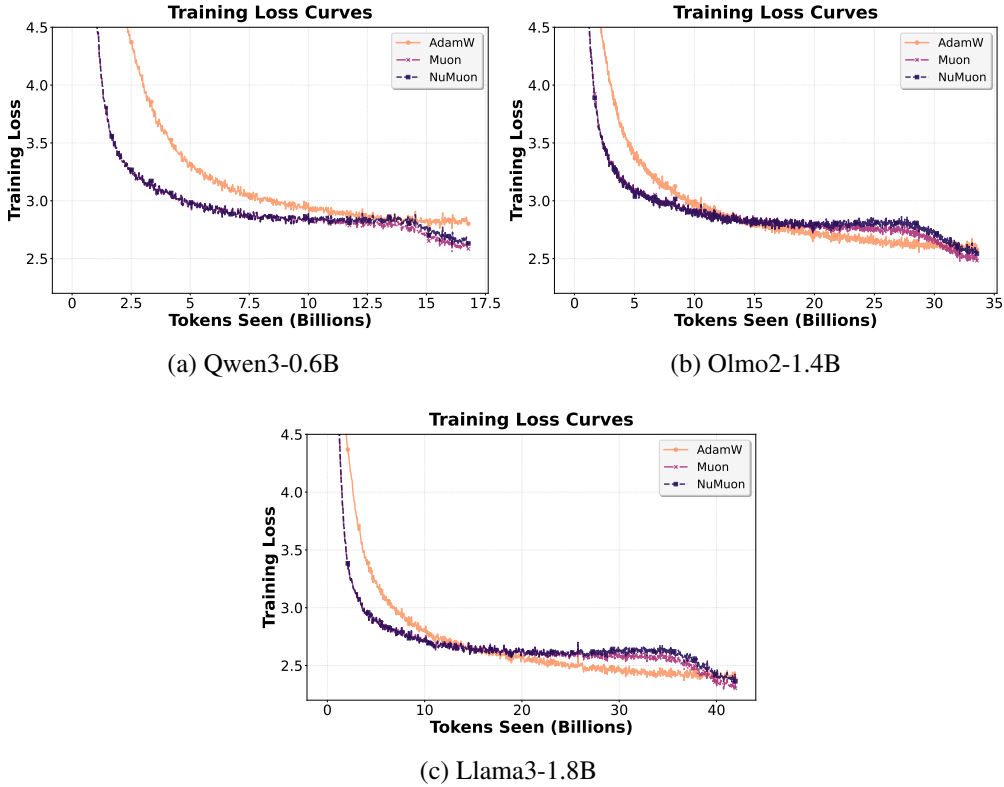


Figure 4: Training loss convergence for language models of size 0.6B-1.8B parameter count. For each model family, we use AdamW, Muon, and NuMuon to train the model. For more details, please see Appendix C.1.

**Convergence.** First, we benchmark the training behavior of NuMuon compared to AdamW and Muon. As shown in Figure 4, NuMuon closely tracks Muon throughout most of training. Toward the end of training and once the ranks across weight matrices stabilize under the cosine rank scheduler, NuMuon exhibits a small deviation from Muon; nevertheless, its final training/validation perplexity remains comparable to Muon and improves over AdamW as reported in Table 1. In terms of training resources, each NuMuon step is slightly slower due to the overhead of managing large SVD approximations (via Block Krylov SVD) when ranks are changing dynamically. As we show in the ablations, using alternative rank schedulers reduces this overhead and narrows the runtime gap. Importantly, GPU memory consumption remains close to Muon and lower than AdamW.

We also report the normalized stable rank of the final trained models across all layers and weight matrices for Qwen3-0.6B, Olmo2-1.4B, and Llama3-1.8B in Figures 14 to 16. These figures show that NuMuon induces a strictly lower stable rank across all weight matrices and layers in our transformer blocks. In the next set of experiments, we demonstrate that this reduced stable rank translates into substantially improved robustness to SVD-based compression, allowing NuMuon-trained models to retain performance at higher compression rates than Muon.

**Compressibility.** Next, we study SVD-based LLM compression and show how NuMuon’s explicit rank-control updates translate into weights that are more amenable to low-rank approximation than those obtained with Muon. We apply ASVD, SVD-LLM, and Dobi-SVD to all pretrained models across compression rates from 20% to 80%, and evaluate the compressed checkpoints on WikiText2 and standard downstream benchmarks. We show a scatter plot of NuMuon’s relative performance improvement against Muon in Figure 5 as well as raw results for Llama3-1.8B at 40% compression in Table 2, and defer the complete set of results

Table 2: WikiText2 validation perplexity and downstream task performance across compressed Llama3-1.8B models using various LLM compression methods 40% compression. Full results for all models and methods can be found in Appendix C.2.

METHOD	OPTIMIZER	VAL. PPL ↓	DOWNSTREAM TASKS							AVG ↑
			ARC-C	ARC-E	H'SWAG	LAM'DA	OPENBkQA	PIQA	W'GRANDE	
ASVD	ADAMW	718.71	22.61	37.25	30.15	6.00	26.40	54.52	49.88	32.40
	MUON	1443.55	24.66	31.90	29.28	7.08	27.80	55.93	50.12	32.40
	NUMUON	20.56 (-98.6%)	<b>32.76</b>	<b>62.88</b>	<b>50.27</b>	<b>42.64</b>	<b>37.20</b>	<b>71.38</b>	<b>56.20</b>	<b>50.48 (+55.8%)</b>
SVD-LLM	ADAMW	27.94	28.41	49.37	40.69	29.52	30.00	65.13	51.22	42.05
	MUON	26.39	26.19	43.14	36.74	28.86	28.20	59.52	53.83	39.50
	NUMUON	19.18 (-27.3%)	<b>31.66</b>	<b>60.77</b>	<b>49.49</b>	<b>38.87</b>	<b>34.80</b>	<b>69.37</b>	<b>57.38</b>	<b>48.91 (+23.8%)</b>
Dobi-SVD	ADAMW	28.83	30.72	49.79	43.15	31.30	33.20	64.69	53.67	43.79
	MUON	20.44	28.16	52.27	46.22	<b>40.29</b>	29.80	63.98	56.35	45.30
	NUMUON	18.63 (-8.9%)	<b>31.31</b>	<b>60.23</b>	<b>51.98</b>	39.59	<b>34.80</b>	<b>70.18</b>	<b>57.54</b>	<b>49.38 (+9.0%)</b>

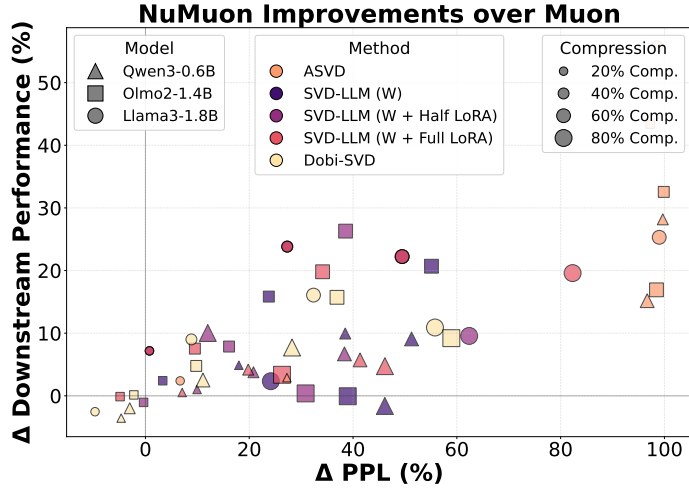


Figure 5: NuMuon’s relative performance against Muon under SoTA LLM compression methods. The scatter plot displays the performance improvement on downstream tasks as well as validation perplexity improvements for all compression methods at all rates. The positive quadrant shows performance improvement.

for all models and compression levels (20-80%) to Appendix C.2 and Tables 6 to 17.

Across all three compression methods at 40-80% compression, NuMuon consistently achieves the strongest downstream average (**4.2-55.8%**) and substantially lower validation perplexity (**up to 99.8%**) than AdamW and Muon trained baselines. This suggests that NuMuon produces weight matrices whose information is concentrated in fewer effective directions, enabling SVD-based methods to discard parameters with less degradation. Moreover, as the compression method improves (e.g., moving from ASVD to SVD-LLM to Dobi-SVD), NuMuon retains a larger fraction of the underlying model’s performance, indicating that better approximators can more effectively exploit the low-rank structure induced by NuMuon.

To show how NuMuon’s superiority could lead to better deployment, we report the validation perplexity against the generation throughput (at batch-size 256) in Figure 2. We see that for a fixed perplexity, NuMuon unlocks a higher compression rate and in turn, faster generation throughput compared to both AdamW and Muon. This mirrors the importance of NuMuon in deployability of trained LLMs.

#### Update-Weight Subspace Alignment.

To gain further insight into the training dynamics of NuMuon and its superior compressibility, we measure how well the optimizer updates aligns with the dominant spectral subspace of the weights. Concretely, for a given weight matrix  $W$  and its update  $\Delta W$ , we form the top- $k$  left-singular subspaces (here  $k = 64$ ) and compute their Grassmann distance. Let  $U_W, U_{\Delta W} \in \mathbb{R}^{d \times k}$  be orthonormal bases spanning these two  $k$ -dimensional subspaces. The principal angles  $\{\theta_i\}_{i=1}^k$  are defined via

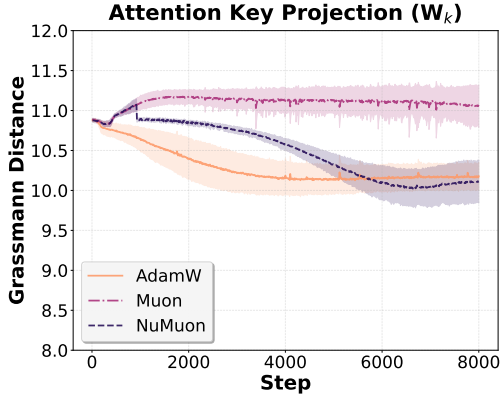


Figure 6:  $d_G(\mathbf{U}_W, \mathbf{U}_{\Delta W})$ . For other weight matrices, please see Figure 18.

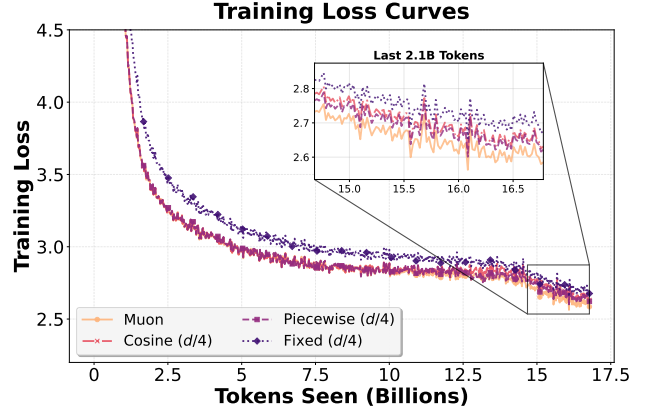


Figure 7: Convergence behavior of rank schedulers used for training Qwen3-0.6B.

Table 3: 80% Dobi-SVD LLM compression performance for Qwen3-0.6B models compared to non-compressed base models under various rank schedulers for NuMuon.

SCHEDULER	TIME/STEP (S)	VAL. PPL ↓		TASK ACC ↑	
		0%	80%	0%	80%
PIECEWISE (0.25)	9.94	20.01	33.39	45.87	37.92
COSINE (0.25)	10.49	20.20	36.10	45.69	35.89
FIXED (0.05)	8.96	29.13	31.93	39.64	38.74
FIXED (0.25)	9.81	21.85	44.69	44.30	34.36
FIXED (0.50)	11.33	20.27	46.66	45.17	34.38
FIXED (0.80)	11.49	19.31	43.70	46.33	34.42
MUON	8.86	19.20	50.31	46.81	33.32

the singular values of  $\mathbf{U}_W^\top \mathbf{U}_{\Delta W}$  as  $\cos(\theta_i) = \sigma_i(\mathbf{U}_W^\top \mathbf{U}_{\Delta W})$ , and the Grassmann distance

$$d_G(\mathbf{U}_W, \mathbf{U}_{\Delta W}) = \left( \sum_{i=1}^k \theta_i^2 \right)^{1/2}.$$

Figure 6 plots this quantity over training for the attention key projection matrix  $\mathbf{W}_k$  in Qwen3-0.6B. We observe that NuMuon maintains a consistently smaller Grassmann distance than Muon, indicating that its updates remain more aligned with the top spectral subspace of  $\mathbf{W}$ . In contrast, Muon applies orthonormalized updates that are less coupled to the evolving spectral geometry of the weights, resulting in larger subspace misalignment that remains almost fixed throughout training. This sustained alignment provides a mechanistic explanation for why NuMuon tends to induce lower stable rank and improved robustness under SVD-based compression.

**Ablation Study.** Next, we study the impact of our design choices on the training and compressibility of LLMs via NuMuon. The most important aspects of our optimizer are (i) the choice of the final update rank and (ii) the rank scheduler, both of which can affect training dynamics and downstream compression. To this end, we ablate the rank scheduler type (cosine (C) vs. piecewise (P) vs. fixed (F)) and the rank budget. For the rank budget, we use the fixed scheduler and vary the rank fraction in  $\{0.05, 0.25, 0.50, 0.80\}$  of the maximum rank, i.e., a fraction of  $\max(d_{\text{in}}, d_{\text{out}})$ . We use Qwen3-0.6B for these experiments to enable a broader ablation sweep, and we use Dobi-SVD for LLM compression as it is the strongest method in our comparisons. The rank fractions are summarized in Figure 11 in the Appendix.

Our training curves for various ranks are shown in Figure 8. As can be seen, decreasing the rank and making

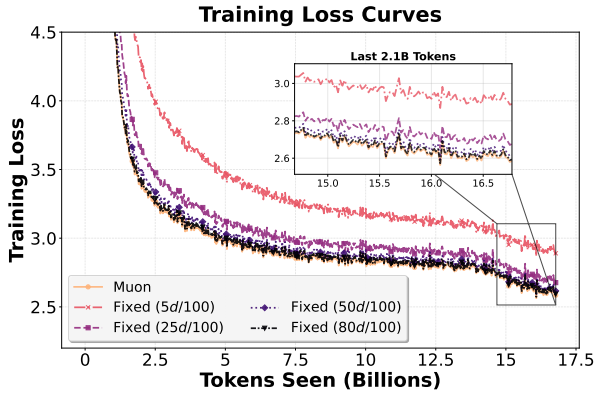


Figure 8: Convergence behavior of various rank budgets ( $\tau$  in our nuclear norm formulation) used for training Qwen3-0.6B models with NuMuon. Muon training loss is also shown for comparison. As seen, NuMuon gets closer to Muon behavior as we increase the rank budget. However, this rank increase provides diminishing returns while hurting the final model’s compressibility.

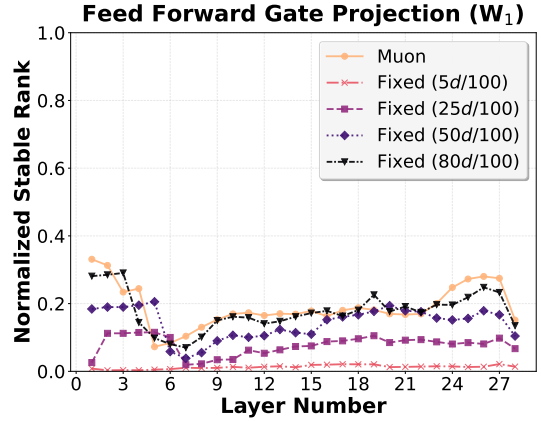


Figure 9: Normalized stable rank for feedforward gate projection weight matrix of Qwen3-0.6B models trained with NuMuon under different ranks/nuclear norm budget. Each subplot shows the stable rank (normalized by the maximum rank) of the converged model across all layers.

it too restrictive harms convergence and results in worse final loss. However, beyond 0.25 the gains from increasing the rank exhibit diminishing returns. Meanwhile, in Figure 9 we observe that a more restrictive nuclear-norm/rank budget induces a lower stable rank across weight matrices and layers, whereas increasing the budget increases the stable rank. This directly translates to compressibility: as shown in Table 3, lower stable-rank (more restrictive) settings typically incur less degradation after 80% compression. However, as discussed above, there is a balance to strike so that the base model remains strong and we do not over-restrict training.

Finally, we compare different scheduler types in Figures 7 and 22. As we see, fixed-rank schedules tend to degrade the base performance more than cosine and piecewise schedules, where NuMuon benefits from a higher-rank period early in training and then transitions to a lower-rank regime (see Section 3.4 for more discussion on this point). In terms of efficiency, low, fixed-rank schedules can be faster per step since they avoid the high-rank Block Krylov SVD regime that arises early with cosine and piecewise schedules (see the Time/Step in Table 3). Nevertheless, training speed is comparable with Muon in all cases. For more details on our ablations, see Appendix C.3.

## 6. CONCLUSION AND FUTURE WORK

In this paper, we studied Muon’s weight space structure and revealed that its spectral geometry, while designed for optimization efficiency, also shapes the compressibility of the learned weights. The emergence of low-rank structure under full-rank updates suggests that effective dimensionality in trained models arises not just from explicit constraints but from the interplay between optimizer dynamics and loss landscape geometry. NuMuon leverages this insight by directly controlling update rank through a nuclear-norm budget, which we showed reduces to a simple top- $k$  truncation of the momentum’s singular directions. The result is an optimizer that retains Muon’s training efficiency while producing weights better suited for aggressive post-hoc compression, achieving substantial gains in the high-compression regime where standard Muon-trained models underperform.

In addition to being beneficial for LLM compression workflows, the factored form of NuMuon’s updates is a natural fit for distributed training over bandwidth-constrained settings (Douillard et al., 2023) and gossip-based protocols (Blot et al., 2016), complementing recent efforts such as DION (Ahn et al., 2025) that approximate Muon for distributed training. We leave exploration of this interesting direction to future work.

## REFERENCES

- Kwangjun Ahn, Byron Xu, Natalie Abreu, Ying Fan, Gagik Magakyan, Pratyusha Sharma, Zheng Zhan, and John Langford. Dion: Distributed orthonormalized updates. *CoRR*, abs/2504.05295, 2025.
- Yifan Bai, Yiping Bao, Guanduo Chen, Jiahao Chen, Ningxin Chen, Ruijue Chen, Yanru Chen, Yuankun Chen, Yutian Chen, Zhuofu Chen, Jialei Cui, Hao Ding, Mengnan Dong, Angang Du, Chenzhuang Du, Dikang Du, Yulun Du, Yu Fan, Yichen Feng, Kelin Fu, Bofei Gao, Hongcheng Gao, Peizhong Gao, Tong Gao, Xinran Gu, Longyu Guan, Haiqing Guo, Jianhang Guo, Hao Hu, Xiaoru Hao, Tianhong He, Weiran He, Wenyang He, Chao Hong, Yangyang Hu, Zhenxing Hu, Weixiao Huang, Zhiqi Huang, Zihao Huang, Tao Jiang, Zhejun Jiang, Xinyi Jin, Yongsheng Kang, Guokun Lai, Cheng Li, Fang Li, Haoyang Li, Ming Li, Wentao Li, Yanhao Li, Yiwei Li, Zhaowei Li, Zheming Li, Hongzhan Lin, Xiaohan Lin, Zongyu Lin, Chengyin Liu, Chenyu Liu, Hongzhang Liu, Jingyuan Liu, Junqi Liu, Liang Liu, Shaowei Liu, T. Y. Liu, Tianwei Liu, Weizhou Liu, Yangyang Liu, Yibo Liu, Yiping Liu, Yue Liu, Zhengying Liu, Enzhe Lu, Lijun Lu, Shengling Ma, Xinyu Ma, Yingwei Ma, Shaoguang Mao, Jie Mei, Xin Men, Yibo Miao, Siyuan Pan, Yebo Peng, Ruoyu Qin, Bowen Qu, Zeyu Shang, Lidong Shi, Shengyuan Shi, Feifan Song, Jianlin Su, Zhengyuan Su, Xinjie Sun, Flood Sung, Heyi Tang, Jiawen Tao, Qifeng Teng, Chensi Wang, Dinglu Wang, Feng Wang, and Haiming Wang. Kimi K2: open agentic intelligence. *CoRR*, abs/2507.20534, 2025.
- Ramakrishna Bairi, Atharv Sonwane, Aditya Kanade, Vageesh D. C., Arun Iyer, Suresh Parthasarathy, Sriram K. Rajamani, Balasubramanyan Ashok, and Shashank Shet. Codeplan: Repository-level coding using llms and planning. *Proceedings of the ACM Software Engineering*, 1(FSE):675–698, 2024.
- Jeremy Bernstein and Laker Newhouse. Modular duality in deep learning. In *Proceedings of the International Conference on Machine Learning (ICML)*, 2025.
- Sumithra Bhakthavatsalam, Daniel Khashabi, Tushar Khot, Bhavana Dalvi Mishra, Kyle Richardson, Ashish Sabharwal, Carissa Schoenick, Oyvind Tafjord, and Peter Clark. Think you have solved direct-answer question answering? try arc-da, the direct-answer AI2 reasoning challenge. *CoRR*, abs/2102.03315, 2021.
- Yonatan Bisk, Rowan Zellers, Ronan Le Bras, Jianfeng Gao, and Yejin Choi. PIQA: reasoning about physical commonsense in natural language. In *Proceedings of the AAAI Conference on Artificial Intelligence*, pages 7432–7439, 2020.
- Michael Blot, David Picard, Matthieu Cord, and Nicolas Thome. Gossip training for deep learning. *CoRR*, abs/1611.09726, 2016.
- DeepSeek-AI, Daya Guo, Dejian Yang, Haowei Zhang, Junxiao Song, Ruoyu Zhang, Runxin Xu, Qihao Zhu, Shirong Ma, Peiyi Wang, Xiao Bi, Xiaokang Zhang, Xingkai Yu, Yu Wu, Z. F. Wu, Zhibin Gou, Zhihong Shao, Zhuoshu Li, Ziyi Gao, Aixin Liu, Bing Xue, Bingxuan Wang, Bochao Wu, Bei Feng, Chengda Lu, Chenggang Zhao, Chengqi Deng, Chenyu Zhang, Chong Ruan, Damai Dai, Deli Chen, Dongjie Ji, Erhang Li, Fangyun Lin, Fucong Dai, Fuli Luo, Guangbo Hao, Guanting Chen, Guowei Li, H. Zhang, Han Bao, Hanwei Xu, Haocheng Wang, Honghui Ding, Huajian Xin, Huazuo Gao, Hui Qu, Hui Li, Jianzhong Guo, Jiashi Li, Jiawei Wang, Jingchang Chen, Jingyang Yuan, Junjie Qiu, Junlong Li, J. L. Cai, Jiaqi Ni, Jian Liang, Jin Chen, Kai Dong, Kai Hu, Kaige Gao, Kang Guan, Kexin Huang, Kuai Yu, Lean Wang, Lecong Zhang, Liang Zhao, Litong Wang, Liyue Zhang, Lei Xu, Leyi Xia, Mingchuan Zhang, Minghua Zhang, Minghui Tang, Meng Li, Miaojun Wang, Mingming Li, Ning Tian, Panpan Huang, Peng Zhang, Qiancheng

- Wang, Qinyu Chen, Qiushi Du, Ruiqi Ge, Ruisong Zhang, Ruizhe Pan, Runji Wang, R. J. Chen, R. L. Jin, Ruyi Chen, Shanghao Lu, Shangyan Zhou, Shanhuang Chen, Shengfeng Ye, Shiyu Wang, Shuiping Yu, Shunfeng Zhou, Shuting Pan, and S. S. Li. DeepSeek-R1: Incentivizing reasoning capability in llms via reinforcement learning. *CoRR*, abs/2501.12948, 2025.
- Misha Denil, Babak Shakibi, Laurent Dinh, Marc’Aurelio Ranzato, and Nando de Freitas. Predicting parameters in deep learning. In *Proceedings of the Annual Conference on Neural Information Processing Systems (NeurIPS)*, pages 2148–2156, 2013.
- Emily L. Denton, Wojciech Zaremba, Joan Bruna, Yann LeCun, and Rob Fergus. Exploiting linear structure within convolutional networks for efficient evaluation. In *Proceedings of the Annual Conference on Neural Information Processing Systems (NeurIPS)*, pages 1269–1277, 2014.
- Tim Dettmers, Mike Lewis, Younes Belkada, and Luke Zettlemoyer. Llm.int8(): 8-bit matrix multiplication for transformers at scale. *CoRR*, abs/2208.07339, 2022.
- Arthur Douillard, Qixuan Feng, Andrei A Rusu, Rachita Chhaparia, Yani Donchev, Adhiguna Kuncoro, Marc’Aurelio Ranzato, Arthur Szlam, and Jiajun Shen. DiLoCo: Distributed low-communication training of language models. *CoRR*, abs/2311.08105, 2023.
- Abhimanyu Dubey, Abhinav Jauhri, Abhinav Pandey, Abhishek Kadian, Ahmad Al-Dahle, Aiesha Letman, Akhil Mathur, Alan Schelten, Amy Yang, Angela Fan, Anirudh Goyal, Anthony Hartshorn, Aobo Yang, Archi Mitra, Archie Sravankumar, Artem Korenev, Arthur Hinsvark, Arun Rao, Aston Zhang, Aurélien Rodriguez, Austen Gregerson, Ava Spataru, Baptiste Rozière, Bethany Biron, Binh Tang, Bobbie Chern, Charlotte Caucheteux, Chaya Nayak, Chloe Bi, Chris Marra, Chris McConnell, Christian Keller, Christophe Touret, Chunyang Wu, Corinne Wong, Cristian Canton Ferrer, Cyrus Nikolaidis, Damien Allonsius, Daniel Song, Danielle Pintz, Danny Livshits, David Esiobu, Dhruv Choudhary, Dhruv Mahajan, Diego Garcia-Olano, Diego Perino, Dieuwke Hupkes, Egor Lakomkin, Ehab AlBadawy, Elina Lobanova, Emily Dinan, Eric Michael Smith, Filip Radenovic, Frank Zhang, Gabriel Synnaeve, Gabrielle Lee, Georgia Lewis Anderson, Graeme Nail, Grégoire Mialon, Guan Pang, Guillem Cucurell, Hailey Nguyen, Hannah Korevaar, Hu Xu, Hugo Touvron, Iliyan Zarov, Imanol Arrieta Ibarra, Isabel M. Kloumann, Ishan Misra, Ivan Evtimov, Jade Copet, Jaewon Lee, Jan Geffert, Jana Vranes, Jason Park, Jay Mahadeokar, Jeet Shah, Jelmer van der Linde, Jennifer Billock, Jenny Hong, Jenya Lee, Jeremy Fu, Jianfeng Chi, Jianyu Huang, Jiawen Liu, Jie Wang, Jiecao Yu, Joanna Bitton, Joe Spisak, Jongsoo Park, Joseph Rocca, Joshua Johnstun, Joshua Saxe, Junteng Jia, Kalyan Vasuden Alwala, Kartikeya Upasani, Kate Plawiak, Ke Li, Kenneth Heafield, Kevin Stone, and et al. The Llama 3 herd of models. *CoRR*, abs/2407.21783, 2024.
- Ruili Feng, Kecheng Zheng, Yukun Huang, Deli Zhao, Michael I. Jordan, and Zheng-Jun Zha. Rank diminishing in deep neural networks. In Sanmi Koyejo, S. Mohamed, A. Agarwal, Danielle Belgrave, K. Cho, and A. Oh, editors, *Proceedings of the Annual Conference on Neural Information Processing Systems (NeurIPS)*, 2022.
- Marguerite Frank, Philip Wolfe, et al. An algorithm for quadratic programming. *Naval research logistics quarterly*, 3(1-2):95–110, 1956.
- Jonathan Frankle and Michael Carbin. The lottery ticket hypothesis: Finding sparse, trainable neural networks. In *Proceedings of the International Conference on Learning Representations (ICLR)*, 2019.
- Elias Frantar and Dan Alistarh. SparseGPT: Massive language models can be accurately pruned in one-shot. In *Proceedings of the International Conference on Machine Learning (ICML)*, pages 10323–10337, 2023.
- Suriya Gunasekar, Blake E. Woodworth, Srinadh Bhojanapalli, Behnam Neyshabur, and Nati Srebro. Implicit regularization in matrix factorization. In *Proceedings of the Annual Conference on Neural Information Processing Systems (NeurIPS)*, pages 6151–6159, 2017.

- Geoffrey E. Hinton, Oriol Vinyals, and Jeffrey Dean. Distilling the knowledge in a neural network. *CoRR*, abs/1503.02531, 2015.
- Jordan Hoffmann, Sebastian Borgeaud, Arthur Mensch, Elena Buchatskaya, Trevor Cai, Eliza Rutherford, Diego de Las Casas, Lisa Anne Hendricks, Johannes Welbl, Aidan Clark, Tom Hennigan, Eric Noland, Katherine Millican, George van den Driessche, Bogdan Damoc, Aurelia Guy, Simon Osindero, Karen Simonyan, Erich Elsen, Oriol Vinyals, Jack W. Rae, and Laurent Sifre. An empirical analysis of compute-optimal large language model training. In *Proceedings of the Annual Conference on Neural Information Processing Systems (NeurIPS)*, 2022.
- Yen-Chang Hsu, Ting Hua, Sungen Chang, Qian Lou, Yilin Shen, and Hongxia Jin. Language model compression with weighted low-rank factorization. In *Proceedings of the International Conference on Learning Representations (ICLR)*, 2022.
- Shengding Hu, Yuge Tu, Xu Han, Chaoqun He, Ganqu Cui, Xiang Long, Zhi Zheng, Yewei Fang, Yuxiang Huang, Weilin Zhao, Xinrong Zhang, Zhen Leng Thai, Kai Zhang, Chongyi Wang, Yuan Yao, Chenyang Zhao, Jie Zhou, Jie Cai, Zhongwu Zhai, Ning Ding, Chao Jia, Guoyang Zeng, Dahai Li, Zhiyuan Liu, and Maosong Sun. MiniCPM: Unveiling the potential of small language models with scalable training strategies. *CoRR*, abs/2404.06395, 2024.
- Wei Huang, Yangdong Liu, Haotong Qin, Ying Li, Shiming Zhang, Xianglong Liu, Michele Magno, and Xiaojuan Qi. BiLLM: Pushing the limit of post-training quantization for llms. In *Proceedings of the International Conference on Machine Learning (ICML)*, 2024.
- Minyoung Huh, Hossein Mobahi, Richard Zhang, Brian Cheung, Pulkit Agrawal, and Phillip Isola. The low-rank simplicity bias in deep networks. *Transactions on Machine Learning Research (TMLR)*, 2023.
- Max Jaderberg, Andrea Vedaldi, and Andrew Zisserman. Speeding up convolutional neural networks with low rank expansions. In *British Machine Vision Conference (BMVC)*, 2014.
- Martin Jaggi. Revisiting Frank-Wolfe: Projection-free sparse convex optimization. In *Proceedings of the International Conference on Machine Learning (ICML)*, pages 427–435, 2013.
- Keller Jordan, Yuchen Jin, Vlado Boza, Jiacheng You, Franz Cesista, Laker Newhouse, and Jeremy Bernstein. Muon: An optimizer for hidden layers in neural networks, 2024. URL <https://kellerjordan.github.io/posts/muon/>.
- Jared Kaplan, Sam McCandlish, Tom Henighan, Tom B. Brown, Benjamin Chess, Rewon Child, Scott Gray, Alec Radford, Jeffrey Wu, and Dario Amodei. Scaling laws for neural language models. *CoRR*, abs/2001.08361, 2020.
- Sehoon Kim, Coleman Hooper, Amir Gholami, Zhen Dong, Xiuyu Li, Sheng Shen, Michael W. Mahoney, and Kurt Keutzer. SqueezeLLM: Dense-and-sparse quantization. In *Proceedings of the International Conference on Machine Learning (ICML)*, 2024.
- Diederik P. Kingma and Jimmy Ba. Adam: A method for stochastic optimization. In *Proceedings of the International Conference on Learning Representations (ICLR)*, 2015.
- Thien Le and Stefanie Jegelka. Training invariances and the low-rank phenomenon: beyond linear networks. In *Proceedings of the International Conference on Learning Representations (ICLR)*, 2022.
- Jingyuan Liu, Jianlin Su, Xingcheng Yao, Zhejun Jiang, Guokun Lai, Yulun Du, Yidao Qin, Weixin Xu, Enzhe Lu, Junjie Yan, Yanru Chen, Huabin Zheng, Yibo Liu, Shaowei Liu, Bohong Yin, Weiran He, Han Zhu, Yuzhi Wang, Jianzhou Wang, Mengnan Dong, Zheng Zhang, Yongsheng Kang, Hao Zhang, Xinran

- Xu, Yutao Zhang, Yuxin Wu, Xinyu Zhou, and Zhilin Yang. Muon is scalable for LLM training. *CoRR*, abs/2502.16982, 2025.
- Ilya Loshchilov and Frank Hutter. Decoupled weight decay regularization. In *Proceedings of the International Conference on Learning Representations (ICLR)*, 2019.
- Miao Lu, Xiaolong Luo, Tianlong Chen, Wuyang Chen, Dong Liu, and Zhangyang Wang. Learning pruning-friendly networks via frank-wolfe: One-shot, any-sparsity, and no retraining. In *Proceedings of the International Conference on Learning Representations (ICLR)*, 2022.
- Prasanna Mayilvahanan, Thaddäus Wiedemer, Sayak Mallick, Matthias Bethge, and Wieland Brendel. LLMs on the line: Data determines loss-to-loss scaling laws. In *Proceedings of the International Conference on Machine Learning (ICML)*, 2025.
- Todor Mihaylov, Peter Clark, Tushar Khot, and Ashish Sabharwal. Can a suit of armor conduct electricity? A new dataset for open book question answering. In *Proceedings of Findings of the Association for Computational Linguistics (EMNLP)*, pages 2381–2391, 2018.
- Cameron Musco and Christopher Musco. Randomized block krylov methods for stronger and faster approximate singular value decomposition. In *Proceedings of the Annual Conference on Neural Information Processing Systems (NeurIPS)*, pages 1396–1404, 2015.
- Team OLMo, Pete Walsh, Luca Soldaini, Dirk Groeneveld, Kyle Lo, Shane Arora, Akshita Bhagia, Yuling Gu, Shengyi Huang, Matt Jordan, Nathan Lambert, Dustin Schwenk, Oyvind Tafjord, Taira Anderson, David Atkinson, Faeze Brahman, Christopher Clark, Pradeep Dasigi, Nouha Dziri, Michal Guerquin, Hamish Ivison, Pang Wei Koh, Jiacheng Liu, Saumya Malik, William Merrill, Lester James V. Miranda, Jacob Morrison, Tyler Murray, Crystal Nam, Valentina Pyatkin, Aman Rangapur, Michael Schmitz, Sam Skjonsberg, David Wadden, Christopher Wilhelm, Michael Wilson, Luke Zettlemoyer, Ali Farhadi, Noah A. Smith, and Hannaneh Hajishirzi. 2 olmo 2 furious. *CoRR*, abs/2501.00656, 2025.
- OpenAI. GPT-4 technical report. *CoRR*, abs/2303.08774, 2023.
- Denis Paperno, Germán Kruszewski, Angeliki Lazaridou, Quan Ngoc Pham, Raffaella Bernardi, Sandro Pezzelle, Marco Baroni, Gemma Boleda, and Raquel Fernández. The LAMBADA dataset: Word prediction requiring a broad discourse context. In *Proceedings of the Conference of the Association for Computational Linguistics (ACL)*, 2016.
- Guilherme Penedo, Hynek Kydlíček, Loubna Ben allal, Anton Lozhkov, Margaret Mitchell, Colin Raffel, Leandro Von Werra, and Thomas Wolf. The fineweb datasets: Decanting the web for the finest text data at scale. In *Proceedings of the Annual Conference on Neural Information Processing Systems Datasets and Benchmarks Track (NeurIPS)*, 2024.
- Thomas Pethick, Wanyun Xie, Kimon Antonakopoulos, Zhenyu Zhu, Antonio Silveti-Falls, and Volkan Cevher. Training deep learning models with norm-constrained LMOs. In *Proceedings of the International Conference on Machine Learning (ICML)*, 2025.
- Alec Radford, Karthik Narasimhan, Tim Salimans, Ilya Sutskever, et al. Improving language understanding by generative pre-training. 2018.
- Sameera Ramasinghe, Thalaisyasingam Ajanthan, Gil Avraham, Yan Zuo, and Alexander Long. Subspace networks: Scaling decentralized training with communication-efficient model parallelism. In *Proceedings of the Annual Conference on Neural Information Processing Systems (NeurIPS)*, 2025.
- Benjamin Recht, Maryam Fazel, and Pablo A. Parrilo. Guaranteed minimum-rank solutions of linear matrix equations via nuclear norm minimization. *SIAM Review*, 52(3):471–501, 2010.

- Artem Riabinin, Egor Shulgin, Kaja Gruntkowska, and Peter Richtárik. Gluon: Making muon & scion great again! (bridging theory and practice of lmo-based optimizers for llms). *CoRR*, abs/2505.13416, 2025.
- Bernardino Romera-Paredes, Mohammadamin Barekatin, Alexander Novikov, Matej Balog, M. Pawan Kumar, Emilien Dupont, Francisco J. R. Ruiz, Jordan S. Ellenberg, Pengming Wang, Omar Fawzi, Pushmeet Kohli, and Alhussein Fawzi. Mathematical discoveries from program search with large language models. *Nature*, 625(7995):468–475, 2024.
- Keisuke Sakaguchi, Ronan Le Bras, Chandra Bhagavatula, and Yejin Choi. Winogrande: An adversarial winograd schema challenge at scale. In *Proceedings of the AAAI Conference on Artificial Intelligence*, pages 8732–8740, 2020.
- Rylan Schaeffer, Brando Miranda, and Sanmi Koyejo. Are emergent abilities of large language models a mirage? In Alice Oh, Tristan Naumann, Amir Globerson, Kate Saenko, Moritz Hardt, and Sergey Levine, editors, *Proceedings of the Annual Conference on Neural Information Processing Systems (NeurIPS)*, 2023.
- Andrei Semenov, Matteo Pagliardini, and Martin Jaggi. Benchmarking optimizers for large language model pretraining. *CoRR*, abs/2509.01440, 2025.
- Wei Shen, Ruichuan Huang, Minhui Huang, Cong Shen, and Jiawei Zhang. On the convergence analysis of muon. *CoRR*, abs/2505.23737, 2025.
- Nadav Timor, Gal Vardi, and Ohad Shamir. Implicit regularization towards rank minimization in relu networks. In *Proceedings of the International Conference on Algorithmic Learning Theory (ALT)*, pages 1429–1459, 2023.
- Thijs Vogels, Sai Praneeth Karimireddy, and Martin Jaggi. PowerSGD: Practical low-rank gradient compression for distributed optimization. In *Proceedings of the Annual Conference on Neural Information Processing Systems (NeurIPS)*, pages 14236–14245, 2019.
- John von Neumann. Some matrix-inequalities and metrization of matrix-space. *Tomsk. Univ. Rev.*, 1:286–300, 1937. Reprinted in: A. H. Taub (Ed.), *John von Neumann Collected Works*, Vol. IV, Pergamon Press, Oxford, 1962, pp. 205–218.
- Lei Wang, Chen Ma, Xueyang Feng, Zeyu Zhang, Hao Yang, Jingsen Zhang, Zhiyuan Chen, Jiakai Tang, Xu Chen, Yankai Lin, Wayne Xin Zhao, Zhewei Wei, and Jirong Wen. A survey on large language model based autonomous agents. *Frontiers of Computer Science*, 18(6), 2024.
- Qinsi Wang, Jinghan Ke, Masayoshi Tomizuka, Kurt Keutzer, and Chenfeng Xu. Dobi-SVD: Differentiable SVD for LLM compression and some new perspectives. In *Proceedings of the International Conference on Learning Representations (ICLR)*, 2025a.
- Xin Wang, Yu Zheng, Zhongwei Wan, and Mi Zhang. SVD-LLM: truncation-aware singular value decomposition for large language model compression. In *Proceedings of the International Conference on Learning Representations (ICLR)*, 2025b.
- Jason Wei, Yi Tay, Rishi Bommasani, Colin Raffel, Barret Zoph, Sebastian Borgeaud, Dani Yogatama, Maarten Bosma, Denny Zhou, Donald Metzler, Ed H. Chi, Tatsunori Hashimoto, Oriol Vinyals, Percy Liang, Jeff Dean, and William Fedus. Emergent abilities of large language models. *Transactions on Machine Learning Research (TMLR)*, 2022.
- Kaiyue Wen, David Hall, Tengyu Ma, and Percy Liang. Fantastic pretraining optimizers and where to find them. *CoRR*, abs/2509.02046, 2025.

- Xiaohan Xu, Ming Li, Chongyang Tao, Tao Shen, Reynold Cheng, Jinyang Li, Can Xu, Dacheng Tao, and Tianyi Zhou. A survey on knowledge distillation of large language models. *CoRR*, abs/2402.13116, 2024.
- Jian Xue, Jinyu Li, and Yifan Gong. Restructuring of deep neural network acoustic models with singular value decomposition. In *Proceedings of the Annual Conference of the International Speech Communication Association (INTERSPEECH)*, pages 2365–2369, 2013.
- An Yang, Baosong Yang, Beichen Zhang, Binyuan Hui, Bo Zheng, Bowen Yu, Chengyuan Li, Dayiheng Liu, Fei Huang, Haoran Wei, Huan Lin, Jian Yang, Jianhong Tu, Jianwei Zhang, Jianxin Yang, Jiayi Yang, Jingren Zhou, Junyang Lin, Kai Dang, Keming Lu, Keqin Bao, Kexin Yang, Le Yu, Mei Li, Mingfeng Xue, Pei Zhang, Qin Zhu, Rui Men, Runji Lin, Tianhao Li, Tingyu Xia, Xingzhang Ren, Xuancheng Ren, Yang Fan, Yang Su, Yichang Zhang, Yu Wan, Yuqiong Liu, Zeyu Cui, Zhenru Zhang, and Zihan Qiu. Qwen2.5 technical report. *CoRR*, abs/2412.15115, 2024.
- An Yang, Anfeng Li, Baosong Yang, Beichen Zhang, Binyuan Hui, Bo Zheng, Bowen Yu, Chang Gao, Chengen Huang, Chenxu Lv, Chujie Zheng, Dayiheng Liu, Fan Zhou, Fei Huang, Feng Hu, Hao Ge, Haoran Wei, Huan Lin, Jialong Tang, Jian Yang, Jianhong Tu, Jianwei Zhang, Jian Yang, Jiayi Yang, Jingren Zhou, Junyang Lin, Kai Dang, Keqin Bao, Kexin Yang, Le Yu, Lianghao Deng, Mei Li, Mingfeng Xue, Mingze Li, Pei Zhang, Peng Wang, Qin Zhu, Rui Men, Ruize Gao, Shixuan Liu, Shuang Luo, Tianhao Li, Tianyi Tang, Wenbiao Yin, Xingzhang Ren, Xinyu Wang, Xinyu Zhang, Xuancheng Ren, Yang Fan, Yang Su, Yichang Zhang, Yinger Zhang, Yu Wan, Yuqiong Liu, Zekun Wang, Zeyu Cui, Zhenru Zhang, Zhipeng Zhou, and Zihan Qiu. Qwen3 technical report. *CoRR*, abs/2505.09388, 2025.
- Xiyu Yu, Tongliang Liu, Xinchao Wang, and Dacheng Tao. On compressing deep models by low rank and sparse decomposition. In *Proceedings of the IEEE Conference on Computer Vision and Pattern Recognition (CVPR)*, pages 67–76, 2017.
- Zhihang Yuan, Yuzhang Shang, Yue Song, Qiang Wu, Yan Yan, and Guangyu Sun. ASVD: activation-aware singular value decomposition for compressing large language models. *CoRR*, abs/2312.05821, 2023.
- Zhihang Yuan, Yuzhang Shang, and Zhen Dong. PB-LLM: partially binarized large language models. In *Proceedings of the International Conference on Learning Representations (ICLR)*, 2024.
- Rowan Zellers, Ari Holtzman, Yonatan Bisk, Ali Farhadi, and Yejin Choi. Hellaswag: Can a machine really finish your sentence? In *Proceedings of the Conference of the Association for Computational Linguistics (ACL)*, pages 4791–4800, 2019.
- Dan Zhao. Combining explicit and implicit regularization for efficient learning in deep networks. In *Proceedings of the Annual Conference on Neural Information Processing Systems (NeurIPS)*, 2022.
- Jiawei Zhao, Zhenyu Zhang, Beidi Chen, Zhangyang Wang, Anima Anandkumar, and Yuandong Tian. GaLore: Memory-efficient LLM training by gradient low-rank projection. In *Proceedings of the International Conference on Machine Learning (ICML)*, 2024.
- Zixuan Zhou, Xuefei Ning, Ke Hong, Tianyu Fu, Jiaming Xu, Shiyao Li, Yuming Lou, Luning Wang, Zhihang Yuan, Xiuhong Li, Shengen Yan, Guohao Dai, Xiao-Ping Zhang, Yuhang Dong, and Yu Wang. A survey on efficient inference for large language models. *CoRR*, abs/2404.14294, 2024.
- Xunyu Zhu, Jian Li, Yong Liu, Can Ma, and Weiping Wang. A survey on model compression for large language models. *Transactions of the Association for Computational Linguistics*, 12:1556–1577, 2024.
- Max Zimmer, Christoph Spiegel, and Sebastian Pokutta. Compression-aware training of neural networks using Frank-Wolfe. *CoRR*, abs/2205.11921, 2022.

## A. PROOFS

### A.1 NUMUON LMO PROOFS

**Proposition 3.1.** Let  $M \in \mathbb{R}^{d_{\text{out}} \times d_{\text{in}}}$  with thin SVD  $M = U \text{diag}(\boldsymbol{\sigma}) V^\top$ , where  $\sigma_1 \geq \sigma_2 \geq \dots \geq 0$  and  $q = \min(d_{\text{out}}, d_{\text{in}})$ . Consider the LMO

$$\min_{\Delta W} \langle M, \Delta W \rangle \text{ s.t. } \|\Delta W\|_2 \leq \rho, \|\Delta W\|_* \leq \tau.$$

There exists an optimal solution of the form  $\Delta W^* = -U \text{diag}(\mathbf{s}^*) V^\top$  for some  $\mathbf{s}^* \in \mathbb{R}_{\geq 0}^q$  where

$$\max_{\mathbf{s} \in \mathbb{R}^q} \sum_{i=1}^q \sigma_i s_i \text{ s.t. } \mathbf{s} \in \mathcal{P}(\rho, \tau) \quad (11)$$

is a linear program over the polytope  $\mathcal{P}(\rho, \tau) := \left\{ \mathbf{s} : 0 \leq s_i \leq \rho \ \forall i, \sum_{i=1}^q s_i \leq \tau \right\}$ .

*Proof.* Let us assume that  $\bar{M} := -M$ . Then, the LMO is equivalent to:

$$- \max_{\Delta W \in \mathcal{W}} \langle \bar{M}, \Delta W \rangle, \quad (15)$$

over  $\mathcal{W} = \{\Delta W : \|\Delta W\|_2 \leq \rho, \|\Delta W\|_* \leq \tau\}$ . The optimal solution of this LMO can be written as:

$$\arg \max_{\Delta W \in \mathcal{W}} \langle \bar{M}, \Delta W \rangle = \arg \max_{\Delta W \in \mathcal{W}} \text{Tr}(\bar{M}^\top \Delta W). \quad (16)$$

Let  $\bar{M} = \bar{U} \text{diag}(\boldsymbol{\sigma}) V^\top$  where  $\sigma_1 \geq \sigma_2 \geq \dots \geq 0$  and  $\bar{U} = -U$ . Let us assume a new variable  $\mathbf{Y} := \bar{U}^\top \Delta W V$ , then we have:

$$\begin{aligned} \text{Tr}(\bar{M}^\top \Delta W) &= \text{Tr}(V \text{diag}(\boldsymbol{\sigma})^\top U^\top \Delta W) \\ &= \text{Tr}(\text{diag}(\boldsymbol{\sigma})^\top U^\top \Delta W V) \\ &= \text{Tr}(\text{diag}(\boldsymbol{\sigma})^\top \mathbf{Y}) \end{aligned} \quad (17)$$

and  $\|\Delta W\|_2 = \|U^\top \Delta W V\|_2$  by unitary invariance. Hence, our LMO is equivalent to:

$$\max_{\mathbf{Y}} \text{Tr}(\text{diag}(\boldsymbol{\sigma})^\top \mathbf{Y}) \text{ s.t. } \|\mathbf{Y}\|_* \leq \tau, \|\mathbf{Y}\|_2 \leq \rho. \quad (18)$$

From von Neumann's trace inequality (von Neumann, 1937), we have:

$$|\text{Tr}(\mathbf{A}^\top \mathbf{B})| \leq \sum_i \sigma_i(\mathbf{A}) \sigma_i(\mathbf{B}), \quad (19)$$

with equality if and only iff the eigenvectors are the same. Thus, the maximum of  $\text{Tr}(\text{diag}(\boldsymbol{\sigma})^\top \mathbf{Y})$  under these constraints is achieved when  $\mathbf{Y}$  shares singular vectors with  $\text{diag}(\boldsymbol{\sigma})$ , i.e., when  $\mathbf{Y} = \text{diag}(\mathbf{s})$  with  $\mathbf{s} \geq 0$ . Under this choice, the constraints become  $0 \leq s_i \leq \rho$  and  $\sum_i s_i \leq \tau$ , and the objective becomes  $\sum_i \sigma_i s_i$ , yielding (11). Negating the maximizer returns  $\Delta W^* = -U \text{diag}(\mathbf{s}^*) V^\top$ .  $\square$

**Proposition 3.2.** Under the assumptions of Proposition 3.1, the optimal solution of the LP in Equation (11)

is  $\mathbf{s}^*$  where, for  $i = 1, \dots, q$  and  $k = \lfloor \tau/\rho \rfloor$ , we have

$$\mathbf{s}_i^* = \begin{cases} \rho, & 1 \leq i \leq \min(k, q), \\ r, & i = k + 1 \text{ and } k + 1 \leq q, \\ 0, & k + 2 \leq i \leq q, \end{cases} \quad (12)$$

and  $r = \tau - k\rho$  is the residual singular value. Consequently,  $\text{rank}(\Delta \mathbf{W}^*) \leq \min(q, \lceil \tau/\rho \rceil)$ .

*Proof.* The feasible region of (11) is the capped simplex  $\{\mathbf{s} \in \mathbb{R}^q : 0 \leq s_i \leq \rho, \sum_i s_i \leq \tau\}$ . Since  $\sigma_1 \geq \sigma_2 \geq \dots \geq 0$ , the objective  $\sum_i \sigma_i s_i$  is maximized by allocating as much mass as possible to the smallest indices  $i$  (largest weights  $\sigma_i$ ), subject to the cap  $\rho$  and the total budget  $\tau$ . Formally, if there exist indices  $i < j$  with  $s_i < \rho$  and  $s_j > 0$ , then moving  $\varepsilon := \min\{\rho - s_i, s_j\}$  mass from  $j$  to  $i$  preserves feasibility and increases the objective by  $\varepsilon(\sigma_i - \sigma_j) \geq 0$ . Repeating this exchange argument yields the greedy fill-in solution in Equation (12), which sets  $s_1 = \rho$ , then  $s_2 = \rho$ , etc., until the budget  $\tau$  is exhausted. The rank bound follows from the number of strictly positive entries of  $\mathbf{s}^*$ .  $\square$

## A.2 CONVERGENCE ANALYSIS

In this section, we provide the convergence analysis of NuMuon. For this analysis, we assume that at iteration  $t$ , given momentum buffer  $\mathbf{M}_t \in \mathbb{R}^{d_{\text{out}} \times d_{\text{in}}}$ , let  $\mathbf{U}_{t,k} \in \mathbb{R}^{d_{\text{out}} \times k}$  and  $\mathbf{V}_{t,k} \in \mathbb{R}^{d_{\text{in}} \times k}$  contain the top- $k$  left and right singular vectors of  $\mathbf{M}_t$ , respectively. NuMuon performs the following update:

$$\begin{aligned} \mathbf{G}_t &\leftarrow \frac{1}{b} \sum_{i=1}^b \nabla f(\mathbf{W}_t, \boldsymbol{\xi}_{t,i}), \\ \mathbf{M}_t &\leftarrow \beta \mathbf{M}_{t-1} + (1 - \beta) \mathbf{G}_t, \\ \mathbf{U}_{t,k}, \mathbf{V}_{t,k} &\leftarrow \text{top-}k \text{ singular vectors of } \mathbf{M}_t, \\ \mathbf{W}_{t+1} &\leftarrow \mathbf{W}_t - \gamma \mathbf{U}_{t,k} \mathbf{V}_{t,k}^\top, \end{aligned} \quad (20)$$

for a fixed learning rate  $\gamma$ .<sup>4</sup> Following standard practice in Muon convergence analysis (Pethick et al., 2025; Riabinin et al., 2025; Shen et al., 2025), we assume the following:

**Assumption 3.3** (Smoothness). The function  $f : \mathbb{R}^{d_{\text{out}} \times d_{\text{in}}} \rightarrow \mathbb{R}$  is  $L$ -smooth with respect to the Frobenius norm:

$$\|\nabla f(\mathbf{W}) - \nabla f(\mathbf{W}')\|_{\text{F}} \leq L \|\mathbf{W} - \mathbf{W}'\|_{\text{F}}.$$

**Assumption 3.4** (Unbiased gradients with bounded variance). The stochastic gradient estimator  $\mathbf{G}_t = \frac{1}{b} \sum_{i=1}^b \nabla f(\mathbf{W}_t; \boldsymbol{\xi}_{t,i})$  satisfies

$$\mathbb{E}[\mathbf{G}_t] = \nabla f(\mathbf{W}_t), \quad \mathbb{E}\|\mathbf{G}_t - \nabla f(\mathbf{W}_t)\|_{\text{F}}^2 \leq \frac{\nu^2}{b},$$

where  $b$  is the batch-size.

Additionally, we also assume that the gradient's energy is concentrated around its top- $k$  singular directions.

**Assumption 3.5** (Bounded Tail Energy). Along the iterates  $\{\mathbf{W}_t\}_{t=0}^{T-1}$ , the gradient tail energy is bounded. In other words, there exists  $\delta_k \geq 0$  such that  $\mathbb{E}[\|\nabla f(\mathbf{W}_t) - (\nabla f(\mathbf{W}_t))_k\|_*] \leq \delta_k$  for all  $t$ , where  $(\nabla f(\mathbf{W}_t))_k$  denotes the best rank- $k$  approximation.

<sup>4</sup>Note that we omit  $\rho$  from Equation (13) and assume it is absorbed into  $\gamma$ .

Next, we will review some definitions and identities that would be used in our proofs.

**Definition A.1.** For a matrix  $\mathbf{A} \in \mathbb{R}^{d_{\text{out}} \times d_{\text{in}}}$  with singular values  $\sigma_1(\mathbf{A}) \geq \dots \geq \sigma_q(\mathbf{A})$ ,  $q = \min(d_{\text{out}}, d_{\text{in}})$ , the Ky Fan  $k$ -norm is defined as:

$$\|\mathbf{A}\|_{(k)} := \sum_{i=1}^k \sigma_i(\mathbf{A}).$$

**Lemma A.2** (Ky Fan norm bounded by Frobenius norm). For any matrix  $\mathbf{A}$  and any positive integer  $k$ ,

$$\|\mathbf{A}\|_{(k)} \leq \sqrt{k} \|\mathbf{A}\|_{\text{F}}. \quad (21)$$

*Proof.* Let  $\sigma_1 \geq \sigma_2 \geq \dots \geq \sigma_q \geq 0$  denote the singular values of  $\mathbf{A}$ . By Definition A.1, the Ky Fan  $k$ -norm is  $\|\mathbf{A}\|_{(k)} = \sum_{i=1}^k \sigma_i$ . Applying the Cauchy–Schwarz inequality yields

$$\|\mathbf{A}\|_{(k)} = \sum_{i=1}^k 1 \cdot \sigma_i \leq \sqrt{\sum_{i=1}^k 1^2} \cdot \sqrt{\sum_{i=1}^k \sigma_i^2} = \sqrt{k} \cdot \sqrt{\sum_{i=1}^k \sigma_i^2}.$$

Since  $\sum_{i=1}^k \sigma_i^2 \leq \sum_{i=1}^q \sigma_i^2 = \|\mathbf{A}\|_{\text{F}}^2$ , the result follows.  $\square$

**Lemma A.3** (Top- $k$  SVD identities). Let  $\mathbf{M} \in \mathbb{R}^{d_{\text{out}} \times d_{\text{in}}}$  have singular value decomposition  $\mathbf{M} = \mathbf{U}\mathbf{S}\mathbf{V}^\top$  with singular values  $\sigma_1 \geq \sigma_2 \geq \dots \geq \sigma_q \geq 0$ , where  $q = \min(d_{\text{out}}, d_{\text{in}})$ . Let  $\mathbf{U}_k \in \mathbb{R}^{d_{\text{out}} \times k}$  and  $\mathbf{V}_k \in \mathbb{R}^{d_{\text{in}} \times k}$  denote the matrices containing the top- $k$  left and right singular vectors, respectively. Then:

- (i)  $\langle \mathbf{M}, \mathbf{U}_k \mathbf{V}_k^\top \rangle = \sum_{i=1}^k \sigma_i(\mathbf{M}) = \|\mathbf{M}\|_{(k)}$ .
- (ii)  $\|\mathbf{U}_k \mathbf{V}_k^\top\|_{\text{F}}^2 = k$ .

*Proof.* (i) Using the cyclic property of trace and the SVD  $\mathbf{M} = \mathbf{U}\mathbf{S}\mathbf{V}^\top$ :

$$\begin{aligned} \langle \mathbf{M}, \mathbf{U}_k \mathbf{V}_k^\top \rangle &= \text{tr}(\mathbf{M}^\top \mathbf{U}_k \mathbf{V}_k^\top) \\ &= \text{tr}(\mathbf{V}_k \mathbf{S} \mathbf{U}^\top \mathbf{U}_k \mathbf{V}_k^\top). \end{aligned}$$

Since  $\mathbf{U}$  has orthonormal columns and  $\mathbf{U}_k$  consists of its first  $k$  columns, we have  $\mathbf{U}^\top \mathbf{U}_k = \begin{bmatrix} \mathbf{I}_k \\ \mathbf{0} \end{bmatrix}$ . Thus  $\mathbf{S} \mathbf{U}^\top \mathbf{U}_k = \begin{bmatrix} \mathbf{S}_k \\ \mathbf{0} \end{bmatrix}$ , where  $\mathbf{S}_k = \text{diag}(\sigma_1, \dots, \sigma_k)$ . Similarly,  $\mathbf{V}_k$  consists of the first  $k$  columns of  $\mathbf{V}$ , so:

$$\begin{aligned} \text{tr}(\mathbf{V}_k \mathbf{S} \mathbf{U}^\top \mathbf{U}_k \mathbf{V}_k^\top) &= \text{tr} \left( \mathbf{V}_k \begin{bmatrix} \mathbf{S}_k \\ \mathbf{0} \end{bmatrix} \mathbf{V}_k^\top \right) \\ &= \text{tr}(\mathbf{V}_k \mathbf{S}_k \mathbf{V}_k^\top) \\ &= \text{tr}(\mathbf{S}_k \mathbf{V}_k^\top \mathbf{V}_k) \\ &= \text{tr}(\mathbf{S}_k) = \sum_{i=1}^k \sigma_i. \end{aligned}$$

(ii) Since  $\mathbf{U}_k$  and  $\mathbf{V}_k$  have orthonormal columns:

$$\begin{aligned}\|\mathbf{U}_k \mathbf{V}_k^\top\|_{\text{F}}^2 &= \text{tr}(\mathbf{V}_k \mathbf{U}_k^\top \mathbf{U}_k \mathbf{V}_k^\top) \\ &= \text{tr}(\mathbf{V}_k \mathbf{I}_k \mathbf{V}_k^\top) \\ &= \text{tr}(\mathbf{V}_k^\top \mathbf{V}_k) \\ &= \text{tr}(\mathbf{I}_k) = k.\end{aligned}$$

Equivalently,  $\mathbf{U}_k \mathbf{V}_k^\top$  has exactly  $k$  singular values equal to 1 and the rest equal to 0, so  $\|\mathbf{U}_k \mathbf{V}_k^\top\|_{\text{F}}^2 = \sum_{i=1}^k 1^2 = k$ .  $\square$

For completeness, we also provide the following Lemma from Shen et al. (2025).

**Lemma A.4** (Momentum Error Bound (Lemma A.3 (Shen et al., 2025))). *Under Assumption 3.4, let*

$$\mathbf{C}_t = \beta \mathbf{C}_{t-1} + (1 - \beta) \nabla f(\mathbf{W}_t)$$

and  $\mathbf{M}_t = \beta \mathbf{M}_{t-1} + (1 - \beta) \mathbf{G}_t$  with  $\mathbf{C}_0 = \nabla f(\mathbf{W}_0)$  and  $\mathbf{M}_0 = \mathbf{G}_0$ . Then

$$\mathbb{E}[\|\mathbf{C}_t - \mathbf{M}_t\|_{\text{F}}] \leq \sqrt{\frac{1 - \beta}{1 + \beta}} \frac{\nu}{\sqrt{b}} + \beta^t \frac{\nu}{\sqrt{b}}.$$

Now, we are ready to prove our main result.

**Theorem 3.6** (Nonconvex Nuclear-Norm Stationarity). *Let  $f : \mathbb{R}^{d_{\text{out}} \times d_{\text{in}}} \rightarrow \mathbb{R}$  be  $L$ -smooth with respect to the Frobenius norm. Assume the stochastic gradient estimator  $\mathbf{G}_t$  is unbiased with variance bounded by  $\nu^2/b$ , where  $b$  is the batch-size. Additionally, assume that the gradient spectra has bound energy outside its top- $k$  components (Assumption 3.5). Let  $\{\mathbf{W}_t, \mathbf{M}_t\}$  be generated by NuMuon with momentum parameter  $\beta$  and constant stepsize  $\gamma$ . Then*

$$\frac{1}{T} \sum_{t=0}^{T-1} \mathbb{E} \|\nabla f(\mathbf{W}_t)\|_* \leq \frac{\mathbb{E}[f(\mathbf{W}_0) - f(\mathbf{W}_T)]}{T\gamma} + \frac{Lk\gamma}{2} + \frac{2\nu\sqrt{k(1-\beta)}}{\sqrt{(1+\beta)b}} + \frac{2\beta\nu\sqrt{k}}{(1-\beta)T\sqrt{b}} + \frac{2k\gamma\beta L}{1-\beta} + \delta_k. \quad (14)$$

*Proof.* Our proof follows the proof of Theorem 4.3 in Shen et al. (2025) with modifying the fully orthogonalized update with the top- $k$  NuMuon updates. In particular, by  $L$ -smoothness of  $f$  we have

$$\begin{aligned}\mathbb{E}[f(\mathbf{W}_t) - f(\mathbf{W}_{t+1})] &\geq \mathbb{E}\left[\gamma \langle \nabla f(\mathbf{W}_t), \mathbf{U}_{t,k} \mathbf{V}_{t,k}^\top \rangle - \frac{L}{2} \gamma^2 \|\mathbf{U}_{t,k} \mathbf{V}_{t,k}^\top\|_{\text{F}}^2\right] \\ &= \mathbb{E}\left[\gamma \langle \mathbf{M}_t, \mathbf{U}_{t,k} \mathbf{V}_{t,k}^\top \rangle - \frac{L}{2} \gamma^2 \|\mathbf{U}_{t,k} \mathbf{V}_{t,k}^\top\|_{\text{F}}^2 + \gamma \langle \nabla f(\mathbf{W}_t) - \mathbf{M}_t, \mathbf{U}_{t,k} \mathbf{V}_{t,k}^\top \rangle\right] \\ &\geq \mathbb{E}\left[\gamma \langle \mathbf{M}_t, \mathbf{U}_{t,k} \mathbf{V}_{t,k}^\top \rangle - \frac{L}{2} \gamma^2 \|\mathbf{U}_{t,k} \mathbf{V}_{t,k}^\top\|_{\text{F}}^2 - \gamma \|\nabla f(\mathbf{W}_t) - \mathbf{M}_t\|_{\text{F}} \|\mathbf{U}_{t,k} \mathbf{V}_{t,k}^\top\|_{\text{F}}\right].\end{aligned}$$

Using Lemma A.3, the above becomes

$$\begin{aligned}\mathbb{E}[f(\mathbf{W}_t) - f(\mathbf{W}_{t+1})] &\geq \mathbb{E}\left[\gamma \|\mathbf{M}_t\|_{(k)} - \frac{L}{2} \gamma^2 k - \gamma \sqrt{k} \|\nabla f(\mathbf{W}_t) - \mathbf{M}_t\|_{\text{F}}\right].\end{aligned}$$

By the reverse triangle inequality for  $\|\cdot\|_{(k)}$  and Equation (21),

$$\|\mathbf{M}_t\|_{(k)} \geq \|\nabla f(\mathbf{W}_t)\|_{(k)} - \sqrt{k}\|\mathbf{M}_t - \nabla f(\mathbf{W}_t)\|_{\mathbb{F}}.$$

Substituting yields

$$\begin{aligned} & \mathbb{E}[f(\mathbf{W}_t) - f(\mathbf{W}_{t+1})] \\ & \geq \mathbb{E}\left[\gamma\|\nabla f(\mathbf{W}_t)\|_{(k)} - \frac{L}{2}\gamma^2k - 2\gamma\sqrt{k}\|\nabla f(\mathbf{W}_t) - \mathbf{M}_t\|_{\mathbb{F}}\right]. \end{aligned} \quad (22)$$

**Bounding**  $\mathbb{E}\left[\|\nabla f(\mathbf{W}_t) - \mathbf{M}_t\|_{\mathbb{F}}\right]$ . Define  $\mathbf{C}_0 = \nabla f(\mathbf{W}_0)$  and for  $t > 0$  let

$$\mathbf{C}_t = \beta\mathbf{C}_{t-1} + (1 - \beta)\nabla f(\mathbf{W}_t).$$

Then, we can write

$$\mathbb{E}\left[\|\nabla f(\mathbf{W}_t) - \mathbf{M}_t\|_{\mathbb{F}}\right] \leq \mathbb{E}\left[\|\mathbf{C}_t - \mathbf{M}_t\|_{\mathbb{F}}\right] + \mathbb{E}\left[\|\nabla f(\mathbf{W}_t) - \mathbf{C}_t\|_{\mathbb{F}}\right].$$

By Lemma A.4 from Shen et al. (2025), for the first term we have

$$\mathbb{E}\left[\|\mathbf{C}_t - \mathbf{M}_t\|_{\mathbb{F}}\right] \leq \sqrt{\frac{1 - \beta}{1 + \beta}} \frac{\nu}{\sqrt{b}} + \beta^t \frac{\nu}{\sqrt{b}}. \quad (23)$$

For the second term at  $t > 0$ , we can write

$$\begin{aligned} & \mathbb{E}\left[\|\nabla f(\mathbf{W}_t) - \mathbf{C}_t\|_{\mathbb{F}}\right] \\ & = \mathbb{E}\left[\|\nabla f(\mathbf{W}_t) - (\beta\mathbf{C}_{t-1} + (1 - \beta)\nabla f(\mathbf{W}_t))\|_{\mathbb{F}}\right] \\ & = \mathbb{E}\left[\beta\|\nabla f(\mathbf{W}_t) - \mathbf{C}_{t-1}\|_{\mathbb{F}}\right] \\ & \stackrel{(a)}{\leq} \mathbb{E}\left[\beta\|\nabla f(\mathbf{W}_{t-1}) - \mathbf{C}_{t-1}\|_{\mathbb{F}} + \beta\|\nabla f(\mathbf{W}_{t-1}) - \nabla f(\mathbf{W}_t)\|_{\mathbb{F}}\right] \\ & \stackrel{(b)}{\leq} \mathbb{E}\left[\beta\|\nabla f(\mathbf{W}_{t-1}) - \mathbf{C}_{t-1}\|_{\mathbb{F}} + \beta L\|\mathbf{W}_{t-1} - \mathbf{W}_t\|_{\mathbb{F}}\right] \\ & = \mathbb{E}\left[\beta\|\nabla f(\mathbf{W}_{t-1}) - \mathbf{C}_{t-1}\|_{\mathbb{F}} + \beta L\gamma\|\mathbf{U}_{t-1,k}\mathbf{V}_{t-1,k}^\top\|_{\mathbb{F}}\right] \\ & = \mathbb{E}\left[\beta\|\nabla f(\mathbf{W}_{t-1}) - \mathbf{C}_{t-1}\|_{\mathbb{F}} + \beta L\gamma\sqrt{k}\right] \\ & \leq \sum_{i=1}^t \beta^i L\gamma\sqrt{k} \leq \frac{\sqrt{k}\beta L\gamma}{1 - \beta}. \end{aligned}$$

where (a) is by triangle inequality and (b) is using Assumption 3.3. Combining with Equation (23) gives

$$\mathbb{E}\left[\|\nabla f(\mathbf{W}_t) - \mathbf{M}_t\|_{\mathbb{F}}\right] \leq \sqrt{\frac{1 - \beta}{1 + \beta}} \frac{\nu}{\sqrt{b}} + \beta^t \frac{\nu}{\sqrt{b}} + \frac{\sqrt{k}\beta L\gamma}{1 - \beta}. \quad (24)$$

**Deriving the Ky Fan Stationarity.** Plugging Equation (24) into Equation (22):

$$\begin{aligned} & \mathbb{E}[f(\mathbf{W}_t) - f(\mathbf{W}_{t+1})] \\ & \geq \mathbb{E}\left[\gamma\|\nabla f(\mathbf{W}_t)\|_{(k)} - \frac{L}{2}\gamma^2k\right] - 2\gamma\sqrt{k}\left(\sqrt{\frac{1 - \beta}{1 + \beta}} \frac{\nu}{\sqrt{b}} + \beta^t \frac{\nu}{\sqrt{b}} + \frac{\sqrt{k}\beta L\gamma}{1 - \beta}\right) \\ & = \mathbb{E}\left[\gamma\|\nabla f(\mathbf{W}_t)\|_{(k)} - \frac{L}{2}\gamma^2k - 2\gamma\sqrt{k}\sqrt{\frac{1 - \beta}{1 + \beta}} \frac{\nu\sqrt{k}}{\sqrt{b}} - 2\gamma\beta^t \frac{\nu\sqrt{k}}{\sqrt{b}} - \frac{2k\gamma^2\beta L}{1 - \beta}\right]. \end{aligned}$$

Summing over  $t = 0, 1, \dots, T-1$  and dividing by  $T\gamma$  yields:

$$\frac{1}{T} \sum_{t=0}^{T-1} \mathbb{E} \|\nabla f(\mathbf{W}_t)\|_{(k)} \leq \frac{\mathbb{E}[f(\mathbf{W}_0) - f(\mathbf{W}_T)]}{T\gamma} + \frac{Lk\gamma}{2} + \frac{2\nu\sqrt{k(1-\beta)}}{\sqrt{(1+\beta)b}} + \frac{2\beta\nu\sqrt{k}}{(1-\beta)T\sqrt{b}} + \frac{2k\gamma\beta L}{1-\beta}. \quad (25)$$

**Completing the Proof.** Now, we need to apply Assumption 3.5 to the above bound. Recall that for any matrix  $\mathbf{G}$ , by the singular value decomposition we have:

$$\|\mathbf{G}\|_* = \sum_{i=1}^k \sigma_i(\mathbf{G}) + \sum_{i>k} \sigma_i(\mathbf{G}) = \|\mathbf{G}\|_{(k)} + \|\mathbf{G} - \mathbf{G}_k\|_*.$$

Applying this to  $\mathbf{G} = \nabla f(\mathbf{W}_t)$  gives

$$\|\nabla f(\mathbf{W}_t)\|_* = \|\nabla f(\mathbf{W}_t)\|_{(k)} + \|\nabla f(\mathbf{W}_t) - (\nabla f(\mathbf{W}_t))_k\|_*.$$

Taking expectation from both sides, using Assumption 3.5, and averaging over  $t$ , we would have:

$$\frac{1}{T} \sum_{t=0}^{T-1} \mathbb{E} \|\nabla f(\mathbf{W}_t)\|_* \leq \frac{1}{T} \sum_{t=0}^{T-1} \mathbb{E} \|\nabla f(\mathbf{W}_t)\|_{(k)} + \delta_k. \quad (26)$$

Putting Equation (26) in Equation (25) completes the proof.  $\square$

#### A.2.1 A NOTE ON THE VALIDITY OF TAIL ASSUMPTION 3.5

Recall that Assumption 3.5 requires a *tail control* condition of the form

$$\mathbb{E} \|\nabla f(\mathbf{W}_t) - (\nabla f(\mathbf{W}_t))_k\|_* \leq \delta_k \quad \text{for all iterates } t, \quad (27)$$

i.e., the nuclear-norm mass outside the top- $k$  singular directions of the gradient is uniformly small along the optimization trajectory. A convenient way to interpret and validate Equation (27) is via the *residual spectral energy* of the gradient after top- $k$  truncation. Let  $\mathbf{G} := \nabla f(\mathbf{W})$  and write its thin SVD as

$$\mathbf{G} = \mathbf{U}\mathbf{S}\mathbf{V}^\top, \quad \mathbf{S} = \text{diag}(\sigma_1, \dots, \sigma_q), \quad q = \min(d_{\text{out}}, d_{\text{in}}),$$

where  $\sigma_1 \geq \dots \geq \sigma_q \geq 0$ , and let  $\mathbf{G}_k = \mathbf{U}_k \mathbf{S}_k \mathbf{V}_k^\top$  be the best rank- $k$  truncation (top- $k$  SVD reconstruction). Define the (squared) Frobenius residual energy

$$\delta_k^{(\text{F})}(\mathbf{W}) := \|\mathbf{G} - \mathbf{G}_k\|_{\text{F}}^2. \quad (28)$$

Then

$$\begin{aligned} \delta_k^{(\text{F})}(\mathbf{W}) &= \|\mathbf{U}\mathbf{S}\mathbf{V}^\top - \mathbf{U}_k \mathbf{S}_k \mathbf{V}_k^\top\|_{\text{F}}^2 \\ &= \|\mathbf{U}(\mathbf{S} - \begin{bmatrix} \mathbf{S}_k \\ \mathbf{0} \end{bmatrix})\mathbf{V}^\top\|_{\text{F}}^2 \\ &= \|\begin{bmatrix} \mathbf{S}_k \\ \mathbf{S}_k^- \end{bmatrix} - \begin{bmatrix} \mathbf{S}_k \\ \mathbf{0} \end{bmatrix}\|_{\text{F}}^2 \\ &= \|\mathbf{S}_k^-\|_{\text{F}}^2 \\ &= \sum_{i>k} \sigma_i^2. \end{aligned} \quad (29)$$

Thus,  $\delta_k^{(\text{F})}$  is exactly the residual spectral energy beyond rank  $k$ . An immediate consequence is that increasing  $k$  can only reduce the residual energy.

**Lemma A.5** (Monotonicity of Residual Energy). *Let  $\delta_k^{(F)}(\mathbf{W})$  be defined as in Equation (28). Then  $\delta_k^{(F)}(\mathbf{W})$  is monotonically decreasing in  $k$ :*

$$\delta_{k+1}^{(F)}(\mathbf{W}) \leq \delta_k^{(F)}(\mathbf{W}) \quad \text{for all } k \geq 1.$$

*Proof.* From Equation (29),

$$\delta_{k+1}^{(F)}(\mathbf{W}) = \sum_{i>k+1} \sigma_i^2 = \sum_{i>k} \sigma_i^2 - \sigma_{k+1}^2 = \delta_k^{(F)}(\mathbf{W}) - \sigma_{k+1}^2 \leq \delta_k^{(F)}(\mathbf{W}), \quad (30)$$

where the inequality follows from  $\sigma_{k+1}^2 \geq 0$ .  $\square$

By Lemma A.5,  $\delta_1^{(F)}(\mathbf{W}) \geq \delta_2^{(F)}(\mathbf{W}) \geq \dots \geq \delta_q^{(F)}(\mathbf{W}) = 0$ . Hence, as long as we show that  $\delta_1^{(F)}(\mathbf{W})$  is bounded and close to zero, the tail assumption of Assumption 3.5 holds for all  $k > 1$ .

**Empirical validation.** To empirically validate this assumption, we measure  $\delta_1^{(F)}(\mathbf{W})$  via

$$\delta_1^{(F)}(\mathbf{W}) = \sigma_1^2(\text{sr}(\mathbf{G}) - 1), \quad (31)$$

since the stable rank is defined as  $\text{sr}(\mathbf{G}) := \|\mathbf{G}\|_{\mathbb{F}}^2 / \sigma_1^2 \geq 1$ . Figure 10 displays this quantity across all transformer block weight matrices for the Qwen3-0.6B models. As shown, this residual typically decreases over the course of training for NuMuon, indicating that the gradient spectrum becomes increasingly concentrated in its leading directions. By Equation (27), this concentration implies a small nuclear tail for modest values of  $k$ , supporting the validity of the tail assumption in Equation (27). Consequently, the Ky Fan  $k$ -norm stationarity guarantees of Theorem 3.6 can be meaningfully converted into approximate nuclear norm stationarity bounds that we derive for NuMuon.

### A.3 FEASIBILITY ATTRACTION

In Section 3.2, we discussed how NuMuon modifies the spectral-norm LMO by incorporating an additional nuclear-norm constraint. While this constraint ensures that each update  $\Delta \mathbf{W}_t$  is low-rank, it is not immediately clear whether the iterates  $\mathbf{W}_t$  themselves converge toward the feasible set. The following lemma establishes that under FW/CG updates, the distance to NuMuon’s feasible set contracts at each iteration, guaranteeing that the iterates are progressively attracted toward feasibility.

**Lemma A.6** (Feasibility Attraction under FW/CG Updates). *Let  $\mathcal{W}_*$  be the NuMuon feasible set in Equation (9), and assume  $\mathcal{W}_*$  is nonempty, closed, and convex. Consider a FW/CG-style update of the form*

$$\mathbf{W}_{t+1} = (1 - \gamma_t) \mathbf{W}_t + \gamma_t \Delta \mathbf{W}_t, \quad \Delta \mathbf{W}_t \in \mathcal{W}_*, \quad \gamma_t \in (0, 1]. \quad (32)$$

*Then the distance to  $\mathcal{W}_*$  contracts:*

$$\text{dist}(\mathbf{W}_{t+1}, \mathcal{W}_*) \leq (1 - \gamma_t) \text{dist}(\mathbf{W}_t, \mathcal{W}_*), \quad (33)$$

*where  $\text{dist}(\mathbf{X}, \mathcal{W}_*) := \inf_{\mathbf{Y} \in \mathcal{W}_*} \|\mathbf{X} - \mathbf{Y}\|_{\mathbb{F}}$ . Consequently,*

$$\text{dist}(\mathbf{W}_T, \mathcal{W}_*) \leq \left( \prod_{t=0}^{T-1} (1 - \gamma_t) \right) \text{dist}(\mathbf{W}_0, \mathcal{W}_*), \quad (34)$$

*and in particular  $\text{dist}(\mathbf{W}_T, \mathcal{W}_*) \rightarrow 0$  whenever  $\sum_{t=0}^{\infty} \gamma_t = \infty$  (e.g., for constant  $\gamma_t = \gamma \in (0, 1]$ , the decay is geometric:  $\text{dist}(\mathbf{W}_T, \mathcal{W}_*) \leq (1 - \gamma)^T \text{dist}(\mathbf{W}_0, \mathcal{W}_*)$ ).*

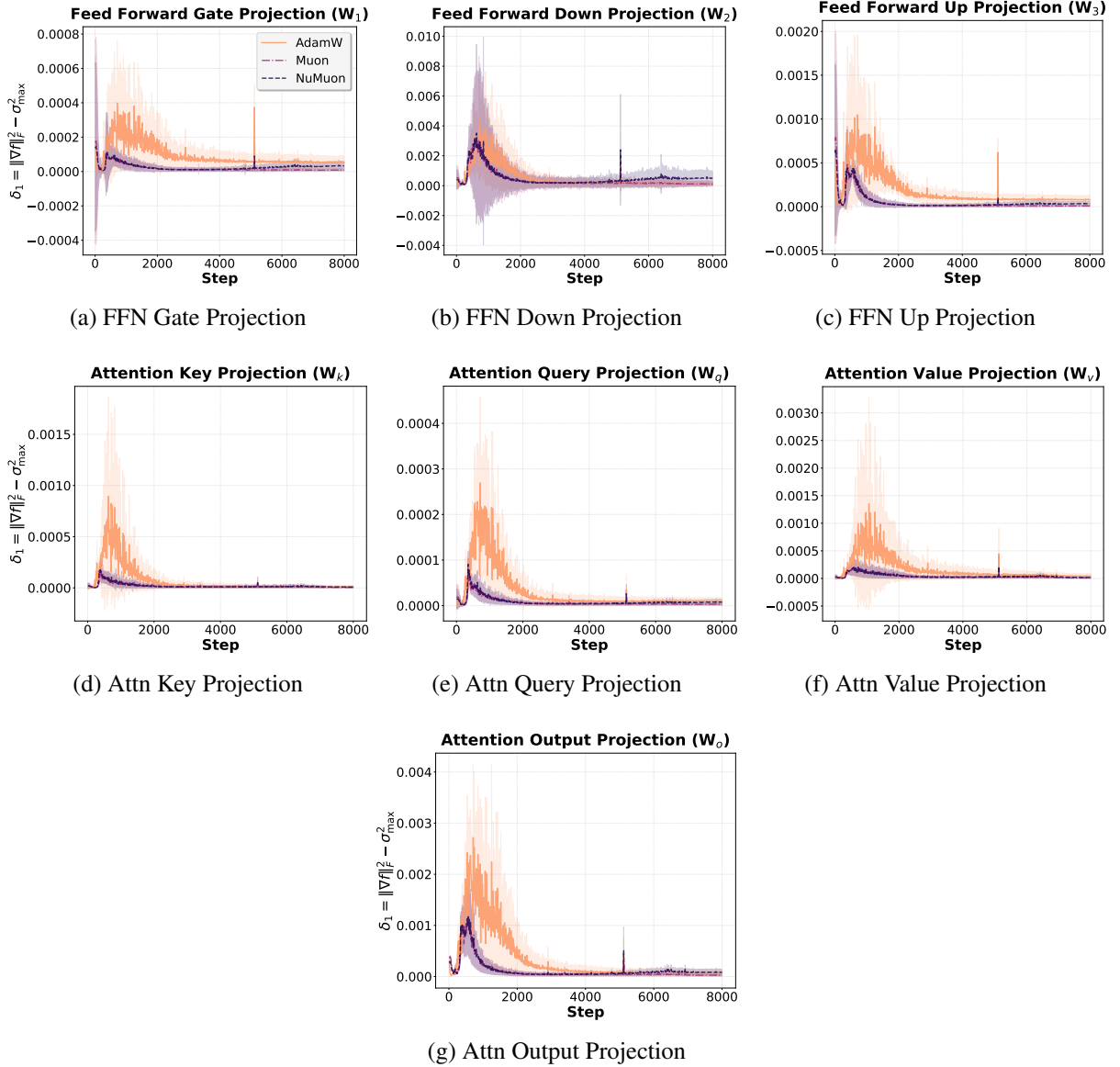


Figure 10:  $\delta_1^{(F)}$  as a proxy for the tail bound in Assumption 3.5. As seen, with NuMuon this quantity gets very close to 0 as training progresses, indicating that our Ky Fan  $k$ -norm stationarity convergence gets very close to the standard nuclear-norm stationarity convergence guarantee of Shen et al. (2025) for Muon. Among all weight matrices, the feedforward output projection  $W_2$  usually exhibits a larger  $\delta_1^{(F)}$  which could potentially require a higher nuclear norm budget. This is interesting research direction which we leave for future work.

*Proof.* Indeed,  $\mathcal{W}_* = \{\Delta W : \|\Delta W\|_2 \leq \rho\} \cap \{\Delta W : \|\Delta W\|_* \leq \tau\}$  is an intersection of two closed convex sets, and is nonempty since  $\mathbf{0} \in \mathcal{W}_*$  so the conditions of the lemma holds. Now let  $P_t \in \arg \min_{Y \in \mathcal{W}_*} \|\mathbf{W}_t - Y\|_F$  be the Frobenius projection of  $\mathbf{W}_t$  onto  $\mathcal{W}_*$ . Since  $\mathcal{W}_*$  is convex and  $\Delta \mathbf{W}_t \in \mathcal{W}_*$ , the convex combination

$$\mathbf{Z}_t := (1 - \gamma_t)P_t + \gamma_t\Delta \mathbf{W}_t$$

also lies in  $\mathcal{W}_*$ . Therefore, by the definition of distance to a set,

$$\text{dist}(\mathbf{W}_{t+1}, \mathcal{W}_*) \leq \|\mathbf{W}_{t+1} - \mathbf{Z}_t\|_F = \|(1 - \gamma_t)(\mathbf{W}_t - P_t)\|_F = (1 - \gamma_t) \text{dist}(\mathbf{W}_t, \mathcal{W}_*),$$

which proves Equation (33). Iterating this inequality yields Equation (34). Finally, if  $\sum_{t=0}^{\infty} \gamma_t = \infty$ , then

**Algorithm 1** Muon / NuMuon Optimizer

---

```

1: Input: Initial parameters  $\mathbf{W}_0$ , learning rate  $\gamma$ , momentum  $\beta$ , rank  $k$ .
2: Initialize: Momentum buffer  $\mathbf{M}_0 = \mathbf{0}$ .
3: for  $t = 0, 1, 2, \dots$  do
4:   Compute gradient  $\mathbf{G}_t = \nabla_{\mathbf{W}} f(\mathbf{W}_t)$ .
5:   Update momentum  $\mathbf{M}_t = \beta \mathbf{M}_{t-1} + (1 - \beta) \mathbf{G}_t$ .
6:   if Muon then
7:     Compute SVD:  $\mathbf{M}_t = \mathbf{U} \mathbf{S} \mathbf{V}^\top$ .
8:      $\bar{\mathbf{M}}_t = \mathbf{U} \mathbf{V}^\top$  ▷ full rank (approx. via Newton-Schulz)
9:   else if NuMuon then
10:    Compute SVD:  $\mathbf{M}_t = \mathbf{U} \mathbf{S} \mathbf{V}^\top$ .
11:     $\bar{\mathbf{M}}_t = \mathbf{U}_{:,1:k} \mathbf{V}_{:,1:k}^\top$  ▷ top- $k$  (approx via Block Krylov SVD)
12:   end if
13:   Update weights  $\mathbf{W}_{t+1} = \mathbf{W}_t - \gamma \bar{\mathbf{M}}_t$ .
14: end for

```

---

$\prod_{t=0}^{T-1} (1 - \gamma_t) \rightarrow 0$ , implying  $\text{dist}(\mathbf{W}_T, \mathcal{W}_*) \rightarrow 0$ . □

**B. ALGORITHMS**

We summarize the differences between Muon and NuMuon in Algorithm 1. Overall, the two methods are similar; however, Muon relies on a Newton–Schulz iteration (see Algorithm 2) to compute an orthonormalized update, whereas NuMuon uses Block Krylov methods to approximate the top- $k$  singular subspace and construct a low-rank update. NuMuon additionally employs a rank scheduler, as discussed in Section 3.4. These changes differentiate NuMuon from Muon and allow it to obtain a final low-rank solution which would greatly benefit downstream weight compression.

**RMS-to-RMS Scaling in Practice.** In practical large-scale implementations, it is common to apply a shape-dependent rescaling to the orthogonalized LMO direction so that the *per-entry RMS* of the update is comparable across matrices with different aspect ratios and can be aligned to typical AdamW update magnitudes (Bernstein and Newhouse, 2025; Liu et al., 2025; Pethick et al., 2025). Concretely, one often uses

$$\text{lmo}_{\mathcal{W}}(\mathbf{M}) = -\rho s(d_{\text{out}}, d_{\text{in}}) \mathbf{U} \mathbf{V}^\top, \quad (35)$$

where  $s(d_{\text{out}}, d_{\text{in}}) = \sqrt{d_{\text{out}}/d_{\text{in}}}$  (or closely related variants), and absorbs  $\rho s(\cdot)$  into the effective stepsize.

**NuMuon’s Rank Schedulers.** NuMuon uses rank schedulers to determine the rank fraction  $k_t$  to compute its truncated updates. We use three family of schedulers in our experiments, which are:

- **Fixed:**  $r(t) = r_0$  (constant rank fraction);
- **Piecewise:**  $r(t) = r_i$  for  $t \in [t_i, t_{i+1})$ ;
- **Cosine decay:**

$$r(t) = \begin{cases} r_{\text{start}}, & 0 \leq t < T_h, \\ r_{\text{end}} + (r_{\text{start}} - r_{\text{end}}) \left(1 + \cos\left(\pi \frac{t - T_h}{T_d}\right)\right) / 2, & \text{o.w.} \end{cases}$$

where  $T$  denotes the total number of steps,  $T_h$  the warm-start period, and  $T_d = \max(1, T - T_h)$  (see Figure 11).

**Algorithm 2** Newton-Schulz Iterative Algorithm for Matrix Orthogonalization

---

```

1: Input: Matrix  $\mathbf{A} \in \mathbb{R}^{n \times m}$ , iterations  $K$ , hyperparameters  $a, b, c \in \mathbb{R}$ .
2: Initialize:  $\mathbf{A}^{(0)} = \mathbf{A} / \|\mathbf{A}\|_F$ .
3: for  $k = 0, 1, \dots, K - 1$  do
4:    $\mathbf{A}^{(k+1)} = a\mathbf{A}^{(k)} + b(\mathbf{A}^{(k)}\mathbf{A}^{(k)\top})\mathbf{A}^{(k)} + c(\mathbf{A}^{(k)}\mathbf{A}^{(k)\top})^2\mathbf{A}^{(k)}$ .
5: end for
6: Return:  $\mathbf{A}^{(K)}$ .

```

---

**Algorithm 3** Randomized Block Krylov Method for Approximate Top- $k$  SVD (Musco and Musco, 2015)

---

```

1: Input: Matrix  $\mathbf{A} \in \mathbb{R}^{m \times n}$ ; target rank  $k$ ; block size  $b \geq k$ ; Krylov iters  $L$ ; (optional) warm-start block  $\mathbf{B}_0 \in \mathbb{R}^{n \times b}$ 
2: Initialize:
3: if  $\mathbf{B}_0$  not provided then
4:   Sample  $\mathbf{B}_0 \sim \mathcal{N}(0, 1)^{n \times b}$ 
5: end if
6:  $\mathbf{B}_0 \leftarrow \text{qr}(\mathbf{B}_0)$ 
7:  $\mathbf{K} \leftarrow []$  ▷ Build orthonormal basis for Krylov subspace
8: for  $i = 1$  to  $L$  do
9:    $\mathbf{T}_i \leftarrow \mathbf{A}\mathbf{B}_{i-1}$ 
10:   $\mathbf{B}_i \leftarrow \mathbf{A}^\top \mathbf{T}_i$ 
11:   $\mathbf{B}_i \leftarrow \text{qr}(\mathbf{B}_i)$ 
12:   $\mathbf{K} \leftarrow [\mathbf{K} \ \mathbf{B}_i]$ 
13: end for
14:  $\mathbf{Q} \leftarrow \text{qr}(\mathbf{K})$ 
15:  $\mathbf{T} \leftarrow \mathbf{A}\mathbf{Q}$  ▷ Project and compute small SVD
16: Compute thin SVD:  $\mathbf{T} = \mathbf{U}_T \mathbf{S}_T \mathbf{V}_T^\top$ 
17:  $\mathbf{U}_k \leftarrow \mathbf{U}_T[:, 1:k]$  ▷ Extract top- $k$  components and lift back
18:  $\mathbf{S}_k \leftarrow \mathbf{S}_T[1:k, 1:k]$ 
19:  $\mathbf{V}_k \leftarrow \mathbf{Q} \mathbf{V}_T[:, 1:k]$ 
20: Return:  $(\mathbf{U}_k, \mathbf{S}_k, \mathbf{V}_k)$ 

```

---

## C. EXTENDED EXPERIMENTAL RESULTS

In this section, we present the full set of experimental results omitted from the main paper due to space constraints.

## C.1 EXPERIMENT SETTINGS AND HYPERPARAMETERS

**Pretraining.** We pretrain three LLMs of different sizes on FineWeb-EDU (Penedo et al., 2024): Qwen3-0.6B (Yang et al., 2025), Olmo2-1.4B (OLMo et al., 2025), and Llama3-1.8B (Dubey et al., 2024). We use the torchtitan library for pretraining on a cluster with 8 NVIDIA A100-SXM4-40GB GPUs,<sup>5</sup> and train each model with AdamW (Loshchilov and Hutter, 2019), Muon (Jordan et al., 2024), and our approach, NuMuon. All models start with a linear warmup. For AdamW, we use a cosine learning rate decay while for Muon and NuMuon we use WSD (Hu et al., 2024), following the benchmarking study of Semenov et al. (2025) which recommends these schedules for best performance. Please see Figure 12 for the details of the rank scheduler. For Muon and NuMuon, we also apply weight decay of 0.1. Finally, for NuMuon we typically use a cosine rank scheduler with a 10% constant period at the beginning of training. We set this scheduler to reach the

<sup>5</sup>Note that for benchmarking the generation throughput in Figure 20, we use a single NVIDIA A100-SXM4-40GB GPU.

final rank before the WSD cooldown stage. We visualize the rank schedule for Qwen3-0.6B in Figure 11 and provide full pretraining hyperparameters in Tables 4 and 5.

**LLM Compression.** After pretraining, we compress the resulting checkpoints using three SVD-based compression methods: ASVD (Yuan et al., 2023), SVD-LLM (Wang et al., 2025b), and Dobi-SVD (Wang et al., 2025a). We use the official default settings provided in each repository<sup>6</sup> and evaluate compressed models on WikiText2 validation perplexity and standard downstream benchmarks (ARC-Easy/Challenge, HellaSwag, LAMBADA (OpenAI), OpenbookQA, PIQA, and Winogrande). For SVD-LLM, we evaluate both the whitening and whitening + LoRA variants; in cases where the LoRA stage was unstable, we report the whitening results for both settings for completeness and note this in the corresponding tables.

Table 4: Model architectures and training configuration.

MODEL CONFIGURATION	QWEN3-0.6B	OLMO2-1.4B	LLAMA3-1.8B
MODEL ARCHITECTURE			
Hidden Dimensions	1024	2048	2048
Number of Layers	28	16	30
Attention Heads	16	32	32
Key-Value Heads	8	8	8
Head Dimension	128	64	64
FFN Dimension Multiplier	–	1.3	1.3
Multiple Of	–	1024	1024
RoPE Theta	1000000	500000	500000
Vocabulary Size	151936	128256	50257
QK Norm	Yes	Yes	No
DISTRIBUTED SETUP			
Data Parallel Replicate Degree	8	8	8
Pipeline Parallel Degree	1	1	1
TRAINING			
Local Batch Size	16	8	2
Global Batch Size	1024	1024	1024
Sequence Length	2048	2048	2048
Total Steps	8000	16000	20000
Dataset	Fineweb-EDU	Fineweb-EDU	Fineweb-EDU
Gradient Clipping (Max Norm)	1.0	1.0	1.0

## C.2 EXTENDED RESULTS

### C.2.1 TRAINING CONVERGENCE

**Loss Curves.** We report training loss trajectories for AdamW, Muon, and NuMuon on all models in Figure 4, illustrating that NuMuon largely tracks Muon with a small late-stage deviation.

**Stable-rank Dynamics.** We also compare stable-rank evolution under each optimizer for the Qwen3-0.6B model in Figure 13, highlighting how rank controlled updates induce lower effective rank during training. Furthermore, we report the stable rank of each weight matrix in the transformer blocks against the layer depth in Figures 14 to 16. As shown, NuMuon produces weight matrices with consistently lower rank than Muon, making it compression friendly.

<sup>6</sup>ASVD: <https://github.com/hahnyuan/ASVD4LLM>.  
 SVD-LLM: <https://github.com/AIoT-MLSys-Lab/SVD-LLM>.  
 Dobi-SVD: <https://github.com/wangqinsi1/Dobi-SVD>.

Table 5: Optimizer configuration and learning rate scheduler settings.

CONFIGURATION	ADAMW	MUON	NUMUON
OPTIMIZER			
Learning Rate	3e-4	1e-2	1e-2
Weight Decay	–	0.1	0.1
Beta1	–	0.9	0.9
Beta2	–	0.95	0.95
Epsilon	1e-8	1e-8	1e-8
MUON/NUMUON-SPECIFIC PARAMETERS			
Scalar Optimizer	–	Lion	Lion
Embedding Optimizer	–	AdamW	AdamW
Head Optimizer	–	AdamW	AdamW
Scalar LR Factor	–	1.0	1.0
Embedding LR Factor	–	0.5	0.5
Head LR Factor	–	1.0	1.0
NUMUON-SPECIFIC PARAMETERS			
Krylov Iterations	–	–	2
Oversample	–	–	8
Rank Scheduler Type	–	–	Cosine
LEARNING RATE SCHEDULER			
Scheduler Type	Cosine	WSD	WSD
Warmup Steps	25%	25%	25%
Minimum LR Factor	0.01	0.01	0.01
Decay Type	Cosine	Cosine	Cosine
Warmdown Ratio	75%	20%	20%

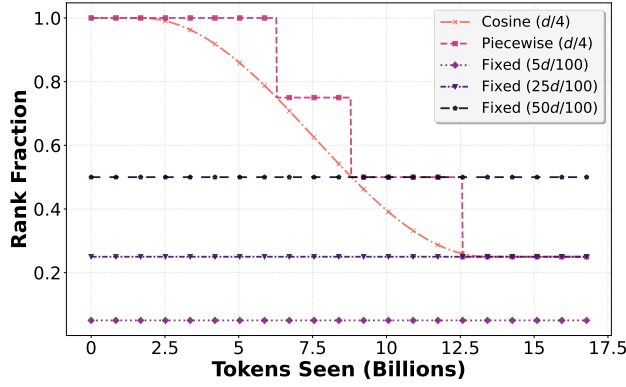


Figure 11: Different rank schedulers used for training Qwen3-0.6B models with NuMuon. Please see Section 3.4 for more details.

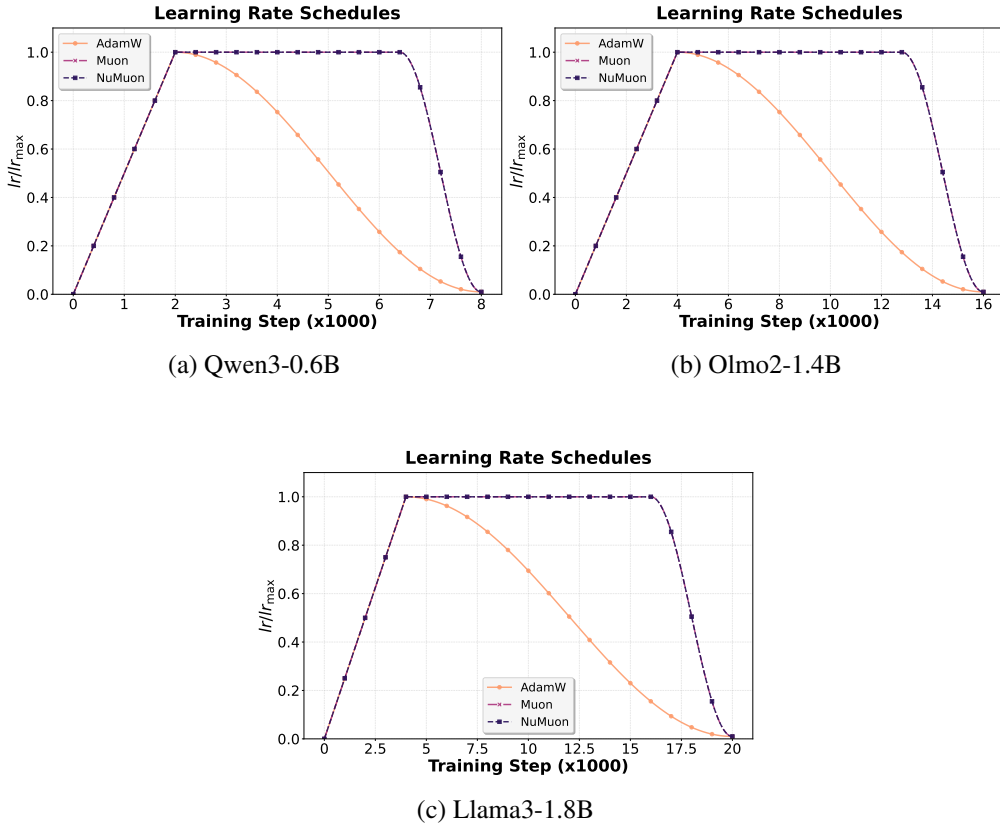


Figure 12: Normalized learning rate scheduler for training language models of size 0.6B-1.8B parameter count. For each model family, we use AdamW, Muon, and NuMuon to train the model. Following Semenov et al. (2025) extensive benchmarks, we use a WSD (Hu et al., 2024) schedule for training Muon and NuMuon, while we use a cosine decay for AdamW. For more details, please see Appendix C.1.

**Subspace Alignment.** We report the Grassmann distance between the top- $k$  right-singular subspaces of  $\mathbf{W}$  and  $\Delta\mathbf{W}$  (here  $k = 64$ ) in Figure 18, demonstrating improved update-weight subspace alignment for NuMuon. For more information, please see Section 5.

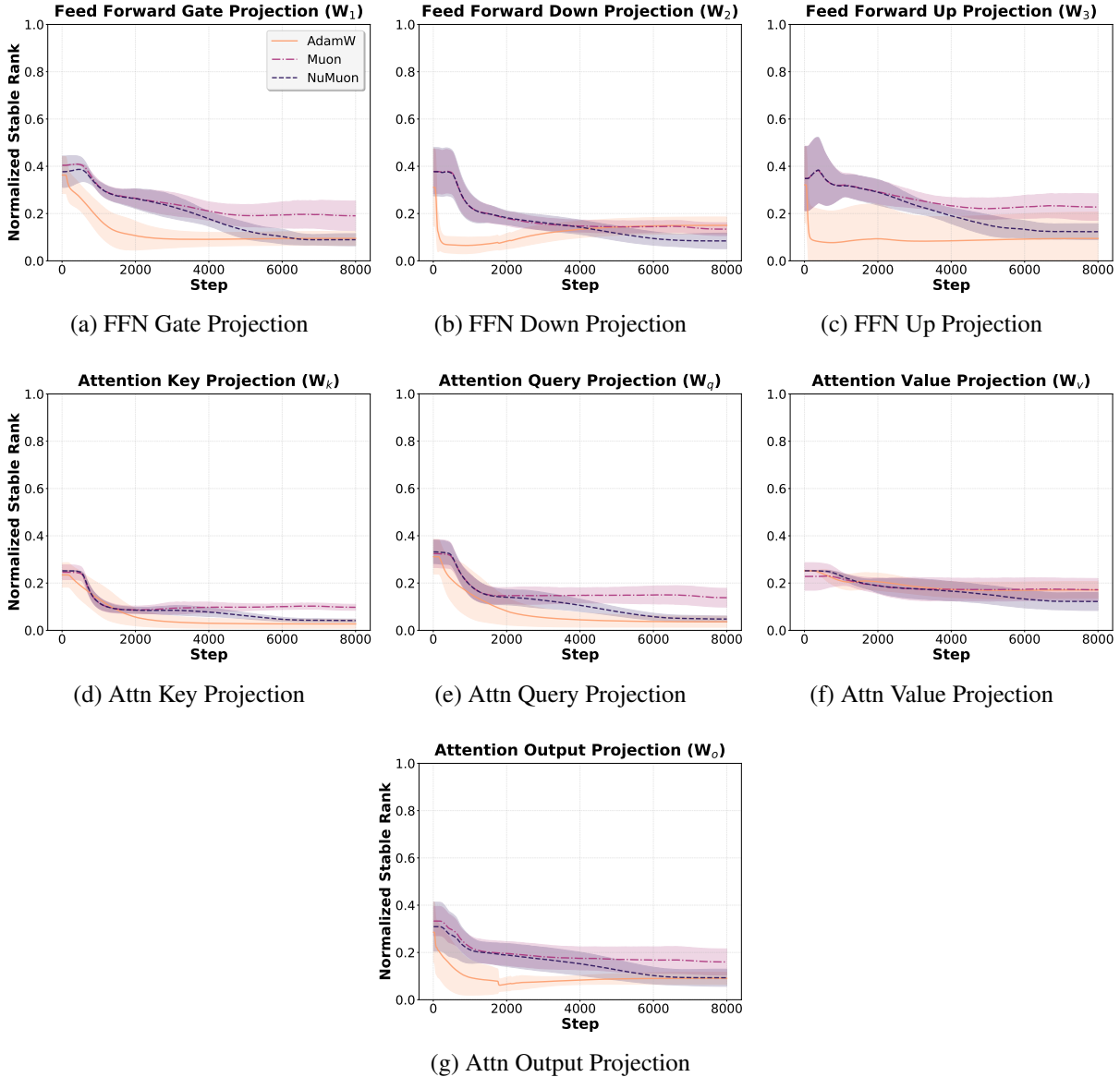


Figure 13: Normalized stable rank evolution for Qwen3-0.6B across training steps for different weight matrices. Each subplot shows the mean stable rank (normalized by the maximum rank), with shaded regions indicating standard deviation across all layers.

### C.2.2 LLM COMPRESSION

We summarize WikiText2 validation perplexity versus compression rate across all methods and models in Figure 19. We see that NuMuon-trained weights degrade more gracefully under aggressive compression rates, illustrating that their lower rank weights are more compressible than Muon. We also report the validation perplexity and detailed downstream benchmark results in Tables 6 to 17.

### C.3 EXTENDED ABLATION STUDIES

**Rank-scheduler Ablations.** Table 18 reports the effect of rank scheduler choice (cosine, piecewise, and fixed) on training efficiency and robustness to aggressive compression (80%) using Dobi-SVD. Consistent with our discussion in the main paper, fixed-rank schedules are typically fastest per step since they avoid an

Table 6: WikiText2 validation perplexity and downstream task performance across compressed Qwen3-0.6B models using ASVD.

COMP.	OPTIMIZER	VAL. PPL	DOWNSTREAM TASKS							AVG
			ARC-C	ARC-E	H'SWAG	LAM'DA	OPENBKQA	PIQA	W'GRANDE	
0%	ADAMW	25.39	27.30	49.66	36.04	27.77	31.20	65.02	49.64	40.95
	MUON	19.20	<b>30.72</b>	<b>57.95</b>	<b>45.56</b>	<b>37.69</b>	33.60	<b>67.74</b>	<b>54.38</b>	<b>46.81</b>
	NUMUON	20.20 (+5.2%)	29.95	55.68	43.51	35.40	<b>34.40</b>	67.41	53.51	45.69 (-2.4%)
20%	ADAMW	61.91	22.53	37.21	30.83	12.13	28.20	54.68	51.70	33.90
	MUON	29.87	<b>28.67</b>	52.06	40.80	30.49	33.80	65.94	<b>52.96</b>	43.53
	NUMUON	21.73 (-27.3%)	28.33	<b>52.27</b>	<b>42.47</b>	<b>37.55</b>	<b>34.20</b>	<b>66.32</b>	52.41	<b>44.79 (+2.9%)</b>
40%	ADAMW	1677.81	24.49	28.83	26.68	0.10	28.40	51.85	47.59	29.71
	MUON	17097.41	<b>24.57</b>	27.31	27.57	1.07	26.20	52.12	50.12	29.85
	NUMUON	54.79 (-99.7%)	23.89	<b>40.49</b>	<b>35.79</b>	<b>24.92</b>	<b>30.60</b>	<b>61.48</b>	<b>50.67</b>	<b>38.26 (+28.2%)</b>
60%	ADAMW	5306.46	25.85	27.78	26.51	0.06	<b>30.60</b>	52.45	50.12	30.48
	MUON	30980.97	25.17	27.06	27.08	0.25	29.20	51.58	47.99	29.76
	NUMUON	1030.72 (-96.7%)	<b>27.13</b>	<b>33.08</b>	<b>30.36</b>	<b>12.98</b>	28.20	<b>57.07</b>	<b>51.14</b>	<b>34.28 (+15.2%)</b>

Table 7: WikiText2 validation perplexity and downstream task performance across compressed Olmo2-1.4B models using ASVD.

COMP.	OPTIMIZER	VAL. PPL	DOWNSTREAM TASKS							AVG
			ARC-C	ARC-E	H'SWAG	LAM'DA	OPENBKQA	PIQA	W'GRANDE	
0%	ADAMW	20.58	30.20	55.47	44.96	34.76	35.80	68.93	50.67	45.83
	MUON	17.80	<b>34.04</b>	<b>60.10</b>	<b>50.94</b>	<b>39.28</b>	<b>37.80</b>	<b>70.46</b>	54.85	<b>49.64</b>
	NUMUON	19.06 (+7.1%)	31.06	59.55	48.40	37.80	37.00	68.99	<b>55.41</b>	48.32 (-2.7%)
20%	ADAMW	35.89	28.07	49.12	40.12	23.09	30.20	64.47	50.67	40.82
	MUON	738.86	22.78	40.19	28.98	2.87	27.40	58.43	50.51	33.02
	NUMUON	20.09 (-97.3%)	<b>30.38</b>	<b>57.24</b>	<b>47.22</b>	<b>36.44</b>	<b>35.20</b>	<b>69.10</b>	<b>55.80</b>	<b>47.34 (+43.4%)</b>
40%	ADAMW	873.00	22.18	32.37	28.62	2.76	27.40	51.80	49.64	30.68
	MUON	39946.67	<b>24.32</b>	25.67	26.06	0.00	27.40	51.36	<b>52.64</b>	29.64
	NUMUON	52.61 (-99.9%)	24.23	<b>50.59</b>	<b>37.02</b>	<b>17.33</b>	<b>30.80</b>	<b>63.60</b>	51.46	<b>39.29 (+32.6%)</b>
60%	ADAMW	40436.60	25.51	26.22	26.26	0.00	26.60	52.29	49.33	29.46
	MUON	29425.49	25.09	25.25	26.74	0.00	<b>27.80</b>	52.61	50.59	29.73
	NUMUON	451.06 (-98.5%)	<b>25.94</b>	<b>39.23</b>	<b>30.71</b>	<b>9.06</b>	<b>27.80</b>	<b>58.76</b>	<b>51.85</b>	<b>34.76 (+16.9%)</b>

Table 8: WikiText2 validation perplexity and downstream task performance across compressed Llama3-1.8B models using ASVD.

COMP.	OPTIMIZER	VAL. PPL	DOWNSTREAM TASKS							AVG
			ARC-C	ARC-E	H'SWAG	LAM'DA	OPENBKQA	PIQA	W'GRANDE	
0%	ADAMW	18.75	33.79	62.67	51.28	40.46	37.00	71.82	55.33	50.34
	MUON	15.39	<b>38.82</b>	<b>67.80</b>	<b>58.35</b>	<b>47.47</b>	<b>41.80</b>	<b>74.37</b>	<b>59.27</b>	<b>55.41</b>
	NUMUON	17.56 (+14.1%)	35.49	65.19	54.96	44.38	38.20	72.91	58.56	52.81 (-4.7%)
20%	ADAMW	27.19	31.57	57.53	46.29	32.25	36.20	68.06	52.01	46.27
	MUON	19.13	34.47	62.71	52.62	42.60	37.60	71.38	56.27	51.09
	NUMUON	17.85 (-6.7%)	<b>35.41</b>	<b>64.18</b>	<b>53.98</b>	<b>44.89</b>	<b>38.40</b>	<b>71.98</b>	<b>57.30</b>	<b>52.31 (+2.4%)</b>
40%	ADAMW	718.71	22.61	37.25	30.15	6.00	26.40	54.52	49.88	32.40
	MUON	1443.55	24.66	31.90	29.28	7.08	27.80	55.93	50.12	32.40
	NUMUON	20.56 (-98.6%)	<b>32.76</b>	<b>62.88</b>	<b>50.27</b>	<b>42.64</b>	<b>37.20</b>	<b>71.38</b>	<b>56.20</b>	<b>50.48 (+55.8%)</b>
60%	ADAMW	10251.84	24.49	29.38	26.50	0.19	30.40	51.85	49.64	30.35
	MUON	26731.09	25.94	26.26	25.86	0.02	28.20	48.69	50.28	29.32
	NUMUON	268.86 (-99.0%)	<b>26.11</b>	<b>39.73</b>	<b>29.66</b>	<b>19.81</b>	<b>33.00</b>	<b>58.43</b>	<b>50.43</b>	<b>36.74 (+25.3%)</b>

Table 9: WikiText2 validation perplexity and downstream task performance across compressed Qwen3-0.6B models using SVD-LLM (Whitening).

Comp.	OPTIMIZER	VAL. PPL	DOWNSTREAM TASKS							AVG
			ARC-C	ARC-E	H'SWAG	LAM'DA	OPENBKQA	PIQA	W'GRANDE	
0%	ADAMW	25.39	27.30	49.66	36.04	27.77	31.20	65.02	49.64	40.95
	MUON	19.20	<b>30.72</b>	<b>57.95</b>	<b>45.56</b>	<b>37.69</b>	<b>33.60</b>	<b>67.74</b>	<b>54.38</b>	<b>46.81</b>
	NUMUON	20.20 (+5.2%)	29.95	55.68	43.51	35.40	<b>34.40</b>	67.41	53.51	45.69 (-2.4%)
20%	ADAMW	39.36	25.17	42.30	31.10	14.30	27.40	56.86	49.96	35.30
	MUON	27.89	26.62	45.33	37.70	28.04	31.40	62.46	<b>53.83</b>	40.77
	NUMUON	22.87 (-18.0%)	<b>27.47</b>	<b>48.65</b>	<b>40.80</b>	<b>31.17</b>	<b>34.60</b>	<b>65.02</b>	51.62	<b>42.76</b> (+4.9%)
40%	ADAMW	142.39	22.61	31.90	26.65	2.17	27.40	51.41	<b>50.75</b>	30.41
	MUON	52.14	23.12	34.68	32.34	18.16	28.00	56.75	49.72	34.68
	NUMUON	32.07 (-38.5%)	<b>24.32</b>	<b>41.29</b>	<b>35.88</b>	<b>23.52</b>	<b>29.60</b>	<b>61.53</b>	<b>50.75</b>	<b>38.13</b> (+9.9%)
60%	ADAMW	545.52	23.89	29.92	26.00	0.21	27.80	51.47	50.43	29.96
	MUON	195.35	22.95	28.11	28.06	3.10	<b>28.20</b>	51.74	50.43	30.37
	NUMUON	95.18 (-51.3%)	<b>25.09</b>	<b>30.77</b>	<b>29.88</b>	<b>12.03</b>	26.80	<b>55.77</b>	<b>51.54</b>	<b>33.13</b> (+9.1%)
80%	ADAMW	1412.22	23.63	27.23	26.59	0.00	28.20	51.03	49.41	29.44
	MUON	1560.59	<b>25.00</b>	<b>27.61</b>	26.31	0.00	<b>29.20</b>	51.58	<b>52.41</b>	<b>30.30</b>
	NUMUON	840.76 (-46.1%)	<b>25.00</b>	26.64	<b>26.95</b>	<b>0.10</b>	27.40	<b>51.96</b>	50.59	29.81 (-1.6%)

Table 10: WikiText2 validation perplexity and downstream task performance across compressed Olmo2-1.4B models using SVD-LLM (Whitening).

Comp.	OPTIMIZER	VAL. PPL	DOWNSTREAM TASKS							AVG
			ARC-C	ARC-E	H'SWAG	LAM'DA	OPENBKQA	PIQA	W'GRANDE	
0%	ADAMW	20.58	30.20	55.47	44.96	34.76	35.80	68.93	50.67	45.83
	MUON	17.80	<b>34.04</b>	<b>60.10</b>	<b>50.94</b>	<b>39.28</b>	<b>37.80</b>	<b>70.46</b>	54.85	<b>49.64</b>
	NUMUON	19.06 (+7.1%)	31.06	59.55	48.40	37.80	37.00	68.99	<b>55.41</b>	48.32 (-2.7%)
20%	ADAMW	26.65	26.11	50.38	39.95	27.60	32.00	65.23	51.85	41.87
	MUON	20.13	<b>30.72</b>	56.31	43.98	<b>37.94</b>	33.80	65.72	<b>56.67</b>	46.45
	NUMUON	19.46 (-3.3%)	29.95	<b>58.84</b>	<b>47.38</b>	36.44	<b>35.20</b>	<b>68.82</b>	56.35	<b>47.57</b> (+2.4%)
40%	ADAMW	51.62	24.57	39.44	32.81	14.07	27.60	56.58	51.46	35.22
	MUON	27.22	25.26	43.98	36.77	30.93	29.20	60.01	53.51	39.95
	NUMUON	20.75 (-23.8%)	<b>28.84</b>	<b>56.94</b>	<b>44.95</b>	<b>35.38</b>	<b>35.40</b>	<b>67.03</b>	<b>55.41</b>	<b>46.28</b> (+15.8%)
60%	ADAMW	221.80	23.63	30.64	27.12	2.31	26.20	52.56	50.75	30.46
	MUON	67.48	23.21	28.87	29.30	15.43	24.80	52.61	52.09	32.33
	NUMUON	30.29 (-55.1%)	<b>24.83</b>	<b>42.47</b>	<b>37.10</b>	<b>26.53</b>	<b>30.40</b>	<b>59.58</b>	<b>52.25</b>	<b>39.02</b> (+20.7%)
80%	ADAMW	1040.87	24.66	24.79	25.62	0.08	25.20	<b>51.63</b>	48.54	28.65
	MUON	474.07	24.83	<b>28.11</b>	26.46	0.70	<b>27.00</b>	50.49	<b>50.36</b>	<b>29.71</b>
	NUMUON	289.28 (-39.0%)	<b>26.02</b>	27.02	<b>26.74</b>	<b>1.11</b>	26.00	50.60	<b>50.36</b>	29.69

Table 11: WikiText2 validation perplexity and downstream task performance across compressed Llama3-1.8B models using SVD-LLM (Whitening).

Comp.	OPTIMIZER	VAL. PPL	DOWNSTREAM TASKS							AVG
			ARC-C	ARC-E	H'SWAG	LAM'DA	OPENBKQA	PIQA	W'GRANDE	
0%	ADAMW	18.75	33.79	62.67	51.28	40.46	37.00	71.82	55.33	50.34
	MUON	15.39	<b>38.82</b>	<b>67.80</b>	<b>58.35</b>	<b>47.47</b>	<b>41.80</b>	<b>74.37</b>	<b>59.27</b>	<b>55.41</b>
	NUMUON	17.56 (+14.1%)	35.49	65.19	54.96	44.38	38.20	72.91	58.56	52.81 (-4.7%)
20%	ADAMW	24.27	29.78	56.19	43.82	35.77	33.40	67.03	53.67	45.67
	MUON	18.04	30.20	58.38	47.86	40.69	34.40	66.54	<b>58.33</b>	48.06
	NUMUON	17.90 (-0.8%)	<b>34.39</b>	<b>63.80</b>	<b>53.32</b>	<b>42.29</b>	<b>37.00</b>	<b>71.71</b>	58.09	<b>51.51</b> (+7.2%)
40%	ADAMW	51.68	23.38	39.02	33.24	14.85	28.00	57.40	52.25	35.45
	MUON	26.39	26.19	43.14	36.74	28.86	28.20	59.52	53.83	39.50
	NUMUON	19.18 (-27.3%)	<b>31.66</b>	<b>60.77</b>	<b>49.49</b>	<b>38.87</b>	<b>34.80</b>	<b>69.37</b>	<b>57.38</b>	<b>48.91</b> (+23.8%)
60%	ADAMW	307.36	23.72	29.21	26.87	0.74	26.60	51.20	49.88	29.75
	MUON	63.75	22.44	31.48	29.69	10.63	24.80	52.99	52.17	32.03
	NUMUON	32.22 (-49.5%)	<b>23.81</b>	<b>45.41</b>	<b>37.54</b>	<b>23.48</b>	<b>29.00</b>	<b>61.15</b>	<b>53.67</b>	<b>39.15</b> (+22.2%)
80%	ADAMW	2672.33	<b>25.00</b>	25.67	26.22	0.00	27.00	50.11	50.43	29.20
	MUON	346.10	24.32	27.53	26.80	0.21	<b>27.20</b>	50.76	50.36	29.60
	NUMUON	262.48 (-24.2%)	24.15	<b>30.09</b>	<b>27.52</b>	<b>1.47</b>	25.60	<b>51.58</b>	<b>51.62</b>	<b>30.29</b> (+2.3%)

Table 12: WikiText2 validation perplexity and downstream task performance across compressed Qwen3-0.6B models using SVD-LLM (Whitening + LoRA).

Comp.	OPTIMIZER	VAL. PPL	DOWNSTREAM TASKS							AVG
			ARC-C	ARC-E	H'SWAG	LAM'DA	OPENBKQA	PIQA	W'GRANDE	
0%	ADAMW	25.39	27.30	49.66	36.04	27.77	31.20	65.02	49.64	40.95
	MUON	19.20	<b>30.72</b>	<b>57.95</b>	<b>45.56</b>	<b>37.69</b>	33.60	<b>67.74</b>	<b>54.38</b>	<b>46.81</b>
	NUMUON	20.20 (+5.2%)	29.95	55.68	43.51	35.40	<b>34.40</b>	67.41	53.51	45.69 (-2.4%)
20%	ADAMW	38.49	25.51	46.21	32.10	19.66	30.60	61.21	50.59	37.98
	MUON	25.84	<b>29.52</b>	<b>51.09</b>	40.22	30.43	32.40	<b>66.87</b>	<b>53.04</b>	43.37
	NUMUON	24.01 (-7.1%)	28.41	49.83	<b>41.40</b>	<b>32.60</b>	<b>35.40</b>	65.18	52.41	<b>43.60</b> (+0.5%)
40%	ADAMW	64.17	22.53	39.18	28.39	9.86	27.60	57.18	51.70	33.78
	MUON	36.36	<b>27.65</b>	45.54	36.33	25.73	31.80	62.02	50.20	39.90
	NUMUON	29.16 (-19.8%)	26.62	<b>47.47</b>	<b>38.10</b>	<b>28.60</b>	<b>32.60</b>	<b>63.71</b>	<b>53.91</b>	<b>41.57</b> (+4.2%)
60%	ADAMW	194.18	22.10	33.50	26.33	2.74	26.00	53.54	49.57	30.54
	MUON	86.75	23.63	37.12	31.25	18.61	27.60	56.80	50.36	35.05
	NUMUON	50.88 (-41.3%)	<b>24.57</b>	<b>41.04</b>	<b>32.60</b>	<b>20.09</b>	<b>30.00</b>	<b>60.55</b>	<b>50.59</b>	<b>37.06</b> (+5.7%)
80%	ADAMW	399.33	21.67	30.09	25.86	0.56	<b>27.60</b>	52.29	49.49	29.65
	MUON	446.48	<b>23.89</b>	31.78	27.33	5.59	26.40	52.77	50.91	31.24
	NUMUON	240.48 (-46.1%)	23.21	<b>33.67</b>	<b>27.45</b>	<b>9.82</b>	27.40	<b>55.71</b>	<b>51.78</b>	<b>32.72</b> (+4.7%)

Table 13: WikiText2 validation perplexity and downstream task performance across compressed Olmo2-1.4B models using SVD-LLM (Whitening + LoRA).

Comp.	OPTIMIZER	VAL. PPL	DOWNSTREAM TASKS							AVG
			ARC-C	ARC-E	H'SWAG	LAM'DA	OPENBKQA	PIQA	W'GRANDE	
0%	ADAMW	20.58	30.20	55.47	44.96	34.76	35.80	68.93	50.67	45.83
	MUON	17.80	<b>34.04</b>	<b>60.10</b>	<b>50.94</b>	<b>39.28</b>	<b>37.80</b>	<b>70.46</b>	54.85	<b>49.64</b>
	NUMUON	19.06 (+7.1%)	31.06	59.55	48.40	37.80	37.00	68.99	<b>55.41</b>	48.32 (-2.7%)
20%	ADAMW	28.69	26.96	52.10	41.15	30.70	32.80	66.21	52.09	43.14
	MUON	21.48	<b>32.76</b>	57.74	46.80	<b>38.19</b>	35.60	<b>68.93</b>	<b>54.70</b>	<b>47.82</b>
	NUMUON	22.53 (+4.9%)	31.66	<b>58.54</b>	<b>47.63</b>	36.72	<b>36.20</b>	<b>68.93</b>	54.62	47.76 (-0.1%)
40%	ADAMW	38.80	26.11	45.79	37.09	20.47	29.00	62.57	52.01	39.01
	MUON	25.61	29.35	51.94	42.51	32.23	32.40	64.96	53.91	43.90
	NUMUON	23.17 (-9.5%)	<b>30.55</b>	<b>55.72</b>	<b>46.51</b>	<b>38.23</b>	<b>35.80</b>	<b>68.23</b>	<b>55.41</b>	<b>47.21</b> (+7.5%)
60%	ADAMW	74.04	23.55	39.18	31.47	9.86	28.00	58.32	47.51	33.94
	MUON	43.80	26.19	36.95	34.17	16.81	28.00	58.11	52.49	36.15
	NUMUON	28.85 (-34.1%)	<b>28.50</b>	<b>50.17</b>	<b>41.67</b>	<b>31.54</b>	<b>31.20</b>	<b>66.32</b>	<b>53.75</b>	<b>43.31</b> (+19.8%)
80%	ADAMW	252.34	22.95	<b>33.00</b>	26.04	2.19	<b>28.80</b>	54.35	50.43	31.11
	MUON	140.29	23.21	29.88	27.48	6.04	26.00	54.24	49.88	30.96
	NUMUON	103.38 (-26.3%)	<b>23.89</b>	32.07	<b>28.16</b>	<b>6.73</b>	27.00	<b>54.95</b>	<b>51.22</b>	<b>32.00</b> (+3.4%)

Table 14: WikiText2 validation perplexity and downstream task performance across compressed Llama3-1.8B models using SVD-LLM (Whitening + LoRA).

Comp.	OPTIMIZER	VAL. PPL	DOWNSTREAM TASKS							AVG
			ARC-C	ARC-E	H'SWAG	LAM'DA	OPENBKQA	PIQA	W'GRANDE	
0%	ADAMW	18.75	33.79	62.67	51.28	40.46	37.00	71.82	55.33	50.34
	MUON	15.39	<b>38.82</b>	<b>67.80</b>	<b>58.35</b>	<b>47.47</b>	<b>41.80</b>	<b>74.37</b>	<b>59.27</b>	<b>55.41</b>
	NUMUON	17.56 (+14.1%)	35.49	65.19	54.96	44.38	38.20	72.91	58.56	52.81 (-4.7%)
20%	ADAMW	21.69	30.03	55.01	46.22	37.69	34.80	68.55	53.83	46.59
	MUON	18.04	30.20	58.38	47.86	40.69	34.40	66.54	<b>58.33</b>	48.06
	NUMUON	17.90 (-0.8%)	<b>34.39</b>	<b>63.80</b>	<b>53.32</b>	<b>42.29</b>	<b>37.00</b>	<b>71.71</b>	58.09	<b>51.51</b> (+7.2%)
40%	ADAMW	27.94	28.41	49.37	40.69	29.52	30.00	65.13	51.22	42.05
	MUON	26.39	26.19	43.14	36.74	28.86	28.20	59.52	53.83	39.50
	NUMUON	19.18 (-27.3%)	<b>31.66</b>	<b>60.77</b>	<b>49.49</b>	<b>38.87</b>	<b>34.80</b>	<b>69.37</b>	<b>57.38</b>	<b>48.91</b> (+23.8%)
60%	ADAMW	49.59	<b>25.09</b>	40.24	33.08	15.04	27.00	58.27	49.72	35.49
	MUON	63.75	22.44	31.48	29.69	10.63	24.80	52.99	52.17	32.03
	NUMUON	32.22 (-49.5%)	23.81	<b>45.41</b>	<b>37.54</b>	<b>23.48</b>	<b>29.00</b>	<b>61.15</b>	<b>53.67</b>	<b>39.15</b> (+22.2%)
80%	ADAMW	226.44	22.61	30.85	26.52	2.23	26.20	53.75	<b>50.83</b>	30.43
	MUON	346.10	<b>24.32</b>	27.53	26.80	0.21	27.20	50.76	50.36	29.60
	NUMUON	61.25 (-82.3%)	23.89	<b>39.35</b>	<b>31.10</b>	<b>15.37</b>	<b>29.60</b>	<b>58.43</b>	50.04	<b>35.40</b> (+19.6%)

Table 15: WikiText2 validation perplexity and downstream task performance across compressed Qwen3-0.6B models using Dobi-SVD.

COMP.	OPTIMIZER	VAL. PPL	DOWNSTREAM TASKS							AVG
			ARC-C	ARC-E	H'SWAG	LAM'DA	OPENBkQA	PIQA	W'GRANDE	
0%	ADAMW	25.39	27.30	49.66	36.04	27.77	31.20	65.02	49.64	40.95
	MUON	19.20	<b>30.72</b>	<b>57.95</b>	<b>45.56</b>	<b>37.69</b>	33.60	<b>67.74</b>	<b>54.38</b>	<b>46.81</b>
	NUMUON	20.20 (+5.2%)	29.95	55.68	43.51	35.40	<b>34.40</b>	67.41	53.51	45.69 (-2.4%)
20%	ADAMW	26.94	26.19	48.95	35.48	28.47	31.00	65.02	49.01	40.59
	MUON	19.90	30.03	<b>57.15</b>	<b>45.58</b>	<b>37.51</b>	33.60	<b>68.93</b>	<b>54.22</b>	<b>46.72</b>
	NUMUON	20.83 (+4.7%)	<b>30.46</b>	54.42	42.95	33.26	<b>34.00</b>	66.87	53.43	45.06 (-3.6%)
40%	ADAMW	27.25	27.05	49.28	35.57	31.05	30.60	64.09	49.72	41.05
	MUON	20.16	<b>30.72</b>	<b>56.06</b>	<b>45.54</b>	<b>33.73</b>	33.20	<b>68.01</b>	53.12	<b>45.77</b>
	NUMUON	20.77 (+3.0%)	29.18	53.58	43.31	32.52	<b>33.80</b>	67.36	<b>54.30</b>	44.86 (-2.0%)
60%	ADAMW	32.64	25.68	42.63	34.45	16.77	32.40	60.83	50.28	37.58
	MUON	24.36	<b>29.01</b>	49.28	41.71	24.94	31.40	64.47	<b>53.12</b>	41.99
	NUMUON	21.66 (-11.1%)	27.65	<b>51.73</b>	<b>42.38</b>	<b>28.95</b>	<b>33.20</b>	<b>65.67</b>	51.78	<b>43.05</b> (+2.5%)
80%	ADAMW	115.94	23.21	31.02	27.38	2.31	26.40	51.20	50.36	30.27
	MUON	50.31	22.95	33.08	31.47	11.00	26.40	56.15	<b>52.17</b>	33.32
	NUMUON	36.10 (-28.2%)	<b>26.19</b>	<b>36.41</b>	<b>35.40</b>	<b>13.62</b>	<b>27.40</b>	<b>60.45</b>	51.78	<b>35.89</b> (+7.7%)

Table 16: WikiText2 validation perplexity and downstream task performance across compressed Olmo2-1.4B models using Dobi-SVD.

COMP.	OPTIMIZER	VAL. PPL	DOWNSTREAM TASKS							AVG
			ARC-C	ARC-E	H'SWAG	LAM'DA	OPENBkQA	PIQA	W'GRANDE	
0%	ADAMW	20.58	30.20	55.47	44.96	34.76	35.80	68.93	50.67	45.83
	MUON	17.80	<b>34.04</b>	<b>60.10</b>	<b>50.94</b>	<b>39.28</b>	<b>37.80</b>	<b>70.46</b>	54.85	<b>49.64</b>
	NUMUON	19.06 (+7.1%)	31.06	59.55	48.40	37.80	37.00	68.99	<b>55.41</b>	48.32 (-2.7%)
20%	ADAMW	23.12	29.18	53.45	43.09	28.45	33.80	67.36	51.14	43.78
	MUON	18.81	<b>31.91</b>	58.59	<b>48.39</b>	<b>35.57</b>	35.20	68.88	<b>56.67</b>	47.89
	NUMUON	19.23 (+2.2%)	31.23	<b>59.97</b>	48.19	35.38	<b>36.20</b>	<b>69.21</b>	55.56	<b>47.96</b> (+0.1%)
40%	ADAMW	34.30	26.28	45.66	37.74	17.48	28.80	62.13	50.51	38.37
	MUON	22.90	27.13	49.37	42.45	<b>32.19</b>	30.80	63.33	<b>55.41</b>	42.95
	NUMUON	20.66 (-9.8%)	<b>27.99</b>	<b>55.01</b>	<b>46.21</b>	29.56	<b>33.60</b>	<b>67.68</b>	54.93	<b>45.00</b> (+4.8%)
60%	ADAMW	127.21	24.49	32.91	29.37	4.17	26.60	54.46	50.04	31.72
	MUON	37.23	24.06	36.95	34.08	22.98	27.60	58.00	<b>54.46</b>	36.88
	NUMUON	23.49 (-36.9%)	<b>27.65</b>	<b>52.27</b>	<b>43.40</b>	<b>23.33</b>	<b>32.40</b>	<b>65.40</b>	54.30	<b>42.68</b> (+15.7%)
80%	ADAMW	930.61	<b>24.40</b>	27.74	25.85	0.19	25.00	52.88	50.20	29.47
	MUON	160.56	24.32	27.40	28.29	3.07	28.20	51.20	51.14	30.52
	NUMUON	65.93 (-58.9%)	23.81	<b>32.32</b>	<b>31.25</b>	<b>8.69</b>	<b>29.20</b>	<b>55.33</b>	<b>52.72</b>	<b>33.33</b> (+9.2%)

Table 17: WikiText2 validation perplexity and downstream task performance across compressed Llama3-1.8B models using Dobi-SVD.

COMP.	OPTIMIZER	VAL. PPL	DOWNSTREAM TASKS							AVG
			ARC-C	ARC-E	H'SWAG	LAM'DA	OPENBkQA	PIQA	W'GRANDE	
0%	ADAMW	18.75	33.79	62.67	51.28	40.46	37.00	71.82	55.33	50.34
	MUON	15.39	<b>38.82</b>	<b>67.80</b>	<b>58.35</b>	<b>47.47</b>	<b>41.80</b>	<b>74.37</b>	<b>59.27</b>	<b>55.41</b>
	NUMUON	17.56 (+14.1%)	35.49	65.19	54.96	44.38	38.20	72.91	58.56	52.81 (-4.7%)
20%	ADAMW	21.42	34.04	56.52	49.41	31.85	35.00	70.13	55.09	47.43
	MUON	16.37	<b>34.56</b>	<b>63.59</b>	<b>54.99</b>	<b>45.97</b>	<b>38.80</b>	71.33	58.01	<b>52.46</b>
	NUMUON	17.96 (+9.7%)	33.96	62.29	53.64	43.10	35.40	<b>71.38</b>	<b>58.17</b>	51.13 (-2.5%)
40%	ADAMW	28.83	30.72	49.79	43.15	31.30	33.20	64.69	53.67	43.79
	MUON	20.44	28.16	52.27	46.22	<b>40.29</b>	29.80	63.98	56.35	45.30
	NUMUON	18.63 (-8.9%)	<b>31.31</b>	<b>60.23</b>	<b>51.98</b>	39.59	<b>34.80</b>	<b>70.18</b>	<b>57.54</b>	<b>49.38</b> (+9.0%)
60%	ADAMW	164.19	23.72	32.53	29.14	2.95	25.80	54.57	50.43	31.31
	MUON	40.55	23.81	34.09	34.13	15.56	25.80	55.77	53.35	34.64
	NUMUON	27.42 (-32.4%)	<b>26.71</b>	<b>45.16</b>	<b>43.86</b>	<b>17.16</b>	<b>31.80</b>	<b>62.89</b>	<b>53.91</b>	<b>40.21</b> (+16.1%)
80%	ADAMW	605.85	<b>24.83</b>	28.03	26.59	0.12	26.80	50.54	48.54	29.35
	MUON	113.19	24.57	28.96	28.83	2.50	26.20	51.63	<b>52.88</b>	30.80
	NUMUON	50.05 (-55.8%)	23.63	<b>35.98</b>	<b>33.45</b>	<b>8.99</b>	<b>27.20</b>	<b>57.24</b>	52.64	<b>34.16</b> (+10.9%)

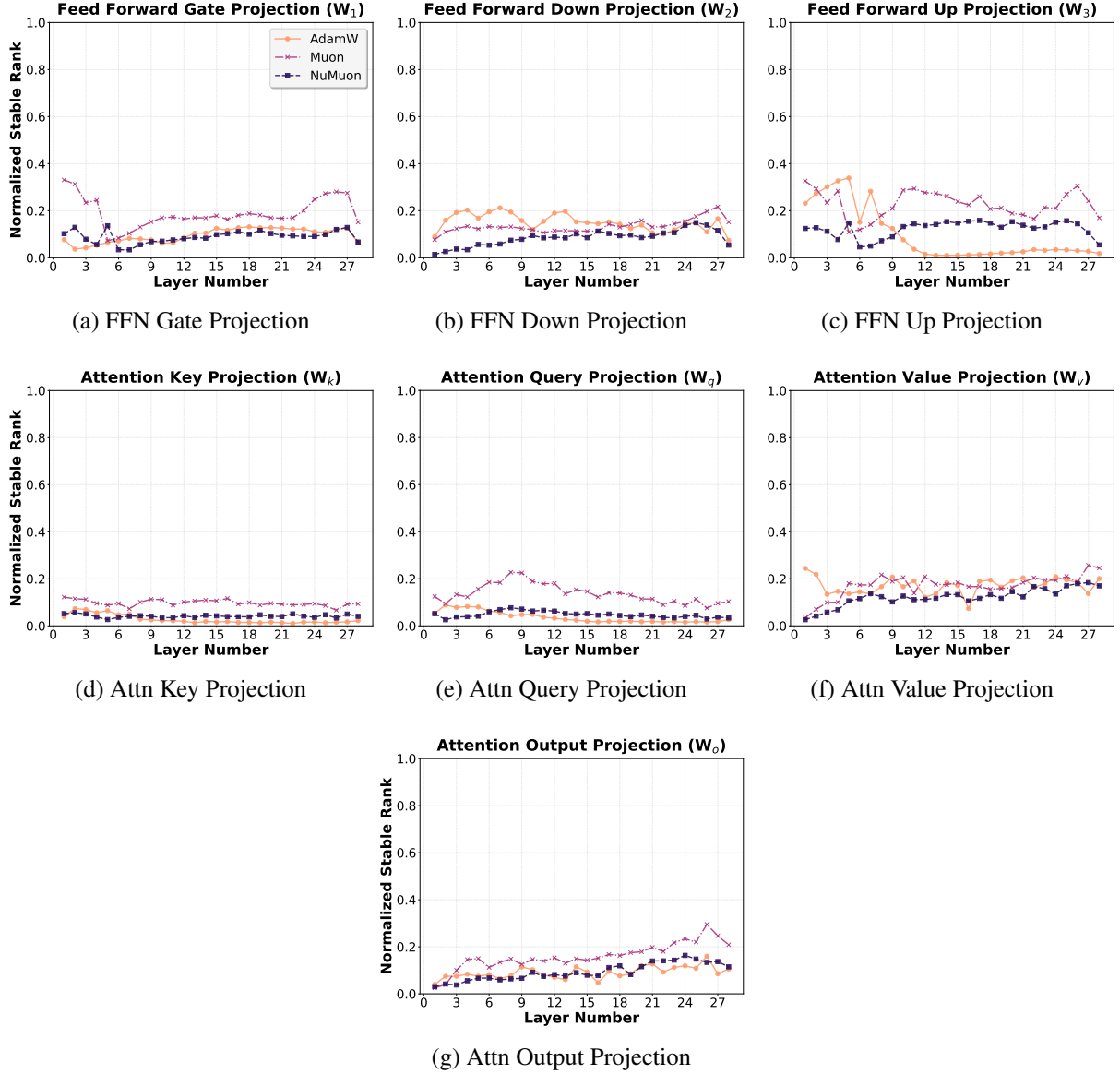


Figure 14: Normalized stable rank for weight matrices of Qwen3-0.6B models. Each subplot shows the stable rank (normalized by the maximum rank) of the converged model across all layers.

early high-rank Block Krylov SVD regime (see Figure 11), but can trade off base performance depending on how restrictive the rank budget is. In contrast, cosine and piecewise schedules benefit from a higher-rank phase early in training and then anneal to a lower-rank regime, which tends to yield better base performance while still improving compressibility relative to full-rank Muon. Across schedulers, NuMuon consistently mitigates the severe degradation observed for Muon at 80% compression, indicating that explicit rank control induces weight structure that is easier to approximate with SVD-based compressors.

**Layerwise Stable-rank under Rank-budget Ablations.** Figure 21 visualizes how changing the rank budget affects the layerwise stable rank of the final model. As expected, tighter budgets produce uniformly lower stable rank across layers and weight matrices, while relaxing the budget increases stable rank and approaches full-rank behavior.

**Layerwise Stable-rank under Scheduler Ablations.** Figure 22 compares scheduler-induced differences in layerwise stable rank. Cosine and piecewise schedules typically yield lower stable rank than full-rank

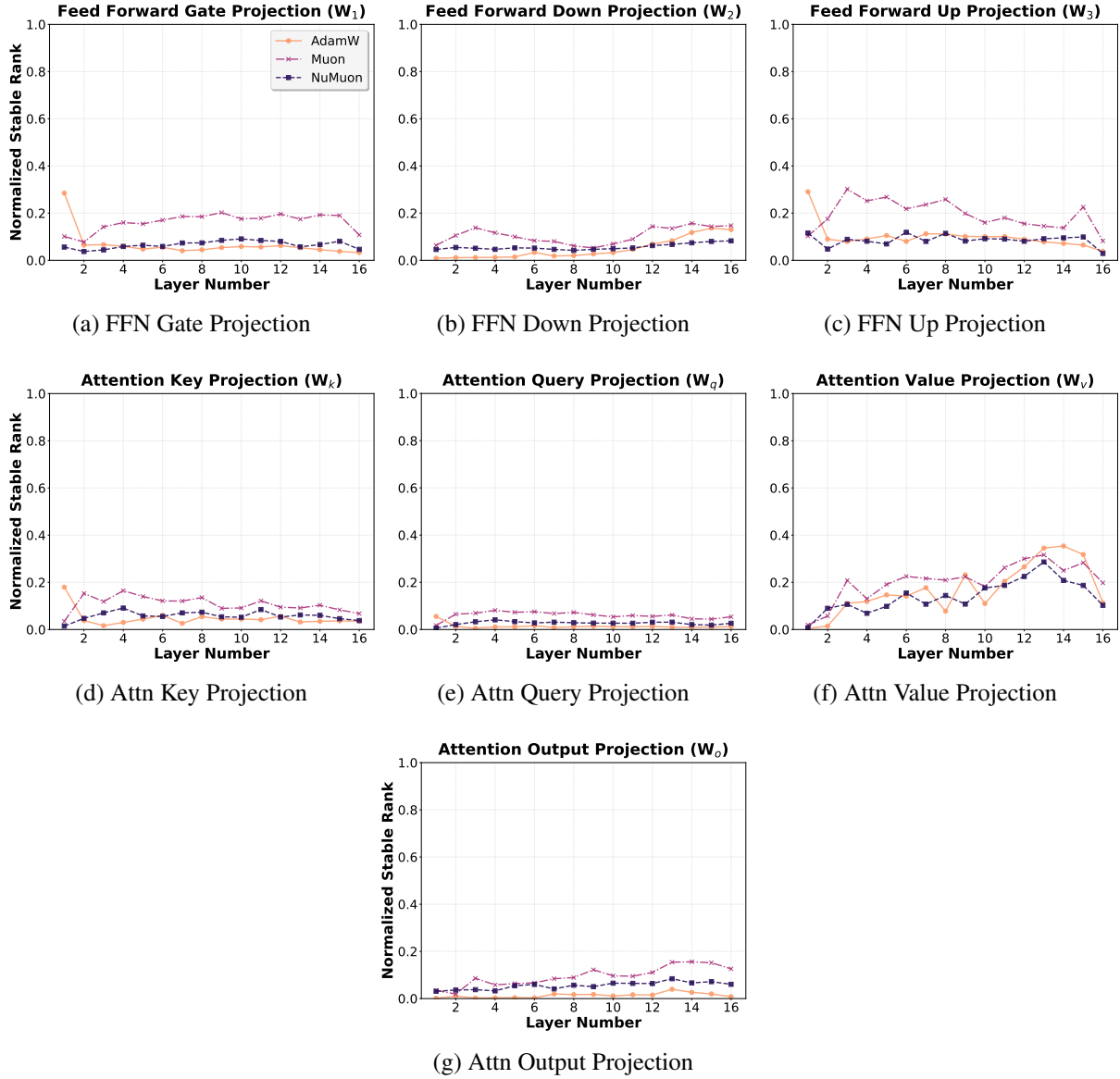


Figure 15: Normalized stable rank for weight matrices of Olmo2-1.4B models. Each subplot shows the stable rank (normalized by the maximum rank) of the converged model across all layers.

Muon while maintaining stronger base performance than the fixed-rank settings, reflecting the benefit of a high-rank warm-start followed by annealing. Taking these results and the loss curves in Figure 7 together, these ablations support the central trade-off in NuMuon: selecting a rank budget and schedule that is low enough to improve compressibility, yet not so restrictive that it impairs optimization.

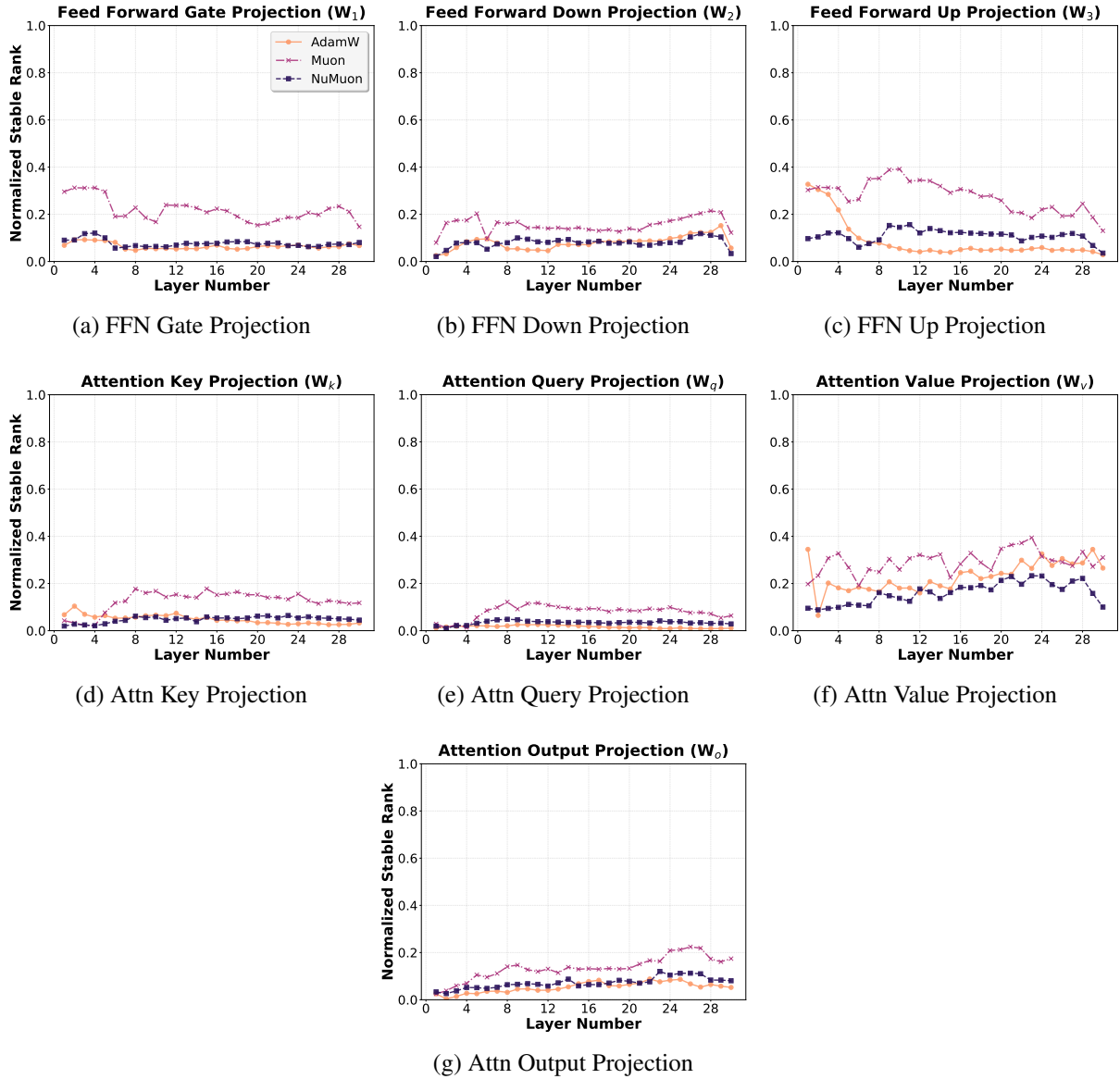


Figure 16: Normalized stable rank for weight matrices of Llama3-1.8B models. Each subplot shows the stable rank (normalized by the maximum rank) of the converged model across all layers.

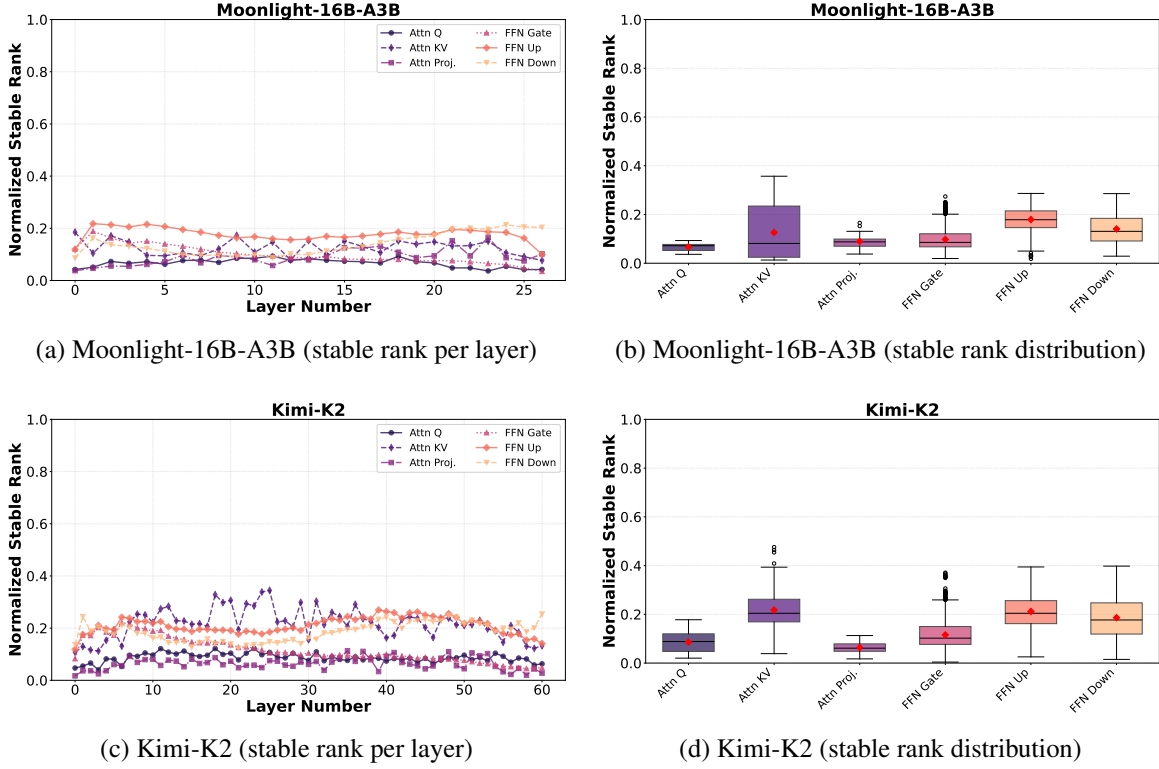


Figure 17: Normalized stable rank of well-known, large-scale models trained via Muon. The plot shows Moonlight-16B-A3B (Liu et al., 2025) (top) as well as Kimi-K2-1T (Bai et al., 2025) (bottom). For each model, we show the distribution of the normalized stable rank (left) as well as its evolution by the layer index (right).

Table 18: WikiText2 validation perplexity and downstream task performance for various rank schedules.

COMP.	OPTIM.	RANK SCHEDULE	VAL. PPL ↓	DOWNSTREAM TASKS						AVG ↑	
				ARC-C	ARC-E	H'SWAG	LAM'DA	OPENBkQA	PIQA		W'GRANDE
0%	ADAMW	-	25.39	27.30	49.66	36.04	27.77	31.20	65.02	49.64	40.95
	MUON	-	19.20	30.72	57.95	45.56	37.69	33.60	67.74	54.38	46.81
	NUMUON	PIECEWISE (25d/100)	20.01	29.69	56.44	43.78	35.51	35.00	67.79	52.88	45.87
		COSINE (25d/100)	20.20	29.95	55.68	43.51	35.40	34.40	67.41	53.51	45.69
		FIXED (5d/100)	29.13	25.60	48.06	33.68	25.13	31.20	63.98	49.80	39.64
		FIXED (25d/100)	21.85	29.01	53.03	41.37	33.30	33.40	66.70	53.28	44.30
		FIXED (50d/100)	20.27	29.52	54.63	43.79	36.64	33.80	67.52	50.28	45.17
FIXED (80d/100)	19.31	30.80	55.68	44.54	36.95	36.00	66.97	53.35	46.33		
80%	ADAMW	-	115.94	23.21	31.02	27.38	2.31	26.40	51.20	50.36	30.27
	MUON	-	50.31	22.95	33.08	31.47	11.00	26.40	56.15	52.17	33.32
	NUMUON	PIECEWISE (25d/100)	33.39	24.91	43.90	32.95	20.20	31.00	62.35	50.12	37.92
		COSINE (25d/100)	36.10	26.19	36.41	35.40	13.62	27.40	60.45	51.78	35.89
		FIXED (5d/100)	31.93	26.96	42.13	36.36	22.39	29.00	62.08	52.25	38.74
		FIXED (25d/100)	44.69	25.85	34.72	33.84	9.57	27.00	57.40	52.17	34.36
		FIXED (50d/100)	46.66	24.91	32.28	32.36	13.55	29.80	56.53	51.22	34.38
FIXED (80d/100)	43.70	23.98	35.82	33.33	14.03	26.20	56.91	50.67	34.42		

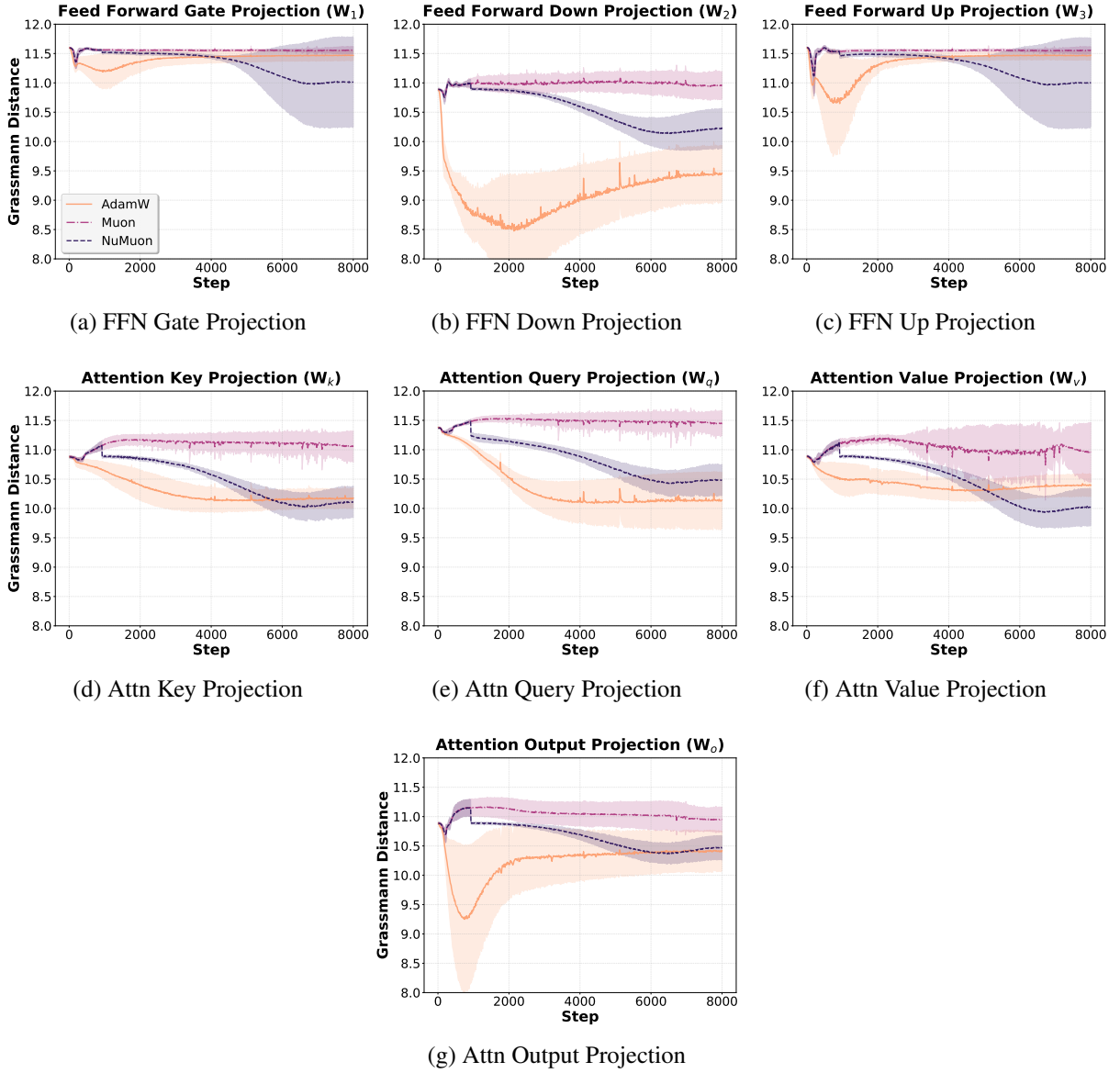


Figure 18: Grassmann distance between the top-64 left singular vectors of the weight space  $\mathbf{W}$  and the optimizer update  $\Delta\mathbf{W}$ . For NuMuon, we use the cosine rank scheduler. As demonstrated, while Muon ignores the structure of the weight space in its updates (high, fixed Grassmann distance), NuMuon gradually concentrates the update’s energy around the top subspaces of the weight space (lower Grassmann distance).

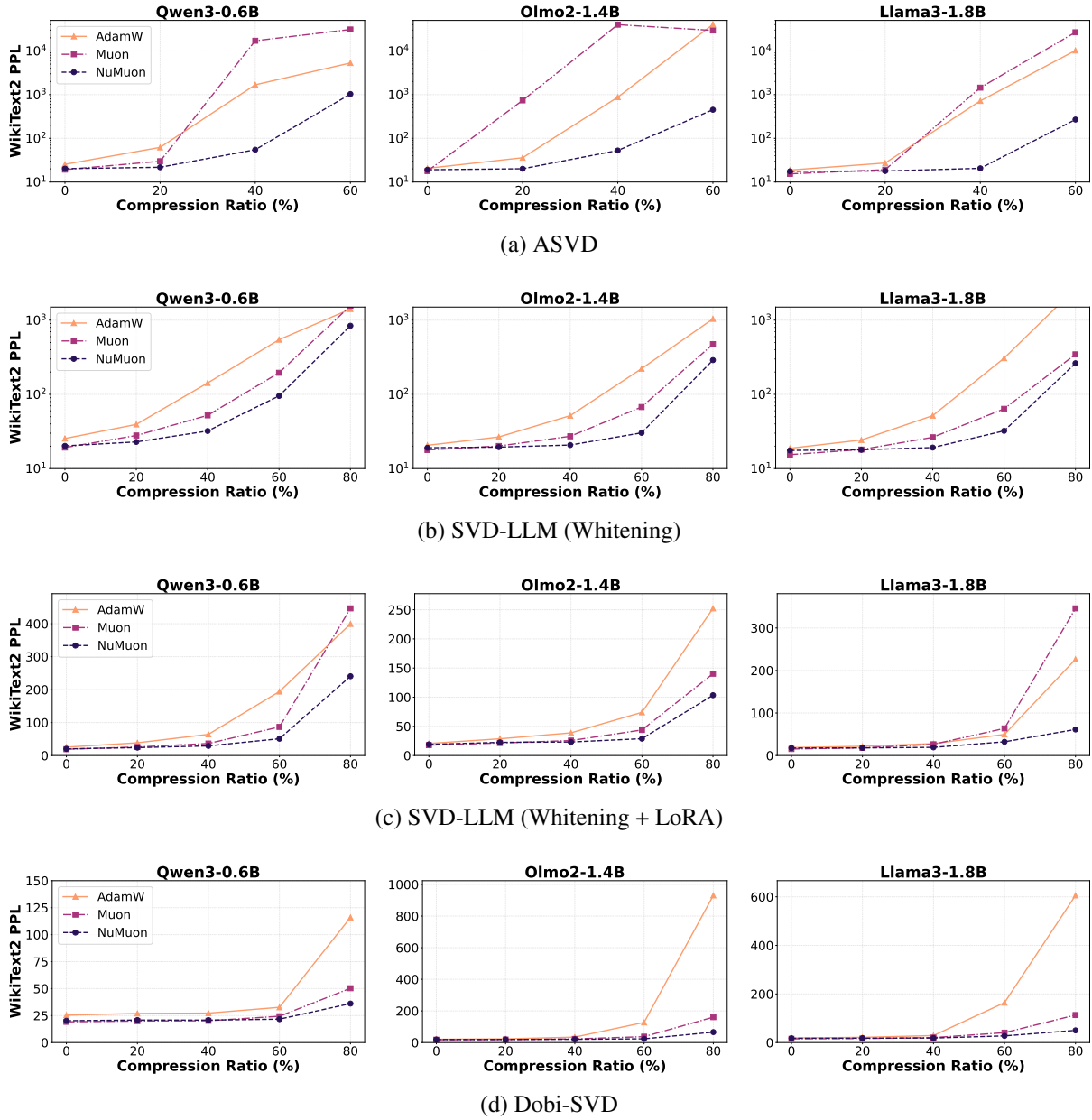


Figure 19: Validation perplexity on WikiText2 dataset for compressed LLMs (Qwen3-0.6B, Olmo2-1.4B, and Llama3-1.8B) using different compression methods. As seen, models pretrained via NuMuon consistently achieve the lowest validation perplexity, yielding better performance at extreme compression ratios.

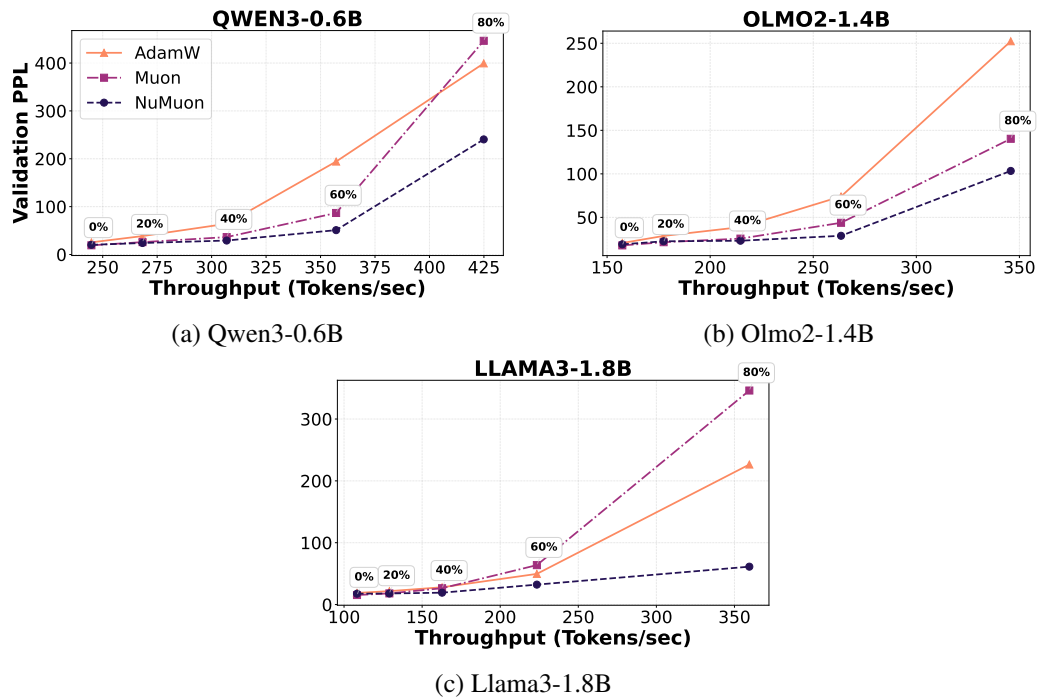


Figure 20: Validation perplexity on WikiText2 against generation inference throughput for Qwen3-0.6B, Olmo2-1.4B, and Llama3-1.8B models compressed via SVD-LLM. NuMuon trained models deliver the lowest perplexity given a throughput, and as such, are far more efficient than AdamW- or Muon-trained models at moderate to extreme compression rates. Also, we observe that as the model size grows, NuMuon-trained models become more amenable to compression.

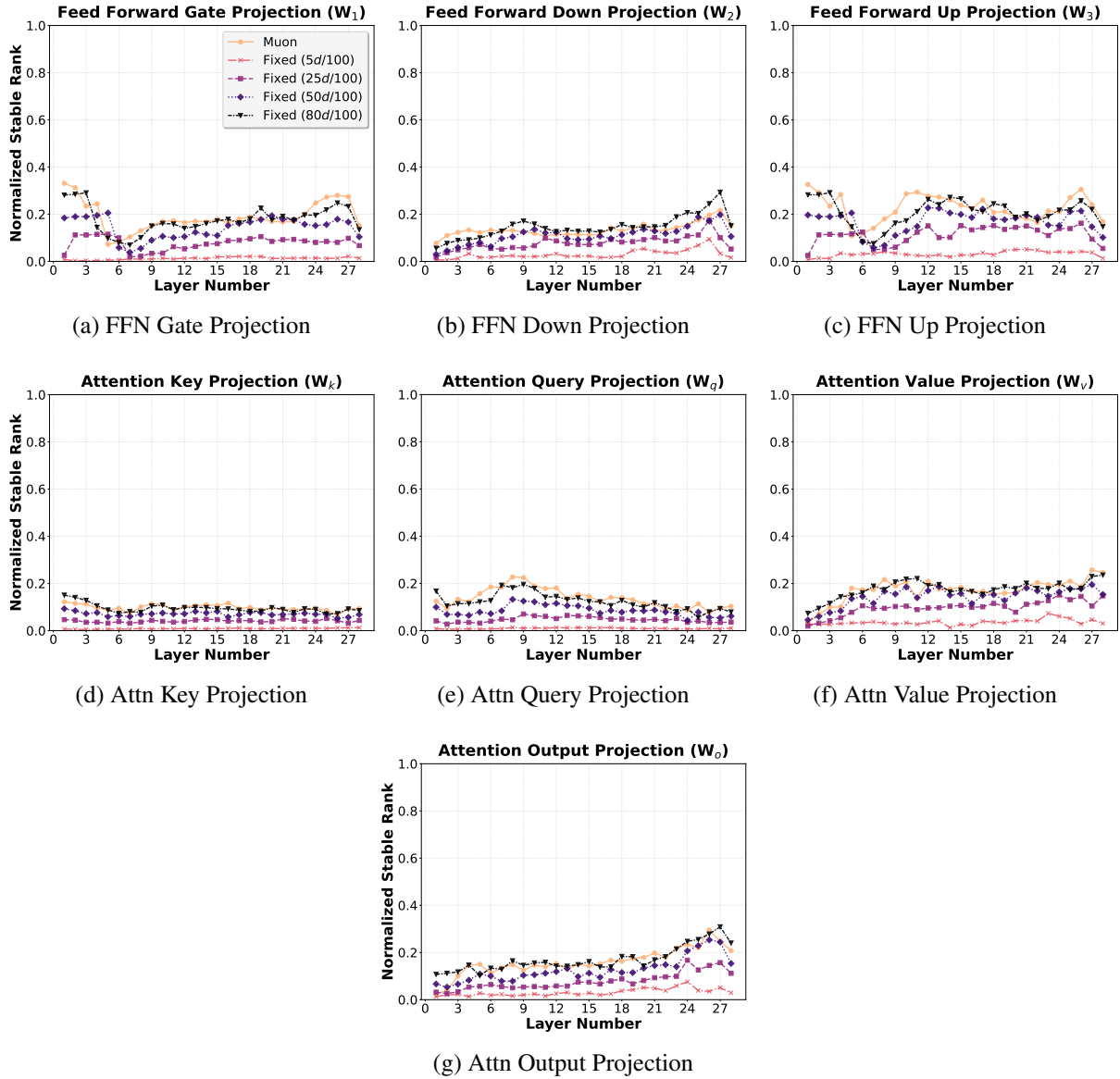


Figure 21: Normalized stable rank for weight matrices of Qwen3-0.6B models trained with NuMuon under different ranks/nuclear norm budget. Each subplot shows the stable rank (normalized by the maximum rank) of the converged model across all layers.

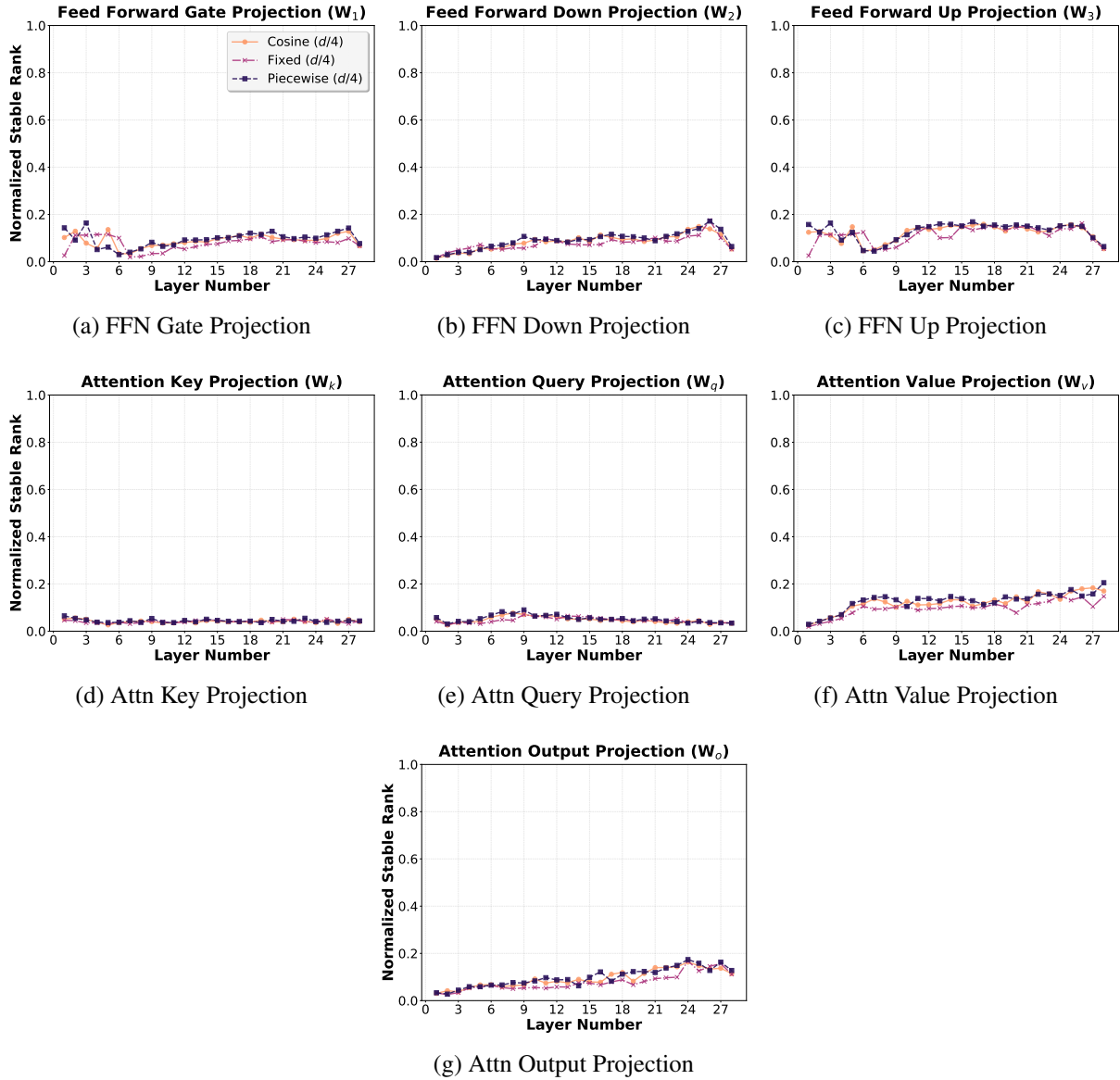


Figure 22: Normalized stable rank for weight matrices of Qwen3-0.6B models trained with NuMuon under different rank schedulers. Each subplot shows the stable rank (normalized by the maximum rank) of the converged model across all layers.